UiT The Arctic University of Norway

Faculty of Science and Technology
Department of Physics and Technology

Seasonal and interannual variability in hydrography and currents along the Nansen Legacy transect across the Barents Sea

Julie Marie Seime Sortland

FYS-3900: Master's thesis in physics - 60 ECTS
December 2023

Abstract

The Barents Sea is an Arctic shelf sea that is an important site for water mass formation and transformation. It is characterized by interactions between Atlantic- and Arctic-origin Waters, and by strong seasonality in terms of alternating atmospheric and sea-ice conditions throughout the year. How these aspects impact the seasonal evolution of the water column properties is yet to be fully understood. In this study, we investigate the hydrographic conditions along the Nansen Legacy (NL) main transect across the Barents Sea and towards the adjacent Nansen Basin in the Arctic Ocean in the period between 2018 and 2022. In particular, we describe the dominant water masses and currents along the transect and investigate the seasonal and interannual variations in water mass characteristics, distribution, and circulation. The dataset includes CTD, S-ADCP, and L-ADCP profiles collected through the NL project. Ancillary data includes atmospheric reanalysis and remotely sensed sea ice data, used to assess how atmospheric and sea ice forcing alters the water column throughout the study period.

Our analysis shows that the NL transects can be divided into three domains reflecting differences in water masses, seasonal evolution, heat- and freshwater content, and flow regimes. In the Nansen Basin and at the Svalbard Continental shelf (81-82° N), the circulation is shaped by the water that is advected in with the Atlantic Water Boundary Current (AWBC) at intermediate depths. The seasonal variations of the AWBC further control the seasonal variations in hydrographic properties in the area, for example in the form of elevated oceanic temperatures during autumn/ early winter. In general, the water column structure in the region follows the typical layering with Polar Water (PW) and/or warm Polar Water (wPW) on top followed by Atlantic Water (AW), modified Atlantic Water (mAW), and Eurasian Basin Deep water (EBDW).

The Northern Barents Sea (77-81° N) is mainly dominated by PW in the upper water column and wPW at lower depths. The water is overall cold and fresh, characteristic of an Arctic domain. The hydrographic properties in the upper water column are shaped by the presence of sea ice cover, which often is extensive during winter and spring in this area. We find that the sea ice cover controls the heat and freshwater content, the stratification, and shape the water

masses in the area.

South of the Polar Front (<76.8° N), warm Atlantic-origin waters dominate the area. On a yearly cycle, the water column progresses from a three-layer, relatively stratified column with wPW, AW, and mAW during summer, to a homogeneous water column consisting of cooled mAW during winter. Here, the water column properties appear to be controlled by local processes, rather than advective ones.

Acknowledgements

Firstly, I want to thank my main supervisor, Angelika Renner, for giving me the opportunity to take on this master's thesis within the Nansen Legacy (NL) Project. Being a part of the big and interdisciplinary research project that the Nansen Legacy represents, has provided me with many valuable experiences and opportunities, - including several field cruises to the high Arctic. I also want to thank you for all the patience and kindness you have shown me during this thesis work, including times of personal ups and downs! I am immensely grateful for having had the opportunity to work with and learn from you!

Further, I must thank my co-supervisor, Polona Itkin. Your academic guidance and encouraging words have been invaluable! To Zoe Koenig, I must express my uttermost gratitude for helping and advising me through my Matlab hardships. The thesis would not have been made without you!

A special thanks must be given to Øyvind Lundesgaard. Thanks for letting me borrow some of your Python scripts, and thanks for the inspirational words you have provided me with during extra hard days. Indeed, I must thank all the people at the Fram Center who've had an open door and who've shared their knowledge. To my fellow office students; Elena and Johanne, you have kept my spirits high and made the coffee breaks extra long. To all of my dear friends and family in Bergen, at Svalbard, and in Tromsø - thanks for all of your love and support. Lastly, thanks to my roommates Sari, Villads, and Molly for keeping me sane during the last couple of weeks.

Contents

Abstract **i**

Acknowledgements **iii**

List of Figures **vii**

List of Tables **xi**

1 Introduction **1**
1.1 Research Purpose and Questions 2

2 Background **5**
2.1 Oceanographic setting of the Study Area 5
2.2 Air-ice-sea interactions 9
2.3 The Nansen Legacy main transect 11

3 Data and Methods **17**
3.1 Hydrographic data 17
3.1.1 Instruments and Processing 19
3.2 Ocean Current Data 20
3.2.1 S-ADCP 21
3.2.2 L-ADCP 22
3.3 Atmosphere and sea ice data 23
3.4 Water Mass Classification 24
3.5 Calculations 26
3.5.1 Fresh Water and Heat Content 26

4 Results **29**
4.1 Atmospheric and Sea ice conditions 29
4.2 Hydrography 33
4.2.1 Water mass classification 40
4.3 Heat and Freshwater Content 50
4.4 Current Measurements 52

5 Discussion **59**
5.1 Atmospheric and sea ice forcing 59
5.2 Currents 62
5.3 Seasonality 64
5.4 Limitations and Future work 66

6 Summary and conclusion **69**

Bibliography **71**

7 Appendix **77**
7.1 Appendix A – Station table 78
7.2 Appendix B – Pcolour plots of CT and SA 80
7.3 Appendix C – P-station profiles including water masses . . . 84

List of Figures

2.1 Map of the Barents Sea, with arrows indicating some of the main current systems in and around the Barents Sea area. Red arrows display the pathway of warm and saline currents of Atlantic origin, while the white arrows indicate colder Arctic Waters and the import of sea ice from the north. The black and grey dots depict the hydrographic stations that make up the Nansen Legacy transect, which is the focus area of this thesis. Source of map: Jones et al. (2023) 9
2.2 Map of the NL main transect, with the positions and numbers of the stations marked by the blue dots on the map. The stations are subscripted as NL1 to NL25. 12
2.3 Conceptual map of the NL transect illustrating different physical and biological environments along the north-to-south gradient. Source: Gerland et al. (2023). 13
2.4 Transect plot of temperature (colored fields) and salinity (black isolines) for the NL transect, where the position of the seven P-stations are indicated with black, dashed lines. The plot displays measurements conducted on the transect in August 2012. Note the different scales in both depth and latitude for the panels. Source of figure: (The Nansen Legacy, 2022) Sampling Protocols: Version 10. The Nansen Legacy Report Series 32/2022. DOI: https://doi.org/10.7557/nlrs.6684 15

3.1 Overview of the NL stations covered for each cruise. The positions of the different NL stations are given in nominal latitude and longitude, with units in decimal degrees E and N, respectively. The blue shading of the NL stations identifies which stations are placed on the continental shelf north of Svalbard. 19

3.2 (a): CT-SA plot displaying the different ranges of conservative temperature, absolute salinity, and/or potential density used for water mass classification in this thesis. Left: Table presenting the same water masses, but with additional information regarding the parameters in the older oceanographic standards of salinity S, potential temperature θ, and potential density σ (EOS-80). Both figures are taken from Sundfjord et al. (2020). 24

4.1 Upper panel: Hovmöller diagram of the ERA-5 12-hourly 2 m air temperature. The temperature is averaged over 30-34° E. The latitude of each process station (P1-P7) is indicated with grey dashed lines. Lower panel: Hovmöller diagram of the daily sea ice concentration (SIC) for the 34° E meridian. The concentration is given in percentage[%] 30
4.2 Top to bottom: Time series of monthly averaged 2 m air temperature, sea surface temperature, sea level pressure, and wind speed for the location of the seven process stations (P1 to P7). 32
4.3 CT-SA diagram of all CTD data from stations on the NL transect from every cruise in our dataset. Dashed grey lines indicate isypycnals. NB. A-twain19 and Mooring20 corresponds to MSC19 and MSC20 cruise, respectively. 34
4.4 Meridional transect plots of conservative temperature (CT) and absolute salinity (SA) against depth (in meters; y-axis) and latitude (° N; x-axis) for the different cruises. The positions of the seven process stations (P1 to P7) are indicated with black dots on top. Note the difference in depth ranges for the two panels; the top panel shows data for the upper 15-350 m of the water column, while the lower panels show the depths from 350 m to 3500 m. 35
4.4 continued. 36
4.4 continued. 37
4.5 Transect plots of Conservative Temperature (CT) and Absolute Salinity (SA) against depth (in meters; y-axis) and latitude (° N; x-axis) for the JC2-1 cruise, displaying the area between P1 and P2 where the PF is expected to be situated. The positions of the four defined NL stations, as well as the positions for the additional CTD stations, are indicated with black arrows at the top of the panels. The grey lines on these plots are isothermals (upper panel) and isohalines (lower panel). . 40

4.6 (Left panels): Classified water masses along each profile conducted at an NL station during its respective cruise. The water masses are classified according to Sundfjord et al. (2020). The top panels show the upper 15-500 m, while the lower panels show the depth from 15 m down to 3500 m. (Right panels): Calculated mean percentage of each water mass for the 7 process stations. 42
4.6 Continued. 43
4.6 Continued. 44
4.7 CT-SA plots displaying the NL data points from each cruise. The CT-SA plot to the left indicate the water mass classification of the single datapoints, while the plot to the right shows the latitude of the datapoits 47
4.7 Continued. 48
4.7 Continued. 49
4.8 Calculated heat and freshwater content in the upper 15-100 m along the NL transect (by latitude (° N); x-axis) for all cruises. 52
4.9 Transect plots of S-ADCP and L-ADCP current velocities against depth (in meters; y-axis) and latitude (° N; x-axis). The left panels display the u-component, while the right panels show the v-component of the current velocities. The positions of the seven process stations are indicated with black dots on top of the panel, while the black arrows at the bottom (for the L-ADCP transects) indicate where measurements are taken. Grey shading indicates the seafloor. 55
4.9 Continued. 56
4.9 Continued. 57

7.1 Name, position, depth, etc. for each defined NL station in the Nansen Legacy main transect. The comment section refers to an associated project and/or the geographical location of the station. Source of table: The Nansen Legacy (2022) Sampling Protocols: Version 10. The Nansen Legacy Report Series 32/2022. DOI: https://doi.org/10.7557/nlrs.6684 78
7.2 Pcolour plots of Conservative Temperature and Absolute Salinity for each of the cruises. Each column refers to a conducted profile. Thus, for some NL stations where several profiles were conducted, several columns are displayed for that same station. 80
7.2 Continued. 81
7.2 Continued. 82

7.3 Profiles of Conservative Temperature for the 7 P-stations, with the corresponding water masses plotted on top. The profiles are shown in chronological order, displaying the evolution throughout the study period. Regarding P7, the displayed profile depth is limited to 15-1000m 84
7.3 Continued. 85
7.3 Continued. 86
7.3 Continued. 87
7.3 Continued. 88
7.3 Continued. 89
7.3 Continued. 90

List of Tables

3.1 Overview of the NL cruise surveys providing the hydrographic data for this thesis. The table includes the cruise name, cruise abbreviation, year, dates, and research vessel for each respective survey. 18
3.2 Data availability of S-ADCP and L-ADCP measurements for each of the NL cruises in our database. 21
3.3 Table with magnetic declination values used for processing L-ADCP raw data. "EMM" refers to the Enhanced Magnetic Model, while "WMM" refers to the World Magnetic Model used to calculate the values. 22

1

Introduction

The Arctic region is warming faster than any other place on Earth, - a phenomenon commonly referred to as the "Arctic amplification" (Previdi et al., 2021). The warming is especially prominent in the climate records of air temperature for the region (e.g., Rantanen et al., 2022), but also shown to extend into the water column (Shu et al., 2022). Concurrent with rising atmospheric and oceanic temperatures, the sea ice in the Arctic is declining in both its extent and thickness (Ivanov et al., 2012; Meredith et al., 2019).

Out of the Arctic region, the Northern Barents Sea is observed to experience the most dramatic warming during the recent decades (Lind et al., 2018), including the highest increase in air temperature (Isaksen et al., 2022) and the biggest reduction in winter sea ice cover (Onarheim et al., 2018). As such, the Barents Sea can be referred to as an Arctic Hotspot for climate change. Studies by Årthun et al. (2021) have shown that the Barents Sea might be ice-free during winter seasons at the end of this century, while some models show the possibility of a winter ice-free Barents Sea even by the year 2050 (Onarheim and Årthun, 2017).

The reduction of sea ice in the Barents Sea can have major impacts on the ocean's current and future state. The declining import of sea ice to the ocean interior, and the subsequent reduction of freshwater input, are shown to reduce ocean stratification and increase vertical mixing (Lind et al., 2018). As a result, the upper 100 m of the water column has become warmer and more saline since the 2000's (Lind et al., 2018).

The Barent Sea is characterized by warm and salty Atlantic-origin Waters from the south meeting and interacting with cold and fresh Arctic Waters from the north (Loeng, 1991). Lately, there has been a shift in the hydrographic properties from a more traditional Arctic condition to an increasing dominance of Atlantic Water, known as "Atlantification"(Polyakov et al., 2017). This shift translates to the ecosystems, and the Barents Sea is one of the polar areas where the changes in ecosystems are most evident (Wold et al., 2023; Gerland et al., 2023).

The Barents Sea is an area that typically experiences large seasonality in terms of variable physical conditions; from the partly sea-ice-covered waters in winter and spring to the open-water conditions that are typical for the summer and autumn season (Gerland et al., 2023). While quite a big interannual variability in hydrography has already been documented for the Barents Sea, the seasonal evolution of the hydrographic environment is yet to be fully explored and understood.

1.1 Research Purpose and Questions

In this thesis, we are investigating the hydrographic conditions along a north-to-south gradient across the Barents Sea, defined as the Nansen Legacy (NL) main transect (see the following section 2.3 for more information). The overarching purpose is to describe the water masses present on the NL transect area during the NL survey period of 2018-2022. We will assess the spatial distribution of water masses along the transect, as well as the temporal evolution throughout the study period. In particular, we will try to elucidate some of the seasonal variations and transformations of the water column properties.

Both the atmosphere and sea ice can modify the hydrographic properties through interactions in the air-ice-ocean interface. For this reason, we are looking into the atmospheric and sea ice conditions during the study period to assess how, and if, the environmental forcing contributes to the variations in water mass over time. However, the water masses do not have to be a local product but can be advected in from downstream areas with current systems. In addition, currents themselves can alter water masses through their mixing effects. Thus, we will also examine the circulation patterns across the transect by looking into ADCP data measured during the same period.

Although the knowledge about the Barents Sea system has advanced during the last decades due to increased research efforts in the area, there is still a lack of observational measurements for the winter and spring seasons (Gerland et al., 2023). With this study, we aim to contribute to fill this gap. The main motivation behind this thesis, however, is to complement the research done by

other working groups within the NL project, by giving a background analysis of the hydrographic environment on the NL transect. From a broader perspective, reports of the present hydrographic conditions can help monitor future changes, both in the Barents Sea and downstream into the Arctic Ocean.

We will be focusing on answering these research questions:

- What are the seasonal variations in water mass characteristics and distribution along the NL transect?
- What does the circulation pattern across the transect look like, and how does it affect the hydrographic properties?
- How did sea ice and atmospheric forcing impact the water column properties during the study period?

2

Background

2.1 Oceanographic setting of the Study Area

The Barents Sea is a shelf sea situated at the doorstep of the Arctic Ocean (see Fig. 2.1). In addition to its shared borders with the Arctic Ocean in the north, it connects to the Norwegian Sea to the west and the Kara Sea to the east. The mean depth of the Barent Sea is merely 230m (Schauer et al., 2002). However, the bathymetry varies substantially throughout the ocean interior and includes several deeper trenches, as well as shoal plateaus and/or banks.

In general, the Barents Sea can be divided into two main domains; one Atlantic and one Arctic (Loeng, 1991). While the southern Barents Sea is dominated by warm and saline Atlantic Water, keeping the ocean surface ice-free for large parts of the year, the northern and central parts of the Barents Sea contain colder, fresher Arctic waters with a seasonally ice-covered surface (Lundesgaard et al., 2022). In the Barents Sea interior, the Atlantic Waters and the Arctic Waters spread and interact. Subsequently, this can lead to the formation of new water masses or water mass transformations (Schauer et al., 2002). To be able to understand the interactions of water masses, as well as the dominant flow regimes in the Barents Sea, we must trace the Arctic and Atlantic Water upstreams.

Once formed back in the Atlantic Ocean, the Atlantic Water (AW) enters the Nordic Seas with the North Atlantic Current (Holliday et al., 2015; Beszczynska-Möller et al., 2011). Some of this AW continues northwards with the Norwe-

gian Atlantic Current (NwAC), mainly steered along the Norwegian continental slope (Beszczynska-Möller et al., 2011). When the NwAC reaches the shelf area southwest of the Barents Sea (at around 72°N), the current splits into two distinct branches (Loeng, 1991; Kolås et al., 2023). One branch brings AW into the Barents Sea through a shallow passage called the "Barents Sea opening" (BSO)(Schauer et al., 2002; Ingvaldsen et al., 2002). The mean temperature and salinity of the AW entering the BSO are found by Aagaard and Woodgate (2001) to be around 4.5°C and 35.1, respectively. The inflow through the BSO is the primary source of warm AW into the Barents Sea, consequently transporting a great amount of heat into the ocean interior (Orvik and Skagseth, 2005).

The complex bathymetry of the Barents Sea interior can impact the circulation within the ocean, for instance, through topographical steering (Kolås et al., 2023). Like so, the Atlantic-origin waters that enter the Barents Sea in the south mainly follow the ocean bathymetry through the Bear Island Through (Loeng, 1991), before bifurcating close to the Central Bank. One branch continues its flow northward along the Hopen Trench. The other branch continues eastward in the southern Barents Sea. This latter branch of AW mainly flows in the upper part of the ocean, with an overall northwards movement Ivanov et al. (2012). Due to the AW being exposed to the atmosphere for large parts of its transit, it gets heavily modified by atmospheric cooling (Lien and Trofimov, 2013), losing as much as $38 \cdot 10^{12}$ W to the atmosphere above (Aagaard and Woodgate, 2001). This supply of heat keeps the southern Barents Sea ice-free for large parts of the year. On its throughflow northwards, the AW is believed to submerge under colder Arctic Waters (Kolås et al., 2023). Ultimately, the water exits the Northern Barents Sea through the St. Anna Trough, continuing into the Arctic Ocean (Schauer et al., 2002; Lien and Trofimov, 2013).

Cold and fresh "Arctic" water enters the Barents Sea in the north (Loeng, 1991). This water forms in the Arctic Ocean through interactions with sea ice, meltwater, and atmospheric cooling (Timmermans and Marshall, 2020). Where the Arctic waters from the north meet the Atlantic waters in the south of the Barents Sea, an oceanographic front is created – known as the Polar Front (PF) (Loeng, 1991). The characteristics of the PF include a steep gradient in temperature and salinity values for the interface between the cold, fresh water and the warm, salty water. In the west-central part of the Barents Sea, the placement of the PF is found to be rather stationary around the 200-250 m isobath in the Hopen Deep (Lien (ed), 2018; Kolås et al., 2023). During the summer season, the front should be prominent from around 50 m depth and downwards (Lien (ed) (2018)). The seasonal and interannual variations in the PF characteristics are known to be minor (Lien (ed), 2018). The PF area is an important site for biological activity, with high primary production and also being a central feeding and nursery/spawning ground for a variety of species (Olsen and von

Quillfeldt, 2003). Thus, this makes the PF an important physical feature that piques the interest of many scientific communities.

Returning to the other branch of the NwAC, which continues its journey northwards west of Svalbard. This branch of Atlantic-origin water flows through the eastern part of the Fram Strait with the West Spitsbergen Current (WSC) (Beszczynska-Möller et al., 2012). North-west of Spitsbergen the WSC splits into three branches carrying Atlantic-origin waters (Koenig et al.). While one branch returns southwards, recirculating back into the Fram Strait, both the Yermak Plateau branch and the Svalbard branch cross the Yermak Plateau with an overall eastward flow. Ultimately, these two branches converge, providing AW to the Atlantic Water Boundary Current (AWBC). The AWBC is topographically steered along the upper continental slope north of Svalbard towards the Siberian Seas, from where it circulates through the main basins of the Arctic Ocean (Woodgate et al., 2001). North of Svalbard, the AWBC descends to intermediate depths (Ivanov et al., 2012) and is capped by a layer of colder and fresher water in the surface (Environmental Working Group, 1997; Meyer et al., 2017). The submerged AW is therefore separated from the ocean-air interface, losing less heat to the atmosphere than the AW in the southern Barents Sea and retaining much of its original heat (and salt) content (Aagaard and Woodgate, 2001; Ivanov et al., 2012). Hence, this branch is considered a more significant heat contributor to the Arctic compared to the temperature-modified Barents Sea AW (Gammelsrød et al., 2009).

In terms of flow characteristics, the AWBC is found to be mainly baroclinic on the stretch between Svalbard and Franz Josefs Land (Pnyushkov et al., 2015). It has a seasonal cycle, where the strongest inflow occurs in late autumn/winter, with a inflow minima in summer (Renner et al., 2018; Fer et al., 2023). The warmest temperature recorded for the current appears in autumn and early winter, and this is also when the largest episodes of vertical heat fluxes are measured for the AWBC (Renner et al., 2018).

The vertical heat flux can result in heat transferred from the submerged AWBC up to the surface, which then has the potential to melt sea ice above or restrict sea ice from forming (Renner et al., 2018; Ivanov et al., 2012). Other times, the AWBC is found close to or at the surface Meyer et al. (2017). In both cases, the AWBC presence is evident in the sea ice extent north and northwest of Svalbard, which is both less and thinner than the surrounding area (Ivanov et al., 2012). In the later years, the sea ice coverage above and around the AWBC positioning has been reported to have high seasonal and interannual variability (Lundesgaard et al., 2021).

The seasonal variation in heat fluxes of the AWBC can be caused by variations of sea ice presence, sea ice meltwater input, wind, and changes in solar radiation

(Renner et al., 2018). It has been hypothesized that input of meltwater from sea ice drift can cap off the layer above the AWBC, increasing the stratification in the upper water column. If the stratification of the surface is sufficient, the vertical heat flux between the AW layer and the surface can be reduced. Thus, the AW heat will not reach the surface, and conditions can be more favorable for sea ice cover in the area (Meyer et al., 2017).

According to findings by Lind and Ingvaldsen (2012); Lundesgaard et al. (2022), branches of the Atlantic-origin waters from the AWBC enter the northern Barents Sea between Svalbard and Franz Josef Land. Here it flows along the deeper trenches connecting the Arctic Ocean to the northern Barents Sea interior. Lundesgaard et al. (2022) has reported a seasonality in this inflow, with larger transport during the autumn and early winter. The seasonally varying inflow was found to be the main driver of ocean temperature variability in the lower and intermediate water column in parts of the northern Barents Sea.

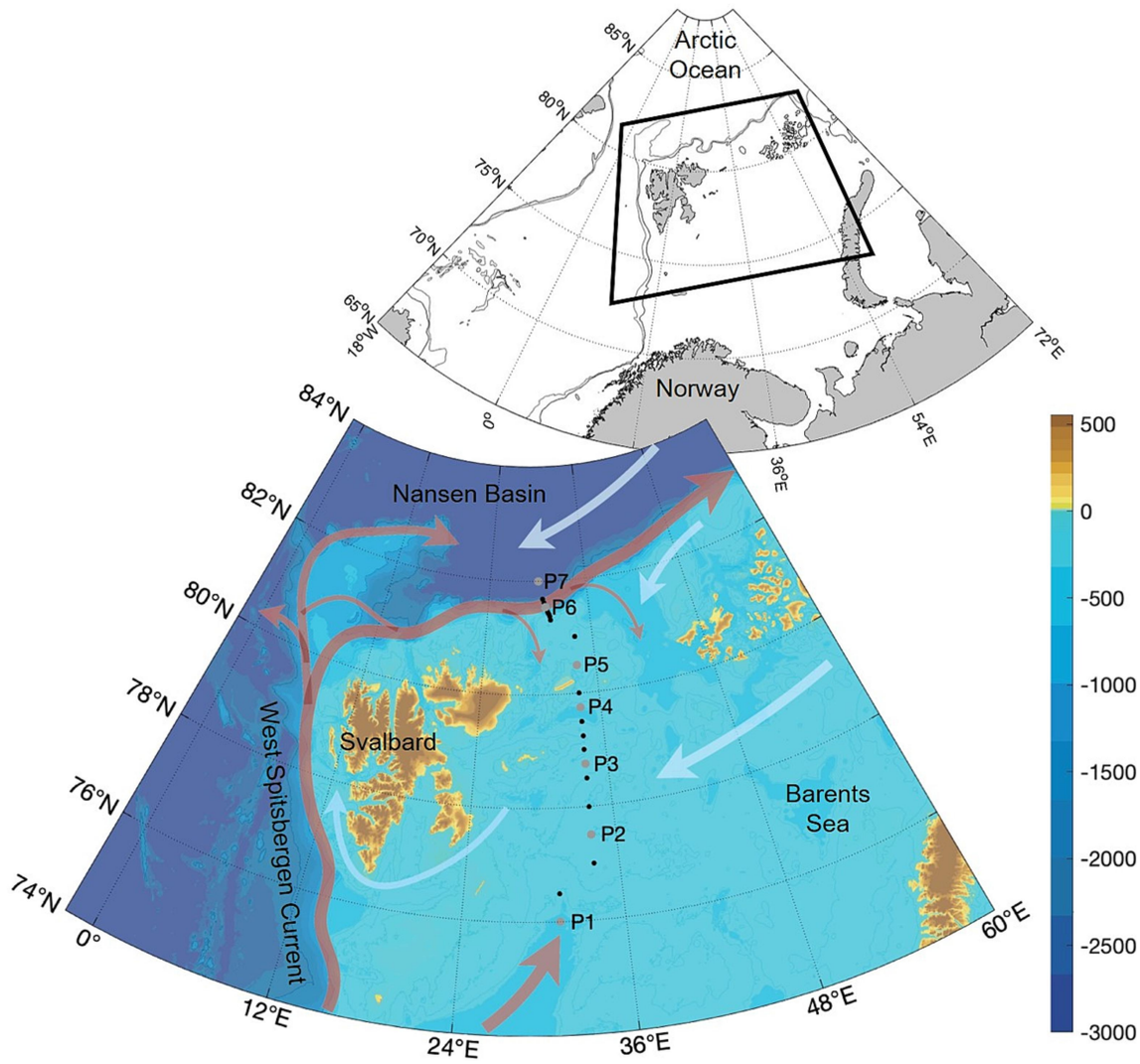

Figure 2.1: Map of the Barents Sea, with arrows indicating some of the main current systems in and around the Barents Sea area. Red arrows display the pathway of warm and saline currents of Atlantic origin, while the white arrows indicate colder Arctic Waters and the import of sea ice from the north. The black and grey dots depict the hydrographic stations that make up the Nansen Legacy transect, which is the focus area of this thesis. Source of map: Jones et al. (2023)

2.2 Air-ice-sea interactions

Not only can water masses form and transform due to mixing in between themselves, but the atmosphere and sea ice also play a major role in modifying water

mass properties (Thomas and Dieckmann, 2010). It often involves complex interactions between the atmosphere, ice, and ocean; among the transfer of heat and/or salt. In this section, we will give a brief introduction to some of the fundamental high-latitude physical processes that take place in the air-ice-sea interface by outlining a typical seasonal cycle in this part of the Arctic.

As autumn brings reduced solar heat, and cooler air temperatures, a heat transfer is set up from the ocean to the atmosphere above. Subsequently, the water at the ocean surface loses heat, resulting in lower water temperatures and increased water density. If this water becomes denser than the water beneath it, the gravitational pull will make the water sink downwards. This vertical movement of water, - known as thermal convection, will proceed until the water reaches a layer with the same density as its own.

If the water cools down to its freezing point, sea ice can form on the ocean surface. However, the freezing point of seawater is not a set value, but rather a function of the the water's salinity. For oceanic water in the Arctic region, the freezing point hovers around -1.8 to −2.0°C (Timmermans and Marshall, 2020). During the freezing process, the seawater expels most of its salt into the underlying water (Aagaard and Woodgate, 2001). The result is a cold, highly saline solution commonly known as "brine". Being both cold and salty, the brine solution is usually denser than the surrounding water, causing the water to sink. This vertical motion, driven by differences in water salinity, is known as haline convection. Again, the water will sink to where it encounters water with the same density.

Under the right circumstances, sea ice can form as early as in autumn in the Barents Sea. Sea ice formation usually starts off in the northern parts of the Barents Sea and then advances further south with time. However, the sea ice in the Barents Sea is not just restricted to the locally produced ice: a substantial amount is often advected in from other sea-ice-producing areas, such as the Kara Sea or the Arctic Ocean shelf, transported by wind and currents (Smedsrud et al., 2013; Lundesgaard et al., 2022). During the winter months, the Barents Sea typically experiences the maximum extent of sea ice, often with a peak by March/April (Smedsrud et al., 2013). The sea ice can reduce the heat transfer between the ocean and the atmosphere, especially if it is covered with a layer of snow. Additionally, the ice can act as a modifier for momentum transfer (Martin et al., 2014).

When solar radiation returns during springtime, in line with increased air temperatures, the sea ice starts to break up and melt. The increased heat input in springtime goes firstly into melting the ice, before it can warm up the ocean surface layer (Ivanov et al., 2012) The ice retreats towards the north, and open water areas start to appear along the southern and western coastlines. The

input of freshwater from the melting sea ice is the main source of freshwater input to the Barents Sea and the Arctic Ocean and contributes to increased stratification of the upper ocean. By July, large parts of the ocean is usually sea-ice-free. With a fresher surface layer, that receives (radiative and sensible) heat input throughout the summer, a more stratified ocean with a low-density surface layer is common for the summer months. As temperatures start to cool off again during autumn, the cycle repeats itself.

Both thermal and haline convection play a crucial role in shaping the mixed layer within the ocean. The mixed layer depth (MLD) is defined as the depth in the upper ocean of which physical properties such as temperature, salinity, and density are relatively well mixed or homogenized. The MLD in the Arctic varies strongly through the seasonal cycle, with deeper MLD during winter (approx. 25m to 50m) compared to summer (approx.5 m to 30 m) (Peralta-Ferriz and Woodgate, 2015). Other processes that can impact the MLD depth involve physical stirring from wind, waves, or tides.

2.3 The Nansen Legacy main transect

The focus area for this thesis is the Nansen Legacy main transect, which was officially established in 2018 with the start-up of the NL project. It is a north-to-south transect that stretches from 76°N in the central Barents Sea up to 82°N in the adjacent Arctic Ocean, with a lateral extension between 30-34°E (see Fig.2.2.). The transect includes 25 hydrographic stations, whereas 7 of these stations are defined as “Process study stations” (P1 to P7, presented in the next section).

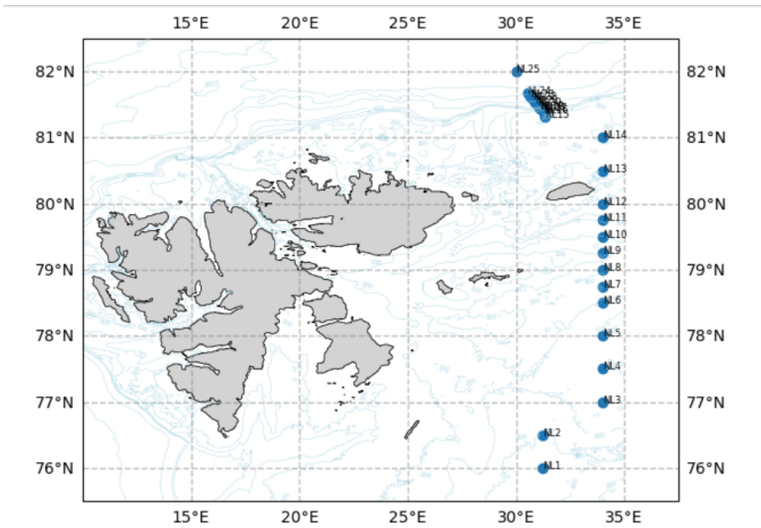

Figure 2.2: Map of the NL main transect, with the positions and numbers of the stations marked by the blue dots on the map. The stations are subscripted as NL1 to NL25.

Stations NL1 to NL14 lie in the central and north-western Barents Sea, where most of them are aligned along the 34 °E meridian. Situated in the relatively shallow Barents Sea, the stations' depths range between 150-330 m. Further north, stations NL15 to NL24 cover the Svalbard continental shelf; an area that borders the Nansen Basin of the Arctic Ocean. On the shelf, the depths increase rapidly, ranging from 190m down to 2800m. Consequently, the stations here are spaced closely to capture potential changes in flow regimes and water properties along the shelf break. Station NL25 is the northernmost station and also the deepest one. Situated well into the Nansen Basin, NL25 represents the deep Arctic Ocean with its 3000 m. Further details regarding station coordinates, station depths, and geographical location/area for all defined NL stations can be found in Table 7.1. in 7.1.

The transect represents a climatic gradient across the Central Barents Sea up towards the Arctic Ocean (Jones et al., 2023); encompassing both Atlantic and Arctic conditions. The transect is situated in the marginal ice zone (MIZ), and thus the the sea ice cover is expected to vary along the gradient and throughout the year. The different physical environments along the transect will again shape and impact the biological communities and ecosystems, as well as the chemical compositions and processes. This is illustrated in a conceptual map of Figure 2.3.

Another conceptual idea behind the NL transect establishment is a so-called

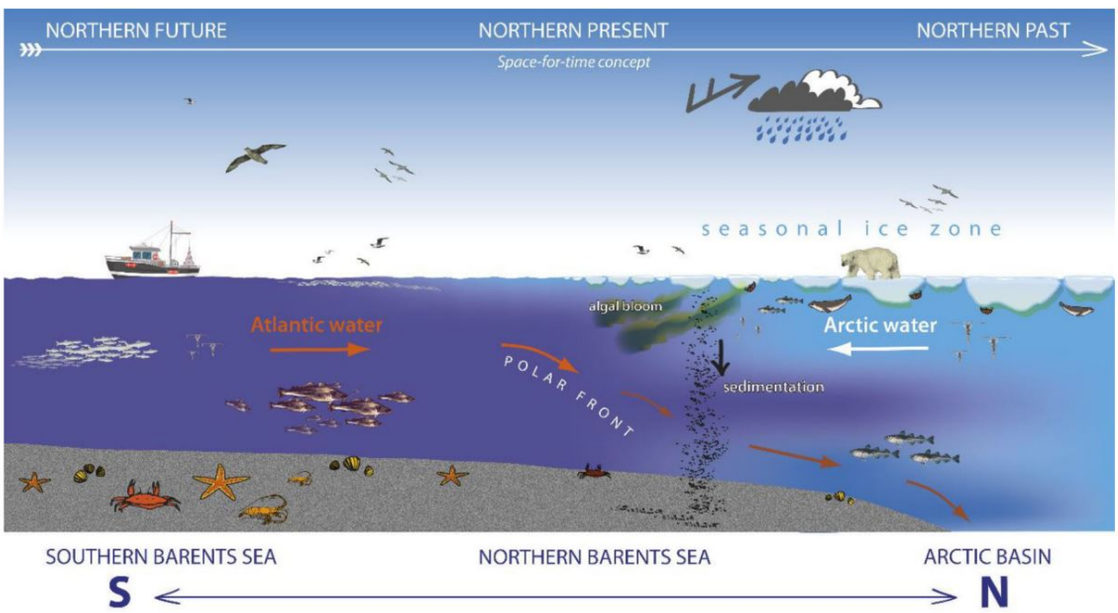

Figure 2.3: Conceptual map of the NL transect illustrating different physical and biological environments along the north-to-south gradient. Source: Gerland et al. (2023).

"space-for-time" investigation (Jones et al., 2023). By examining the areas that nowadays are Atlantic water-dominated, we can learn how the northern Barents Sea may develop in the future, with the expected retreat of sea ice and a stronger Atlantic signal. Additionally, investigations of areas that are Arctic-dominated may give us knowledge about past conditions, with a stronger presence of sea ice and colder waters.

Process study stations (P-stations)

The seven "Process study stations" or "P-stations" are, as the name suggests, a selection of the 25 NL stations designated to study different physical, biological, and/or geological processes. The positions of the seven process stations along the transect can be seen in Fig. 2.4.

P1 (also named NL1), is situated in the central Barents Sea and is the southernmost station of the transect. Situated in the Hopen Trench with a station mean depth of 322 m, P1 represents the Atlantic domain of the Barents Sea.

P2 (NL4), P3 (NL7), P4 (NL11), and P5 (NL13) are situated in the Central and Northern Barents Sea, within the Arctic domain. This should be reflected in

the hydrographic properties of the stations, which are expected to be of Arctic characteristics. For the lower water column of P3 and P4, separate inflowing branches of Atlantic-origin water can be present. At P4 the Atlantic-origin branch comes from the north, as described by Lundesgaard et al. (2022). Whilst at P3 the branch is a continuation of the northward flowing Atlantic-carrying branch along the Hopen Trench from the south (Kolås et al., 2023).

P6 (NL21) is situated at the end of the Svalbard continental shelf with a mean depth of 865 m. Here, the shelf is sloping steeply down towards the deeper Arctic Ocean. At intermediate depth, the core of the Atlantic Water Boundary current should be a prominent feature.

P7 (NL25) is the northernmost station of the transect, located in the Nansen Basin of the Arctic Ocean. With a mean depth of 3000 m, it is a deep water station ideal for comparing water from the Arctic Ocean with the shallower Barents Sea stations.

Unless specified otherwise, the information regarding the Process study stations has been sourced from The Nansen Legacy (2022).

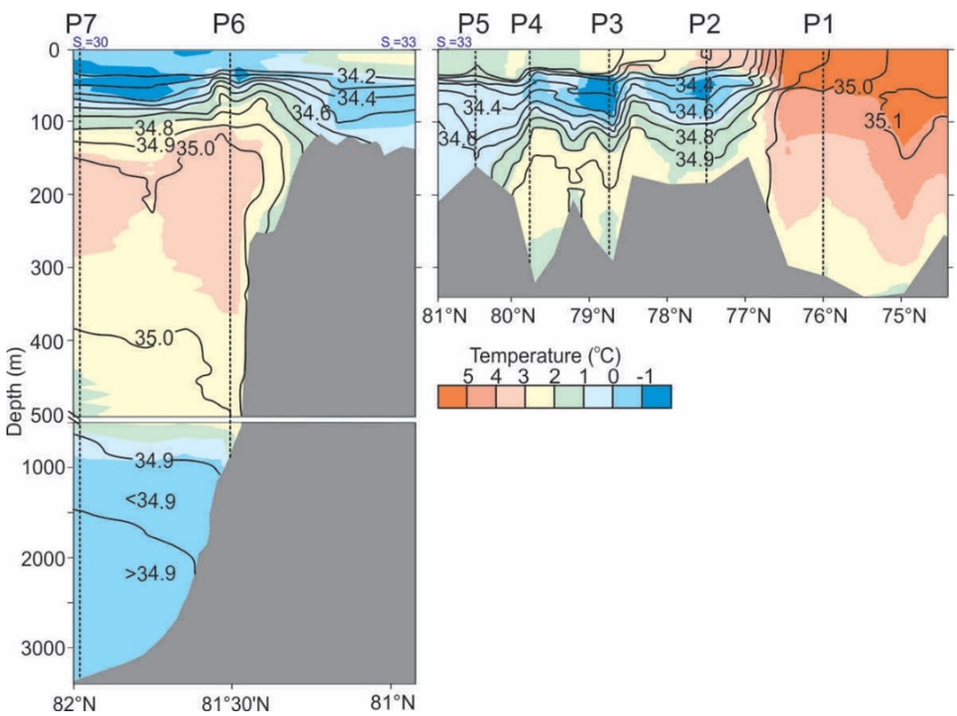

Figure 2.4: Transect plot of temperature (colored fields) and salinity (black isolines) for the NL transect, where the position of the seven P-stations are indicated with black, dashed lines. The plot displays measurements conducted on the transect in August 2012. Note the different scales in both depth and latitude for the panels. Source of figure: (The Nansen Legacy, 2022) Sampling Protocols: Version 10. The Nansen Legacy Report Series 32/2022. DOI: `https://doi.org/10.7557/nlrs.6684`

3

Data and Methods

3.1 Hydrographic data

The foundation of this thesis are the hydrographic measurements of water column temperature and salinity collected through various cruises to the Barents Sea that were conducted as part of the NL project between 2018 and 2022. A significant effort of this thesis went into the identification of NL cruises that did measurements on one or several of the standard stations on the NL transect, and the extraction and classification of these data points. This narrowed down the number of relevant cruises to 11, shown in Table 3.1.

The selection includes four Joint Cruises (JC1-2, JC2-1, JC2-2, JC3), four Seasonal Study Cruises (SSQ3, SSQ4, SSQ1, SSQ1), two service cruises to the moorings on the Svalbard continental shelf and in the Barents Sea (MSC19, MSC20) and a paleooceanographic survey (Paleo). Most of these surveys were conducted during the separate years of 2019 and 2021, as the research activity planned in 2020 was largely put on hold due to the COVID-19 pandemic.

The hydrographic resolution along the NL transect varies considerably from cruise to cruise. This impacts how much information we can obtain regarding the hydrographic environment on the transect. The varying spatial coverage was due to various factors, such as the study focus for each survey, ship time, sea ice conditions, etc. An overview of the NL station coverage for each cruise in our database can be seen in Fig.3.1.

Cruise Name	Abbreviation	Year	Dates	Research Vessel
Joint Cruise 1-2	JC1-2	2018	08.08 - 20.08	Kronprins Haakon
Paleo Cruise	Paleo	2018	27.09 - 17.10	Kronprins Haakon
Seasonal Study Q3	SSQ3	2019	05.08 - 25.08	Kronprins Haakon
A-Twain	MSC19	2019	12.11 - 26.11	Kronprins Haakon
Seasonal Study Q4	SSQ4	2019	28.11 - 14.12	Kronprins Haakon
Mooring Service Cruise	MSC20	2020	06.10 - 26.10	G.O.Sars
Seasonal Study Q1	SSQ1	2021	04.03 - 18.03	Kronprins Haakon
Seasonal Study Q2	SSQ2	2021	29.04 - 18.05	Kronprins Haakon
Joint Cruise 2-1	JC2-1	2021	20.07 - 25.07	Kronprins Haakon
Joint Cruise 2-2	JC2-2	2021	26.08 - 22.09	Kronprins Haakon
Joint Cruise 3	JC3	2022	22.02 - 10.03	Kronprins Haakon

Table 3.1: Overview of the NL cruise surveys providing the hydrographic data for this thesis. The table includes the cruise name, cruise abbreviation, year, dates, and research vessel for each respective survey.

The selection of data points for each NL station was primarily based on how well the coordinates of the cruise measurements matched the coordinates of the defined NL stations. The table shows that the cruises with the highest number of NL stations covering the transect were the Q-cruises (Q1, Q2, Q3 and Q4) and two of the J-cruises (JC2-1 and JC3). In addition, the MSC19 cruise covered several of the NL stations of the shelf north of Svalbard.

		Lon	Lat	JC1-2	Paleo	SSQ3	MSC19	SSQ4	MSC20	SSQ1	SSQ2	JC2-1	JC2-2	JC3
NL1	P1	31,2200	76,0000	yes	no	yes	no	yes	yes	yes	yes	yes	yes	yes
NL2		31,2200	76,5000	no	no	no	no	yes	no	yes	yes	yes	no	no
NL3		34,0000	77,0000	no	no	no	no	yes	no	yes	yes	yes	no	no
NL4	P2	34,0000	77,5000	yes	no	yes	no	yes	yes	yes	yes	yes	no	no
NL5		34,0000	78,0000	no	no	yes	no	yes	no	yes	yes	yes	no	no
NL6		34,0000	78,5000	no	no	yes	no	no	no	yes	yes	yes	no	no
NL7	P3	34,0000	78,7500	yes	yes	yes	no	yes	no	yes	yes	yes	no	no
NL8		34,0000	79,0000	no	no	yes	no	no	no	yes	yes	yes	no	no
NL9		34,0000	79,2500	no	no	yes	no	yes	no	yes	yes	yes	no	no
NL10		34,0000	79,5000	no	no	yes	no	no	no	yes	yes	yes	no	no
NL11	P4	34,0000	79,7500	yes	yes	yes	no	yes	no	yes	yes	yes	no	no
NL12		34,0000	80,0000	no	no	yes	yes	yes	no	yes	yes	yes	no	no
NL13	P5	34,0000	80,5000	yes	no	yes	no	yes	no	yes	yes	yes	no	yes
NL14		34,0000	81,0000	no	no	yes	no	yes	no	yes	yes	yes	no	yes
NL15		31,3487	81,3098	no	no	yes	yes	yes	no	yes	yes	yes	no	yes
NL16		31,2933	81,3822	no	no	yes	yes	no	no	yes	yes	yes	no	yes
NL17		31,2468	81,4107	no	no	yes	yes	no	no	yes	yes	yes	no	yes
NL18		31,1448	81,4318	no	no	yes	yes	yes	no	yes	yes	yes	no	yes
NL19		31,0775	81,4580	no	no	yes	yes	no	no	yes	yes	yes	yes	yes
NL20		30,9618	81,5025	no	no	yes	yes	yes	no	yes	yes	yes	no	yes
NL21	P6	30,8548	81,5463	no	yes	yes	yes	yes	no	yes	yes	yes	no	yes
NL22		30,7667	81,5895	no	no	yes	yes	no	no	yes	yes	yes	no	yes
NL23		30,6647	81,6165	no	no	yes	yes	yes	no	yes	yes	yes	no	yes
NL24		30,5258	81,6828	no	no	yes	yes	yes	no	yes	yes	yes	no	yes
NL25	P7	30,0000	82,0000	no	yes	yes	no	no	no	yes	yes	yes	no	yes

Figure 3.1: Overview of the NL stations covered for each cruise. The positions of the different NL stations are given in nominal latitude and longitude, with units in decimal degrees E and N, respectively. The blue shading of the NL stations identifies which stations are placed on the continental shelf north of Svalbard.

3.1.1 Instruments and Processing

The hydrographic data was collected with a Conductivity-Temperature-Depth (CTD) sensor of type Sea-Bird SBE911+. The instrument was mounted on a General Oceanics rosette and lowered into the water either over the side (cruise MSC20) or through a so-called "moonpool" in the ship's hangar (most of the cruises onboard R/V Kronprins Haakon). Data were collected and pre-processed using SBE software.

Water that was sampled at the very bottom of each CTD cast, was analyzed in the lab at IMR Bergen after the cruises using a Guideline salinometer and IAPSO standard seawater to calibrate the CTD's conductivity sensor. The cruise files generated through the NL project are open-access data and can be downloaded at the Norwegian Marine Data Centre's website (`https://www.nmdc.no/`) in

NetCDF format.

The deployment of CTD through a moonpool can cause disturbances in the upper water column. For this reason, we have removed the upper 15 m of data from the measured profiles during post-processing. We have also removed salinity values fresher than 25 g kg^{-1}, as values below this threshold are assumed to be unrealistic for oceanic waters below 15 m depth in the study region. Further post-processing of the CTD data involved converting the seawater properties of practical salinity, in situ or potential temperature, and density into absolute salinity (SA), conservative temperature (CT), and potential density (σ_0). The data was converted according to the TEOS-10 standard for oceanography (`https://www.teos-10.org/`), using the Gibbs Seawater toolbox package for Python by McDougall and Barker (2011).

3.2 Ocean Current Data

Acoustic Doppler Current Profilers (ADCPs) are hydroacoustic instruments used to measure ocean current velocities. The instruments utilize the principle of the Doppler shift effect to determine the speed and direction of the water flow. It operates by emitting sound waves into the water column and then measures the frequency shift (Doppler shift) of the reflected waves.

Different types of ADCP instruments are available depending on the desired depth range and resolution of the measurements. In this thesis, we look at data from two different velocity measurements: S-ADCP and L-ADCP data. S-ADCP stands for "shipboard" ADCP. As the name implies, these instruments are mounted on the ship and can record profiles of current velocities continuously while the vessel is moving over the water column. L-ADCP on the other hand, refers to "lowered" ADCP. These instruments are typically mounted on the CTD frame and lowered through the water column. The measurements are recorded during the CTD deployment and therefore only provide measurements at CTD stations compared to the continuous along-track S-ADCP data. In exchange, the L-ADCP instrument can record data for the entire water column. By comparing the L-ADCP data against the S-ADCP data, it can hopefully give us a more complete picture of the ocean currents on the transect. An overview of the S-ADCP and L-ADCP data availability for the NL transect during the study period can be found in Table 3.2.

Cruise Abbr.	S-ADCP	L-ADCP	Comment
JC1-2	✓	x	
Paleo	x	x	
SSQ3	✓	✓	
MSC19	x	✓	L-ADCP not processed
SSQ4	✓	✓	
MSC20	x	x	
SSQ1	✓	✓	
SSQ2	✓	✓	
JC2-1	✓	✓	
JC2-2	✓	✓	
JC3	✓	✓	S-ADCP not processed

Table 3.2: Data availability of S-ADCP and L-ADCP measurements for each of the NL cruises in our database.

3.2.1 S-ADCP

The S-ADCP data was measured onboard R/V Kronprins Haakon with a 150 kHz ADCP RDI Ocean Surveyor ADCP mounted on the drop keel (in open water) or in the hull of the vessel (when moving through sea ice). The raw data was processed by H. Cannaby at IMR, using the CODAS software developed at the University of Hawaii (`https://currents.soest.hawaii.edu/docs/adcp_doc/index.html`). The S-ADCP files are open-source data and can be found on the webpage of the Norwegian Marine Data Centre (`http://metadata.nmdc.no/metadata-api/landingpage/3e03daeeb8c946786104b01099db5a34`). The exception is the S-ADCP data for the JC3 cruise, processed by A. Renner at IMR for this thesis (unpublished data).

The S-ADCP data was provided in NetCDF file format and further handled in MATLAB. The files contained measurements as 5 minute averages in 5 m depth bins, with current velocities recorded down to approximately 350m depth. We removed the tidal current signal from the data using the (barotropic) 5-kilometer Arctic Ocean Tidal Inverse Model (AOTIM-5) (`https://arcticdata.io/catalog/view/doi%3A10.18739%2FA2S17SS80#urn%3Auuid%3A5c25d8a2-7e5e-4dfc-98c6-b27d2016f3e4`), including the Tide Model Driver (TMD) version 2.5, Toolbox for MATLAB. Removing the tidal component from the velocity measurements reveals the non-tidal elements of the currents. Further data handling involved restricting the data points to the approximate area of the NL transect.

3.2.2 L-ADCP

The L-ADCP data was collected using two RDI 300 kHz Workhorse ADCPs equipped with an external battery pack, mounted on the CTD frame, and lowered during the CTD casts. One of the two instruments functioned as an uplooker, the other as a downlooker.

The L-ADCP data was provided as raw files and thus needed some extensive processing before the data could be further handled. The first step of the L-ADCP processing involved removing the effects of horizontal instrument motion from the velocity measurements. To achieve this, we applied a method called the "Velocity inversion method", first described by Visbeck (2002). The specific software we utilized was the "LDEO IX Version 14", which can be downloaded from the LDEO server (`https://www.ldeo.columbia.edu/cgi-bin/ladcp-cgi-bin/hgweb.cgi`).

The magnetic declination value, a correcting factor for the angle offset between the geographic north and the magnetic north, was calculated for each cruise data and implemented into the processing script(s). Two models were used for the calculations; the Enhanced Magnetic Model (1900-2019) for the cruises conducted in 2018 and in the early 2019, and the World Magnetic Model (2019-2024) for the later cruises. More information regarding the models can be found at the NOAA webpage (`https://www.ngdc.noaa.gov/geomag/calculators/magcalc.shtml`). As the value of the magnetic declination changes according to the geographical position, it may differ across the NL transect. To simplify the process, we used the mean of the calculated values for three process stations (P1, P3 and P7) as the representative value for all stations. The values utilized for each cruise can be found in Table 3.3.

Cruise Abbr.	Magnetic Declination value	Model
SSQ3	22	EMM
SSQ4	23	EMM
SSQ1	22	WMM
SSQ2	23	WMM
JC2-1	23	WMM
JC2-2	missing	WMM
JC3	24	WMM

Table 3.3: Table with magnetic declination values used for processing L-ADCP raw data. "EMM" refers to the Enhanced Magnetic Model, while "WMM" refers to the World Magnetic Model used to calculate the values.

The processing scripts were run with CTD time-series (i.e., averaged to 1 s

instead of 1 m) files including GPS track data, as well as S-ADCP files (the same files as mentioned in the previous section). These files work as constraints for the L-ADCP data, with aim of improving the quality of the processing output. L-ADCP raw data are a complex data source, known to contain noise, outliers, or simply bad data. Running the raw files through the processing scripts should, however, account for, and filter out, the worst data. We also performed a rough visual check of the output L-ADCP profiles for quality control.

We did receive a variety of error warnings during processing, some of which could not be resolved. The most common warning was in regards to "Large compass deviation". While this warning is something that could be worth looking into for future work, we assume that the current direction should be somewhat reliable due to it having been constrained by S-ADCP data during the processing.

As with the S-ADCP data, the L-ADCP data was de-tided by subtracting the tidal signal (obtained from the AOTIM-5 model) from the measured current velocities. Further data handling involved removing the data points that did not coincide with the NL transect for each cruise file.

The L-ADCP raw files were provided by the Institute of Marine Research, and are not yet published.

3.3 Atmosphere and sea ice data

In this thesis, we use information about the atmospheric and Sea ice conditions during the study period to complement the analysis of the hydrographic conditions.

The atmospheric data was obtained from the reanalysis product ERA5, freely accessible via the Copernicus Climate Change Service (`https://cds.climate.copernicus.eu/cdsapp#!/dataset/reanalysis-era5-single-levels?tab=form`). The downloaded dataset includes the atmospheric parameters of air temperature (at 2m level), sea surface temperature (SST), u and v- components of wind speed (at 10m level), and atmospheric pressure at mean sea level (slp). We used the ERA5 hourly data on single levels product, and downloaded data points 2 times per day (for 00 and 12UTC; Hersbach et al., 2023).

Sea ice data is obtained from the EUMETSAT Ocean and Sea Ice product (OSI-SAF, `https://osi-saf.eumetsat.int/products/osi-401-d`), and involves daily means of sea ice concentration values. This data is based on remotely sensed observations from passive microwave and synthetic aperture radar on a 10km

grid resolution (EUMETSAT Ocean and Sea Ice Satellite Application Facility, 2023).

3.4 Water Mass Classification

In the field of oceanography, it is common practice to identify different bodies of water based on their physical or chemical properties. Such classifications typically include defined ranges of temperature, salinity, and/ or density, and are often set for a particular geographical area. In this thesis, we have used the water mass (WM) classifications by Sundfjord et al. (2020). They include eight different water masses, categorized in particular for the NL transect area of the Northern Barents Sea and the adjacent Arctic Ocean. The classification was developed to complement the research from the NL project by providing a common reference regarding water masses. The respective ranges of temperature, salinity, and/or density are presented in 3.2 in the TEOS-10 standard units of Conservative Temperature (CT), Absolute Salinity (SA), and Potential density σ_0. A brief description of the water mass characteristics and their origin is given below. If not stated otherwise, the information is based on the report by Sundfjord et al. (2020).

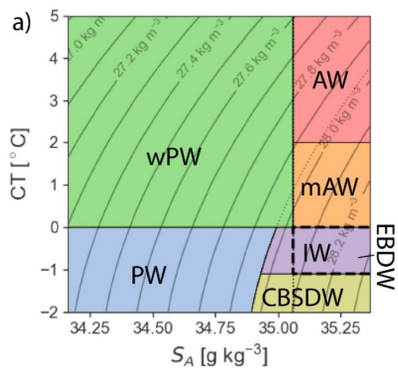

PW (Polar Water)	CT <= 0.0°C, σ_0 <= 27.97 kg m^{-3} (θ <= 0.0°C, σ_0 <= 27.97 kg m^{-3})
wPW (warm Polar Water)[1]	CT > 0.0°C, S_A < 35.06 g kg^{-1} (θ > 0.0°C, S < 34.9)
AW (Atlantic Water)	CT > 2.0°C, S_A >= 35.06 g kg^{-1} (θ > 2.0°C, S >= 34.9)
mAW (modified Atlantic Water)	0.0°C < CT <= 2.0°C, S_A >= 35.06 g kg^{-1} (0.0°C < θ <= 2.0°C, S >= 34.9)
IW (Intermediate Water)	-1.1°C < CT <= 0.0°C, σ_0 > 27.97 kg m^{-3} (-1.1°C < θ <= 0.0°C, σ_0 > 27.97 kg m^{-3})
CBSDW (Cold Barents Sea Dense Water)	CT <= -1.1°C, σ_0 > 27.97 kg m^{-3} (θ <= -1.1°C, σ_0 > 27.97 kg m^{-3})
EBDW (Eurasian Basin Deep Water) Note: to be used for data from North of the Barents Sea (e.g. > 500 m isobath)	-1.1°C < CT <= 0.0°C, SA > 35.06 g kg^{-1} (-1.1°C < θ <= 0.0°C, S > 34.9)

Figure 3.2: (a): CT-SA plot displaying the different ranges of conservative temperature, absolute salinity, and/or potential density used for water mass classification in this thesis. Left: Table presenting the same water masses, but with additional information regarding the parameters in the older oceanographic standards of salinity S, potential temperature θ, and potential density σ (EOS-80). Both figures are taken from Sundfjord et al. (2020).

As previously described in the introduction, Atlantic Water (AW) is a warm and saline water mass with origins in the Atlantic Ocean. AW has been defined by various ranges of temperature and salinity up through research history, but is classified by Sundfjord et al. (2020) as water with conservative temperatures above 2*C and absolute salinity from 35.06 g kg^{-1} or higher.

Modified Atlantic Water (mAW) stems from the warm AW, but has lost some of its initial heat. mAW typically retains much of the same salinity values as the AW, due to limited mixing with other water masses. In the report, mAW has been classified as water with conservative temperatures from 0* to 2*C, and with absolute salinity from 35.06 g kg^{-1} and higher. Together, mAW and AW make up what we refer to as Atlantic-origin or Atlantic-influenced water throughout this thesis.

On the other hand, the water mass of Polar Water (PW) is cold and relatively fresh. This WM is found in connection with cold melt water from sea ice. PW classifies as water below 0*C, and with potential density of 27.97 kg/m3 or below.

Warm Polar Water (wPW) is an offspring from the PW and can be formed in two ways; either from PW that has been heated up through solar radiation, or as a resulting mixture of PW and Atlantic-type of water (AW or mAW). wPW classifies as water above 0*C, and salinity values below 35.06 g kg^{-1}.

Further in the classification, we find two water masses that have somewhat overlapping water column properties; Eurasian Basin Deep Water (EBDW) and Intermediate Water (IW). Common for both of them, is that the water is cold and rather saline. To separate the two wm, we use the geographical location of the water. Eurasian Basin Deep Water, is as the name suggests, found in the Eurasian Basin of the Arctic Ocean. This WM resides in the deep water column below the 500m isobath on the Svalbard continental shelf and northward into the basin. The water has the same salinity limit as the Atlantic-type of water of 35.06 g kg^{-1} and higher, but with temperatures colder than mAW. The temperature range for EBDW is set from 0.0*C to -1.1*C.

Meanwhile, IW is geographically limited to the Barents Sea. It is also colder than mAW and shares the same temperature range as EBDW of 0.0*C to -1.1*C. However, the IW is classified based on density rather than salinity. The density limit restrain the wm to water of 27.97 or higher.

Lastly, we have Cold Barents Sea Deep Water (CBSDW). The water mass is geographically restricted to the Barents Sea Proper (an area which lies in the Northern/central Barents Sea). Here, it resides in the deep water due to its high density. The WM classifies as water below -1.1*C, and with the same density limit as IW of 27.97 or higher.

Water mass classifications, such as the one we are using from Sundfjord et al. (2020), are useful in the sense that they can tell us something about how and/or where the water was formed. However, we must make the reader aware that such classifications are merely a tool, and do not represent set boundaries in the

physical world. Furthermore, the ranges are not static and are in ever-change due to climate change, as well as due to seasonal and interannual variations of the water column properties.

3.5 Calculations

3.5.1 Fresh Water and Heat Content

For this thesis, we have calculated the relative Freshwater content (FWC) and the Heat content (HC) for the upper 15-100m of the water column. Similar calculations have previously been performed by Lind et al. (2018) and Koenig et al. (2023) for the corresponding area. However, they have both included the upper 15m of the water column in their calculations. Due to the differences in depth range, our calculations can not be directly compared in absolute values to their results. Furthermore, we have used conservative temperature and absolute salinity instead of in-situ temperature and practical salinity, and the HC is calculated relative to the freezing point temperature of -1.9° C instead of 0° C as done by Lind et al. (2018) and Koenig et al. (2023).

Fresh Water content

To investigate the distribution of freshwater input along the NL transect, the amount of freshwater [m] in the upper water column was calculated as follows:

$$FWC = \int_0^Z \frac{S_0 - S(z)}{S_0}\, dz \tag{3.1}$$

Here, S_0 is the reference salinity, set 35.06 $\mathrm{g\,kg^{-1}}$. This choice of reference is selected to give the amount of water fresher than the AW. Furthermore, $S(z)$ is the absolute salinity as a function of depth z, and Z the depth of the respective water column.

Heat Content

To get an estimate of the heat (Q $[J\,m^{-2}]$) stored in the upper water column along the transect, the following equation was used:

$$Q = c \cdot \rho_0 \cdot \int_0^Z (T(z) - T_f) dz \tag{3.2}$$

Here, c is the constant of specific heat capacity for seawater set to 3991.87 $J \cdot kg^{-1} \cdot K^{-1}$ (IOC et al., 2010). ρ is the reference density of seawater, with a value of 1027 $kg\,m^{-3}$ and T_f is the freezing point temperature of sea water of -1.9$^{\circ}C$. Choosing to calculate the ocean HC relative to the freezing temperature provides an estimate of the amount of heat potentially available to melt sea ice on the surface. Furthermore, $T(z)$ is the conservative temperature as a function of the depth z, and Z is the total depth of the water column.

4

Results

4.1 Atmospheric and Sea ice conditions

The following section presents the atmospheric and sea ice conditions for the NL transect during the study period. We have included the period from the 1st of January 2018, to get insights into the environmental settings leading up to the first cruise campaign in August 2018.

Figure 4.1 reveals the distinct seasonal pattern of warmer air temperatures during the summer season and colder air temperatures during the winter season for all latitudes. There is a latitudinal asymmetry, where there are generally warmer air temperatures in the southern part of the transect compared to the northern part. There is also an asymmetry along the time axis, displaying some interannual variability in the air temperature. An example of this (interannual) variation can be seen for the winter season of 2019/2020 with a longer, more extensive period of cold temperatures relative to the other years. In contrast, the subsequent summer of 2020 experienced a prolonged period of warm temperatures, in particular for the southern part of the transect.

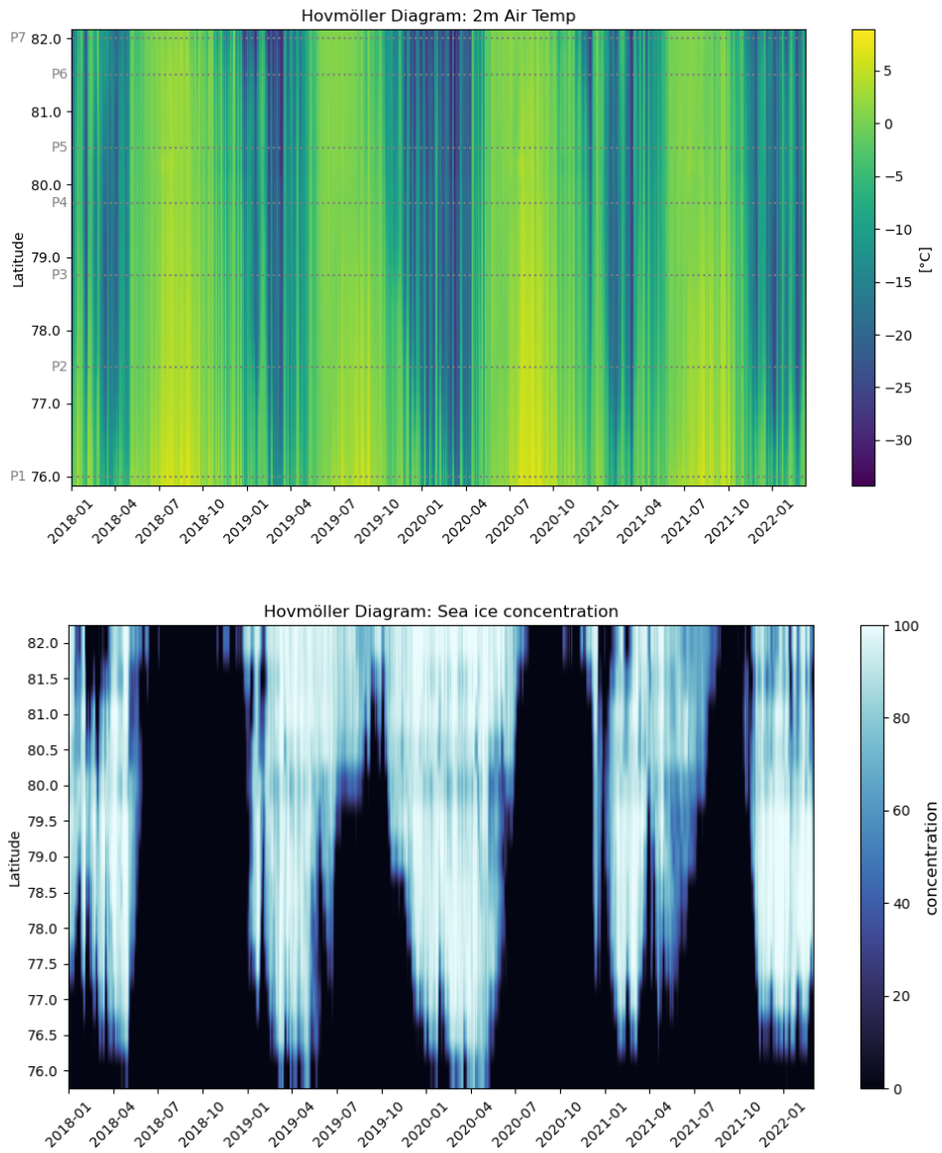

Figure 4.1: Upper panel: Hovmöller diagram of the ERA-5 12-hourly 2 m air temperature. The temperature is averaged over 30-34° E. The latitude of each process station (P1-P7) is indicated with grey dashed lines. Lower panel: Hovmöller diagram of the daily sea ice concentration (SIC) for the 34° E meridian. The concentration is given in percentage[%]

The seasonal cycle is also visible for the sea ice concentration (see Figure 4.1), displaying an overall picture of substantial coverage of the transect during winter and early spring, and less-to-no sea ice during summer and early autumn.

In general, sea ice covers the northern part of the transect first, albeit the onset of sea ice in the Northern Barents Sea (approx. south of 81° N) is seen to follow close after. Although the sea ice arrives first in the north, the northernmost part of the transect does not necessarily exhibit the most extensive sea ice coverage. This is especially evident for the winter of 2018, when the area north of 81° N experienced periods of open water, whilst the Northern and Central Barents Sea was sea-ice covered. The latest onset of sea ice is seen for the southern part of the transect, where the sea ice also retreats first. Besides a few occasions during the winter/spring season of 2018/2019 and again in 2019/2020, the sea ice typically does not reach south of ~ 76° N.

The timing of the sea ice onset varies from year to year. For the four winter seasons during the study period, the onset of sea ice for (large parts of) the NL transect occurs around December/January 2018/2019, October/November 2019, December 2020, and November/December 2021, respectively. The whole transect was ice-free during summer and autumn 2018, late summer/autumn 2020, and autumn 2021. However, the summer and autumn of 2019 stand out with barely any period of open waters north of ~ 81°N. This makes it into an almost continuous period of sea ice coverage between 2019 and mid-2020 for the northern part of the transect. Besides this latter event, both diagrams exploit a similar visual pattern, where periods of low air temperatures typically align with high ice concentrations.

In Figure 4.2 we have plotted the monthly average 2 m air temperature, sea surface temperature (SST), sea level pressure (SLP), and wind speed for the location of the seven process stations during the study period. Again, there is a clear seasonal cycle, with a distinct difference between summer and winter periods seen for both the 2 m air temperature and the SST. As depicted in the Hovmöller diagram, the figure displays a prolonged period of cold air temperatures during winter 2019/2020 for all latitudes. The figure also reveals that the winter of 2018/2019 was rather cold. In relative terms, the winters of 2018, 2021, and 2022 were warm.

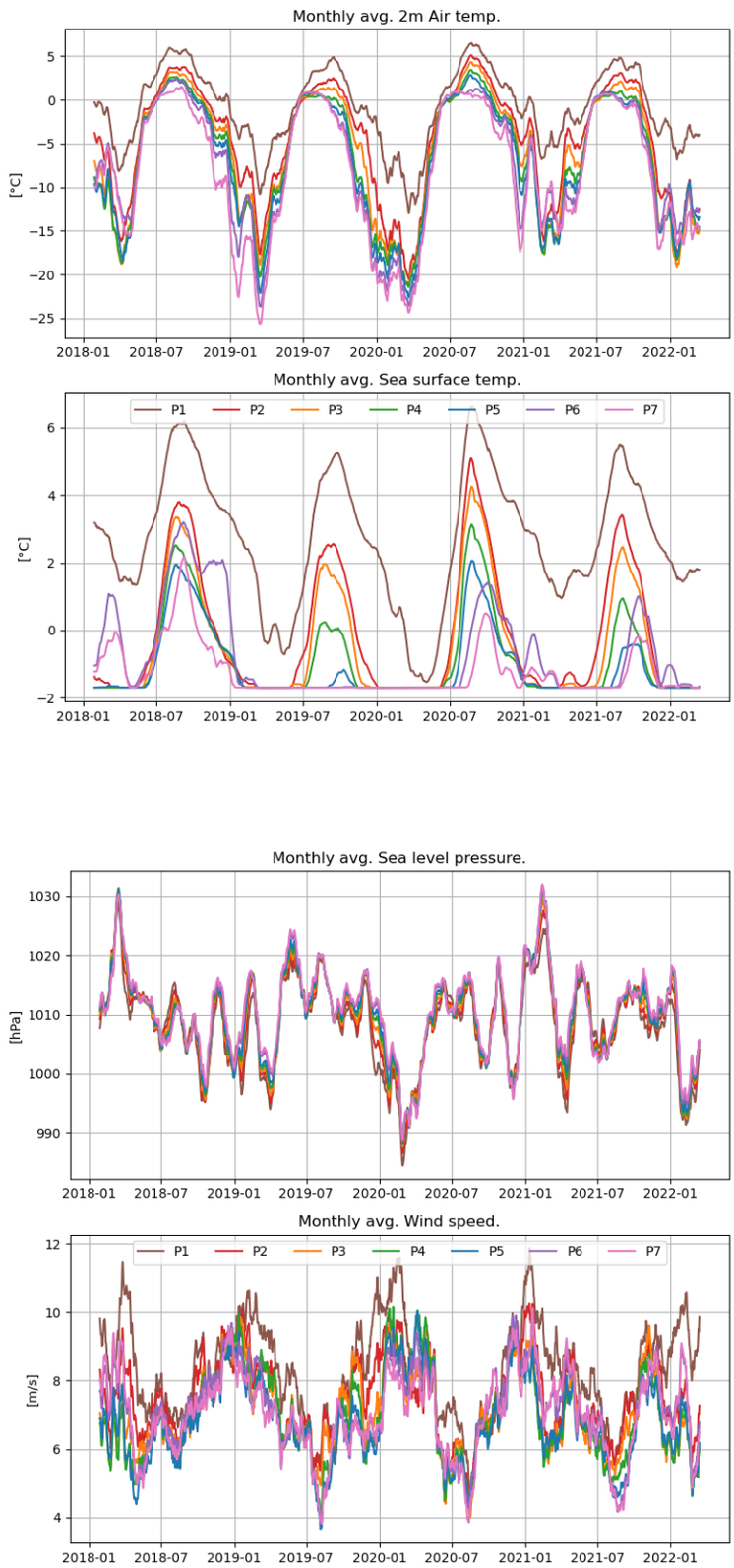

Figure 4.2: Top to bottom: Time series of monthly averaged 2 m air temperature, sea surface temperature, sea level pressure, and wind speed for the location of the seven process stations (P1 to P7).

Among the seven P-stations, P1 stands out with distinctly warmer atmospheric temperatures throughout. The coldest air temperatures were generally found at P7, although at certain periods during the winter/spring period of 2018, 2021, and 2022, the air temperature was colder in the Northern Barents Sea (at P5, P4, P3, and occasionally also at P2). The lowest air temperatures occurred during winter/spring 2019 and winter/spring 2020, with a temperature minimum at P7 down to -32°C and -35°C, respectively (raw data, not shown).

The interannual, seasonal, and lateral variations described for the atmospheric temperature are largely reflected in the trends for the SST. Additionally, the presence of sea ice at the water's surface is also evident in the SST values. Periods of high sea ice concentration seen in Fig.4.1 correspond to low values of SST, often down to freezing point temperature. Conversely, when the sea surface becomes ice-free during springtime, the SST starts to rise again. There was no seasonal rise in SST at P7 and P6 during the summer of 2019, and the temperatures hovered around freezing point. This corresponds to the prolonged period of sea ice cover for the two stations in the north, as previously described. The raw data (not shown) shows occurrences of SST reaching the freezing point temperature at P1 during winter/spring 2019 and winter/spring 2020. Again, this can be matched with the periods of ice cover down to P1 during these two years. For all the other P-stations, SST reaches down to the freezing point temperature during the winter or spring season.

Furthermore, Fig.4.2 reveals that the patterns of sea level pressure (SLP) (on a monthly scale) were similar across all stations, with rather small variations in pressure values. Visual analysis of the data does not reveal any discernible seasonality for the SLP. For the wind speed parameter, a seasonal cycle is more prominent. It appears to be an overall pattern of increased wind speeds during winter, and lower wind speeds during late summer. The wind speeds seem particularly high at P1 during late winter/spring, while the lowest wind speeds are generally found at P5 and P7 during the summer time wind speed minimum.

4.2 Hydrography

In this section, we present the hydrographic data in our dataset. Figure 4.3 shows all CTD profiles conducted at NL stations from the different cruises in CT-SA space. Initially, we can see that there is some variability between the cruises, indicating that the water properties do differ either in time or space. Overall, the CTD profiles display a triangular shape, with some points differing from this main triangle.

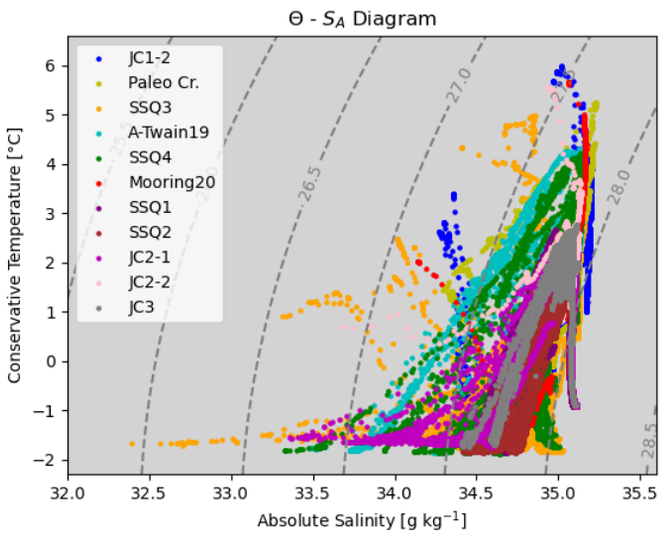

Figure 4.3: CT-SA diagram of all CTD data from stations on the NL transect from every cruise in our dataset. Dashed grey lines indicate isypycnals. NB. A-twain19 and Mooring20 corresponds to MSC19 and MSC20 cruise, respectively.

To unveil the variation in water mass properties throughout the study period, we have plotted transects of conservative temperature and absolute salinity along the NL transect for each cruise, in chronological order (see Fig.**??**). However, transect have not been made for the MSC20 in October 2020 and the JC2-2 cruise in July 2021 due to the low coverage of only 2 NL stations each. The transect plots are made using a spline-Laplacian interpolation method with 30km search radius and no smoothing (Pickart and Smethie Jr, 1998). (NB. The same temperature and salinity data are also presented as pcolor plots in Appendix 7.2, showcasing the data without (horizontal) interpolation. These plots may also give the reader a better visual impression of the varying number of conducted NL stations for each cruise.)

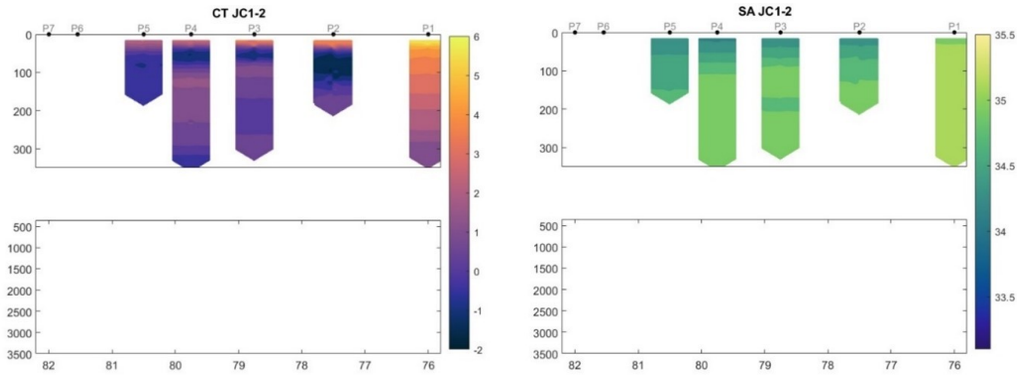

(a) JC1-2: August 2018

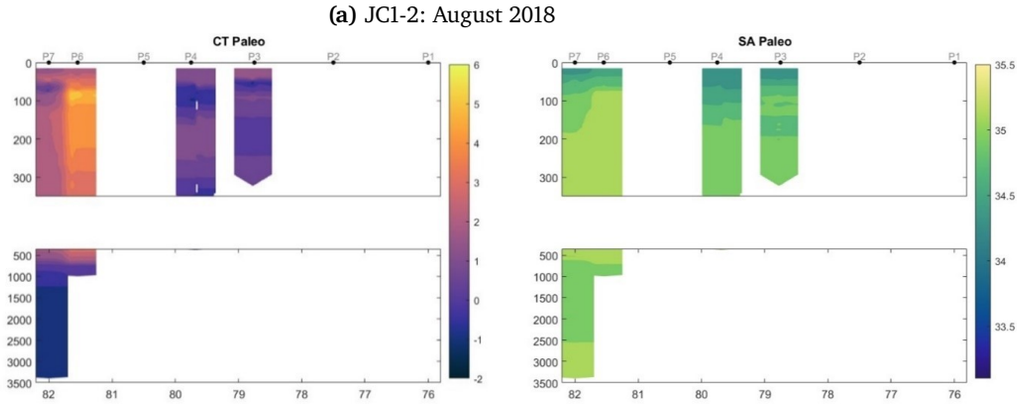

(b) Paleo: October 2018

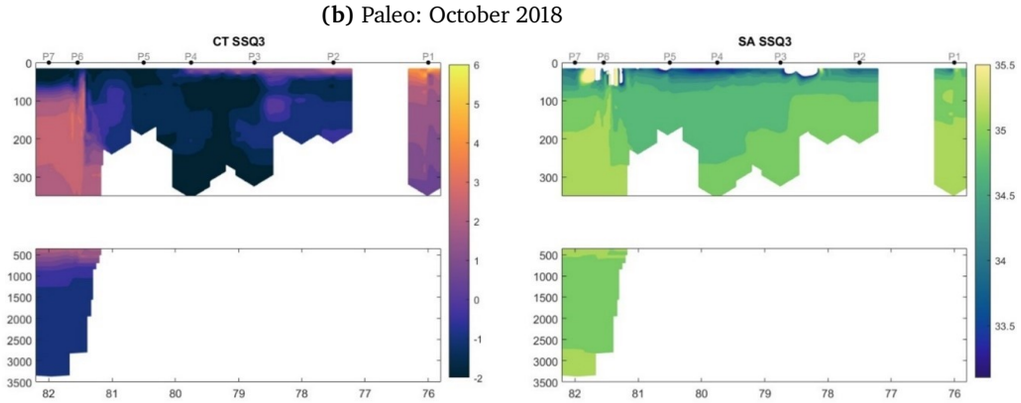

(c) SSQ3: August 2019

Figure 4.4: Meridional transect plots of conservative temperature (CT) and absolute salinity (SA) against depth (in meters; y-axis) and latitude (° N; x-axis) for the different cruises. The positions of the seven process stations (P1 to P7) are indicated with black dots on top. Note the difference in depth ranges for the two panels; the top panel shows data for the upper 15-350 m of the water column, while the lower panels show the depths from 350 m to 3500 m.

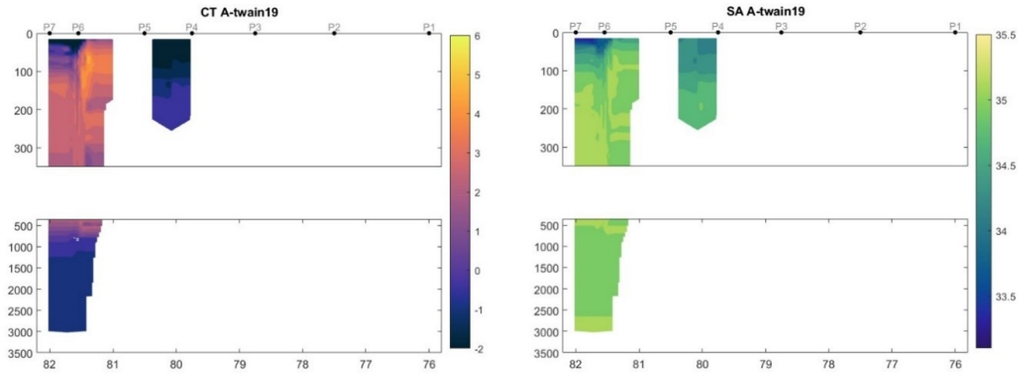

(d) MSC19 (also know as A-twain): November 2019

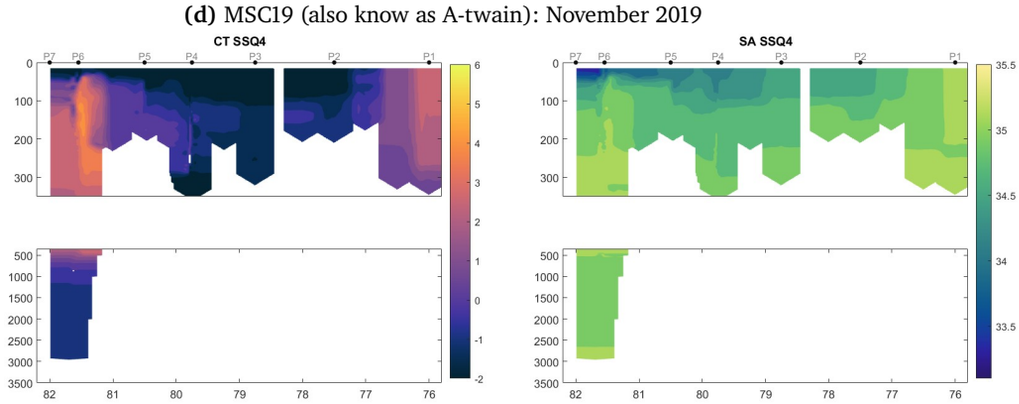

(e) SSQ4: November/December 2019

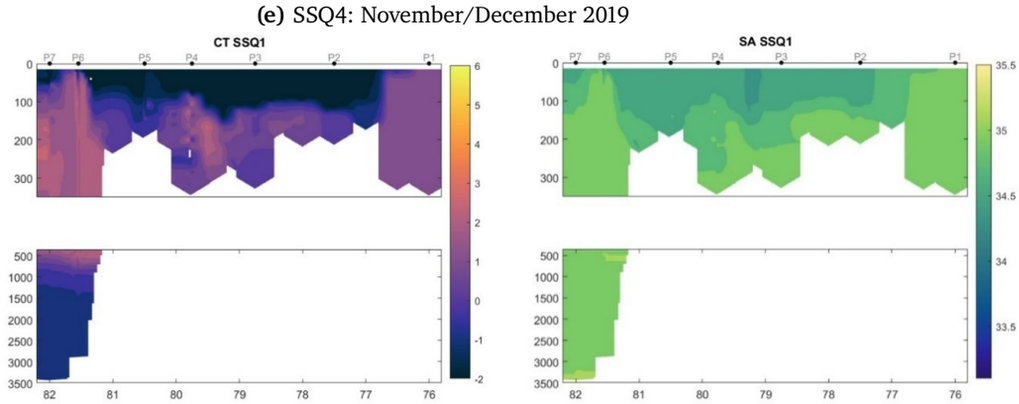

(f) SSQ1: March 2021

Figure 4.4: continued.

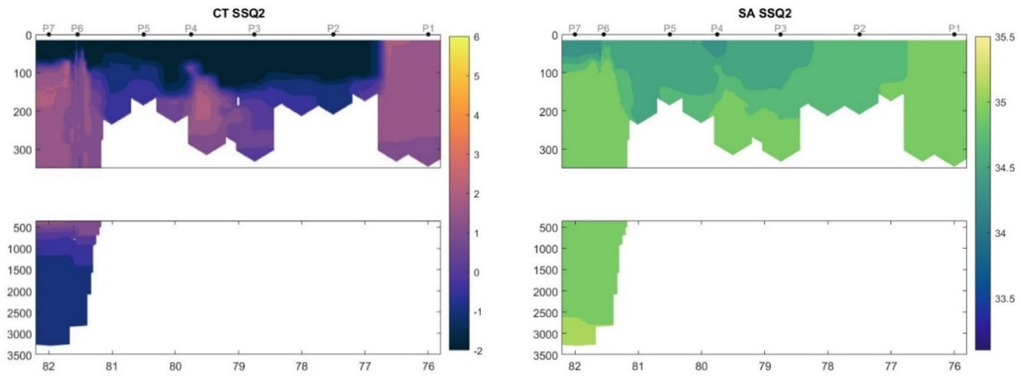

(g) SSQ2: May 2021

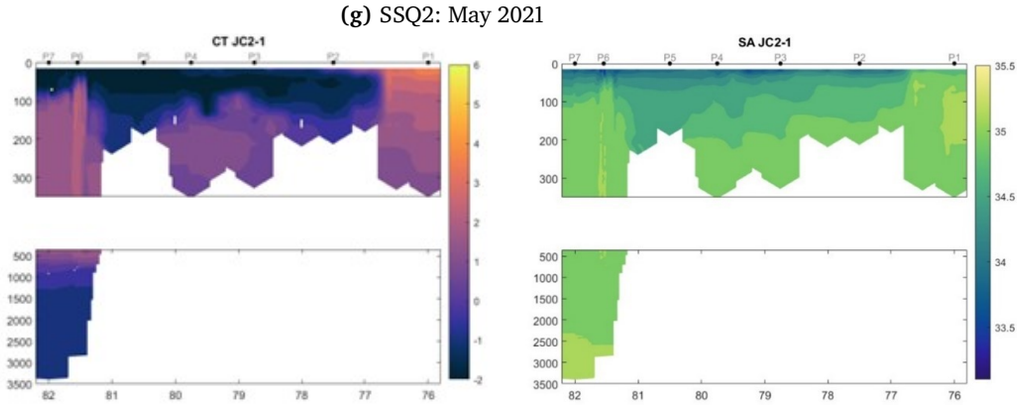

(h) JC2-1: July 2021

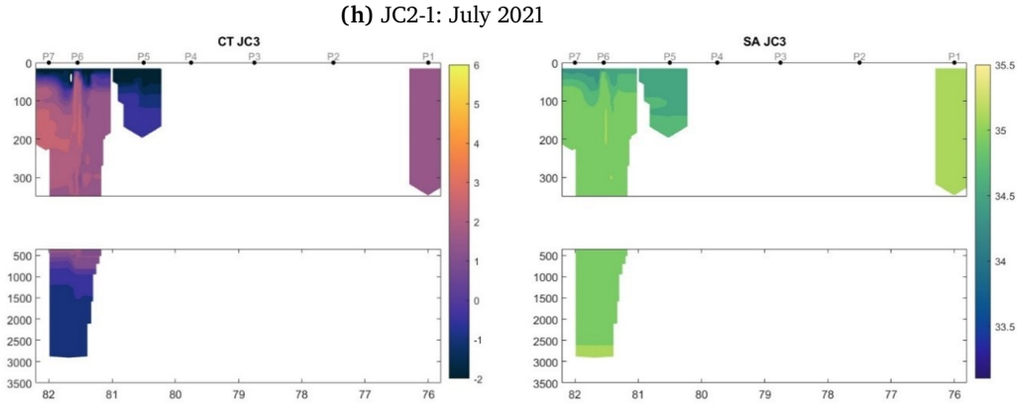

(i) JC3: February/March 2022

Figure 4.4: continued.

One of the most prominent features on the transects is that of the Atlantic Water Boundary Current (AWBC), which can be seen as relatively warm and salty water on the continental shelf (north of 81° N). The core of the AWBC,

which refers to the layer containing the temperature and salinity maxima, can be seen in the close vicinity of P6 for most transects. The highest temperatures recorded for the AWBC during the study period occurred in autumn and early winter. During the Paleo cruise in October 2018, a temperature maximum of above 5° C was measured at around 80-100 m depth for station P6. However, due to the low coverage of NL station on the shelf area of that particular cruise, it is uncertain whether the measurements at P6 indeed capture the core of the AWBC. Thus, we can not exclude the possibility of even higher AWBC temperatures in the close vicinity of P6. Furthermore, we see that the warming signal from the AWBC water reaches all the way into the upper water column, with water temperatures above 2° C measured at 15 m water depth during the Paleo cruise.

In 2019, warm AWBC core temperatures exceeding 4° C were measured for the MSC19 cruise in November and the SSQ4 cruise in November/December. In both instances, it appears that the core was positioned slightly to the south of P6, around 81.37° N and 81.47° N on the continental shelf, respectively. For the MSC19 cruise, the core was situated at approximately 50-100 m depth, with a warming signal from the AWBC again prominent all the way into the surface water at 15 m level. Just weeks/days later during the SSQ4 cruise, the warm salty water from the AWBC looks to be capped off by a thin layer of cold, fresher water at the surface. The AWBC core had then receded downwards to approximately 100-180m depth.

During instances of temperature maxima in autumn and early winter, we can fairly easily locate the core of the AWBC. At other times, the core is less prominent in the temperature and salinity data, and we need additional information to pinpoint its location. The latter is the case for the SSQ1 and SSQ2 cruises, in March and May of 2021, when the AWBC appears to have a temperature minimum.

The Atlantic-origin water from the AWBC impacts the surrounding waters, and the vertical extent of warm and salty water can generally be seen from the shelf area stretching further north into the Nansen Basin at intermediate depths. In periods of elevated temperatures within the AWBC, this warming signal is also evident in this respective layer. For the water column in the deeper parts of the shelf area and the Nansen Basin, the temperatures decrease down to sub-zero values. The salinity remains in the same range as for the Atlantic-origin layer ($SA > 35.06\,g\,kg^{-1}$), but often with a slight increase in salinity towards the very bottom of the Nansen Basin. The water column properties seem to remain relatively constant throughout the study period for this layer.

Continuing southward into the Northern Barents Sea (approx. between 81 and 77° N), the water overall becomes colder and also slightly fresher. The transects

do, however, reveal substantial interannual variability in the water column properties for this area. The measurements for August (JC1-2) and October (Paleo) in 2018 show relatively warm and saline water compared to the same area in other years, with some intricate layering of alternating temperature and salinity values throughout the water column. That summer, a relatively warm surface layer was present for the whole area. The next year, a summer surface layer was also visible during August (SSQ3), but this layer was considerably fresher and not particularly warm. Throughout the 2019 measurements, this area was characterized by cold temperatures reaching all the way to the bottom. In 2021, cold temperatures were again measured in the upper and intermediate water column, while warmer and more saline water was recorded in the lower water column in the approximate area between P3 and P4.

Another distinct feature on the transects is the gradient in temperature and salinity between stations P1 and P2. This gradient can be recognized as the Polar Front (PF) area, an important physical and biological region. From the pcolor plots of the same temperature and salinity data in Appendix 7.2, the plots for SSQ1, SSQ2, and JC2-1 display a rather distinct change in temperature values between the columns for station NL2 and NL3. A temperature gradient from NL2 to NL3 can also be seen for SSQ4, although not so prominent. Overall, this indicates that the placement of the PF can be narrowed down to an area between approximately 76.5° N and 77° N.

One of the cruises (JC2-1) in the dataset had extra CTD measurements conducted in between the defined NL stations for the stretch between NL2 and NL3. In Fig. 4.5 we have plotted a close-up of the JC2-1 transects for conservative temperature and absolute salinity, with these extra CTD measurements included. The figure shows a clear temperature gradient with almost vertical isolines in the vicinity of 76.8°N. The approximate depth of the front can be placed around 50 m depth and downwards. This aligns with previously described characteristics for the PF during summer (Lien (ed), 2018). The location of 76.8°N also seems to coincide well with the location of the 200 m isobath. In contrast to the temperature gradient, the gradient in salinity is more distinct in the upper $\sim$ 50 m at this location, making it more of a surface front.

South of the PF the water is warm and salty for all measurements, signaling a region that is largely influenced by Atlantic conditions all year round. There are however some seasonal variations in the water column properties throughout the years. During summer, the upper water column heats up, creating a vertical temperature gradient towards the bottom. At the same time, the surface also freshens slightly. On the contrary, during late winter and spring, the water properties tend to be fairly homogeneous throughout the column. The latter condition can be seen for March 2021 (SSQ1), May 2021 (SSQ2), and February/March 2022 (JC3).

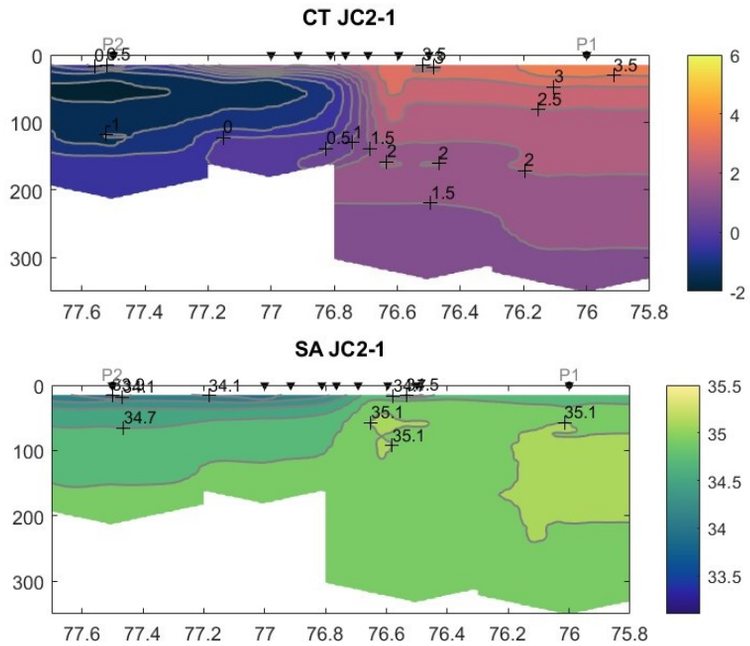

Figure 4.5: Transect plots of Conservative Temperature (CT) and Absolute Salinity (SA) against depth (in meters; y-axis) and latitude (° N; x-axis) for the JC2-1 cruise, displaying the area between P1 and P2 where the PF is expected to be situated. The positions of the four defined NL stations, as well as the positions for the additional CTD stations, are indicated with black arrows at the top of the panels. The grey lines on these plots are isothermals (upper panel) and isohalines (lower panel).

4.2.1 Water mass classification

Moreover, we want to investigate how the different water column properties across the transect translate into the different water masses using the classification by Sundfjord et al. (2020). In Figure 4.6 (left panels), we have created pcolor plots for each cruise, where each column displays the categorized water mass throughout the water column. (Again, we have not produced plots for JC2-2 and MSC20, due to the low station coverage on the NL transect). Note that the plot sometimes displays several columns for each NL station, reflecting the number of profiles conducted at that station. With this in mind, the pcolor plots should not be interpreted as continuous, lateral transects.

In Fig. 4.6 (right panels), we have calculated the mean percentage of each water mass for the 7 process stations. The percentage refers to the fraction of the water column that is classified as the specific water mass. The mean was calculated by averaging the percentage of each water mass over the number

of conducted profiles. In addition, we have plotted CT profiles for the seven P-stations, with water masses on top of the profiles in Appendix. 7.3.

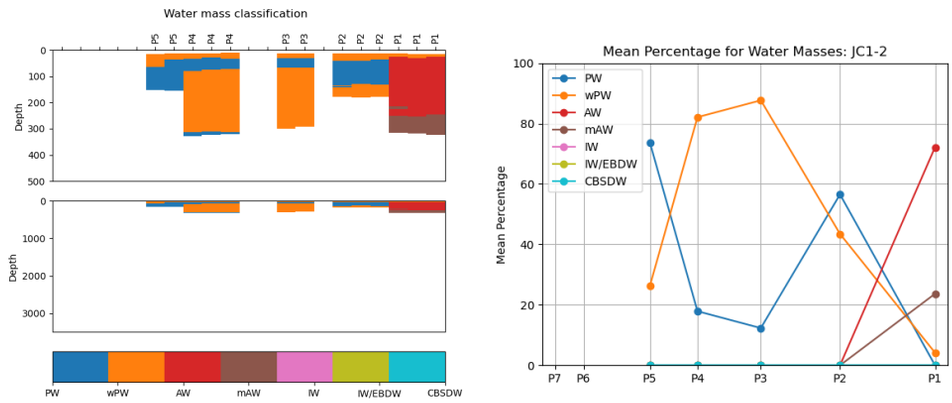

(a) JC1-2: August 2018

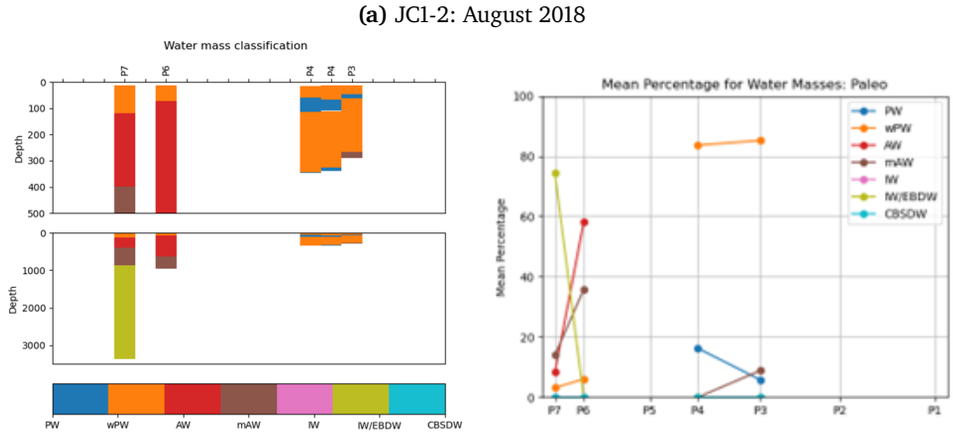

(b) Paleo: October 2018

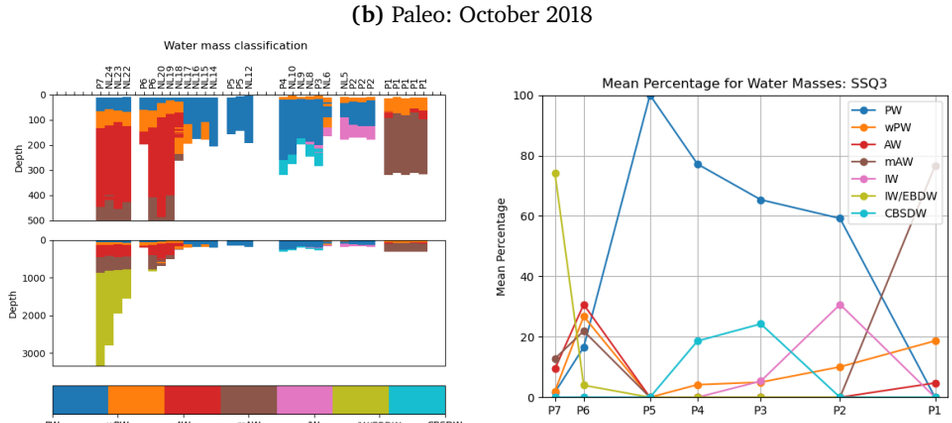

(c) SSQ3: August 2019

Figure 4.6: (Left panels): Classified water masses along each profile conducted at an NL station during its respective cruise. The water masses are classified according to Sundfjord et al. (2020). The top panels show the upper 15-500 m, while the lower panels show the depth from 15 m down to 3500 m. (Right panels): Calculated mean percentage of each water mass for the 7 process stations.

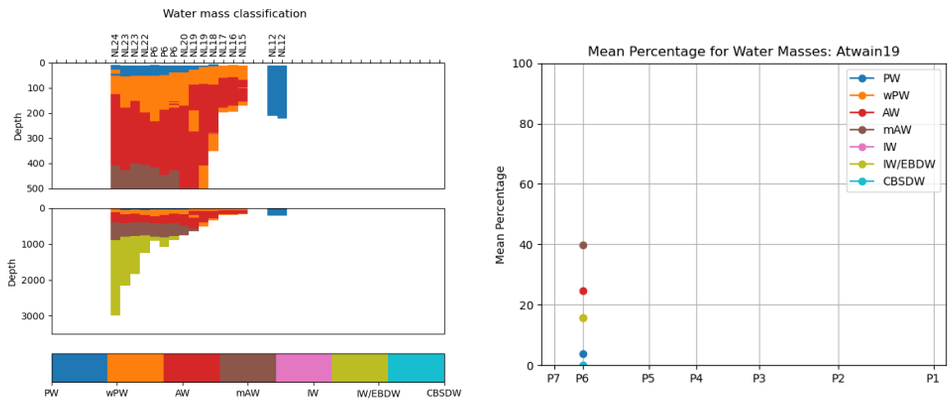

(d) MSC19: November 2019

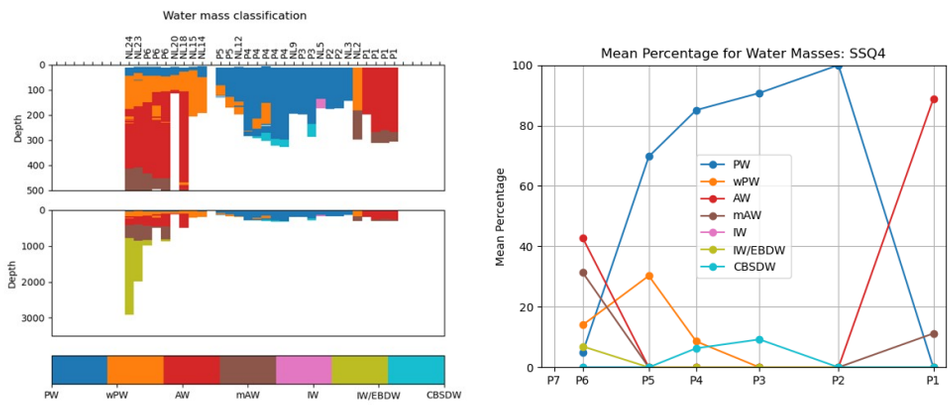

(e) SSQ4: November/December 2019

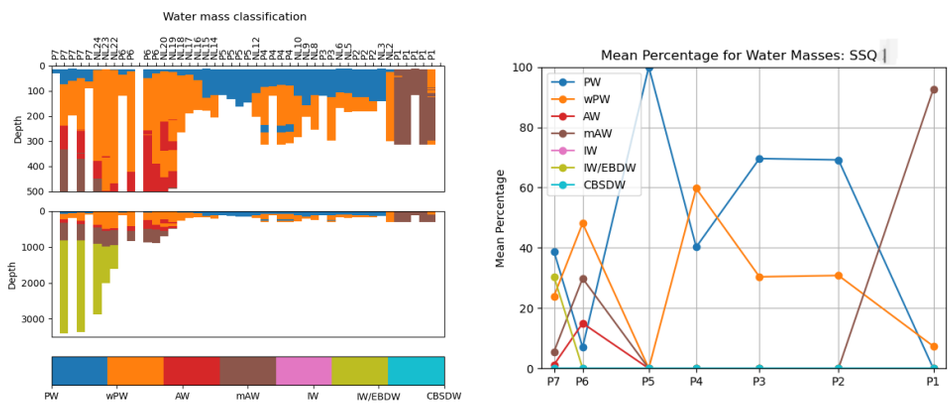

(f) SSQ1: March 2021

Figure 4.6: Continued.

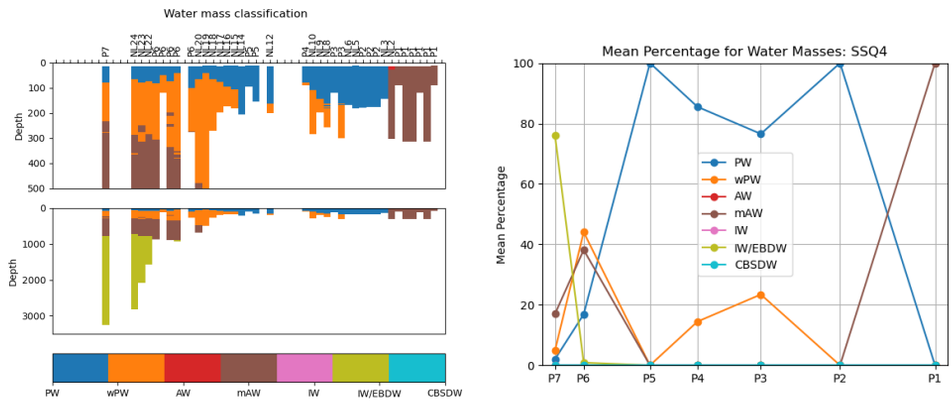

(g) SSQ2: May 2021

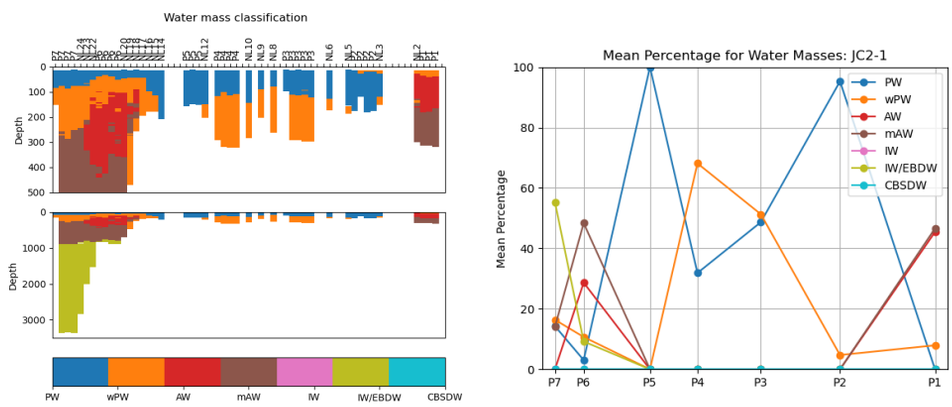

(h) JC2-1: July 2021

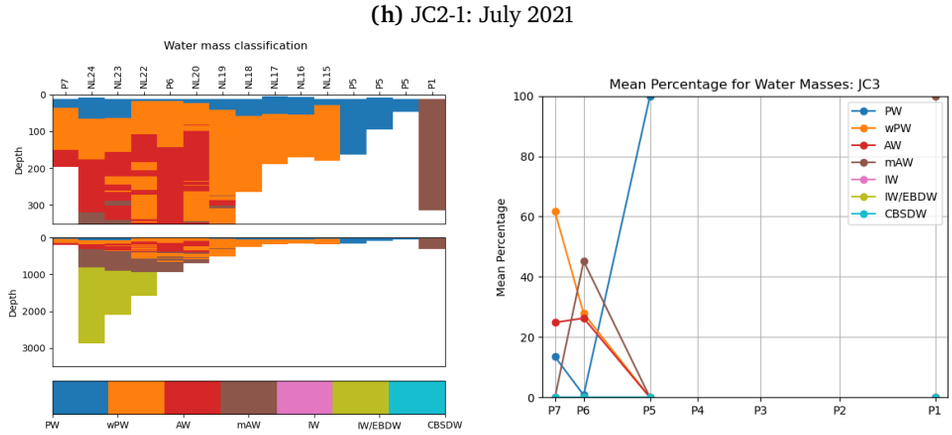

(i) JC3: February/March 2022

Figure 4.6: Continued.

The water which has temperatures above 2° C and salinity above 35.06 g kg^{-1} in the vicinity of the AWBC core on the transect plots, translates to “pure” AW

in the pcolor plots. This AW is sometimes more centered around P6 (as seen for JC2-1), although at most times the AW water mass occupies larger vertical areas of the shelf and into the Nansen basin (as seen for Paleo, SSQ3, SSQ1, and JC3). For transects missing measurements at P7, it is unknown how far this AW layer really stretches. There is also an instance in May 2021 (SSQ2) where no "pure" AW is recorded for the stations on the shelf. For all of the measurements, mAW can be found under the AW layer. This watermass stretches across the whole shelf area and extends into the Nansen basin. The depth of this layer is rather variable, but can in most cases be found from 300-400 m depth down to approximately 8-900m.

Beneath the Atlantic-origin layer of both AW and mAW, the cold and saline water column classifies as the overlapping wm of IW/EBDW. This water mass occupies the deep and intermediate water column from 800/900 m down to the seafloor. Vertically, this layer spans from the deeper parts of the continental shelf and into the Nansen Basin. Based on the waters' geographical location, and the depths in which the watermass resides (>500 m), the water can be determined to be EBDW. Above the Atlantic-influenced water from the AWBC, a layer of wPW appears for all measurements. The depth and height of this wPW layer do however vary throughout the study period. Typically, the wPW is found somewhere between 50-300 m, although it can reach even higher in the water column for the stations close to P6. During the Paleo cruise in October 2018, the wPW even occupied the surface layer. However, in most instances, the wPW at the shelf is capped by a layer of PW at the top.

As previously described for the transect plots, the Northern Barents Sea (between P5 to P2) exhibits more Arctic-like conditions with fresh and cold water in relative terms. This is reflected in the prevalent water masses, where polar water such as PW and wPW is characteristic of the area. The layering and composition of these two water masses do however exhibit some interannual and seasonal variations.

The interannual variation in water mass characteristics previously described for the area do translate into some other watermasses besides polar water. For example, in August (SSQ3) and November/December 2019 (SSQ4), Cold Barents Sea Deep Water (CBSDW) was recorded in the area between P3 and P4. Here it occupied the lower part of the water column towards the bottom. In the first instance, it was recorded at several NL stations, suggesting a continuous occupation of the lower part of the trench between P3 to P4. Additionally, the water mass of Intermediate water (IW) was recorded close to P2 for the same two cruises (SSQ3 and SSQ4).

South of the PF, the area is characterized by the three watermasses wPW, AW and mAW. During summer there is a general 3-layer structure of WM found at

P1; with wPW at the top, AW in the intermediate layer, and AW towards the bottom. The depth of each layer has some interannual variability. In August 2018 (JC2-1) there was a shallow layer of wPW at the top, a significant/prominent layer of AW in the intermediate layer, and a modest layer of mAW beneath. The next August (SSQ3) we measure a more prominent layer of wPw at top, a modest layer of AW beneath, and a deep layer of mAW towards the bottom. The summer of 2021 (JC2-1) the conditions are somewhat in between these two previous summers; with a substantial layer of wPW at top, and approximately equal parts of AW and mAW below.

The only measurements we have for this area during the autumn season were in November 2019 (SSQ4), and show that AW was prominent from the surface and down, with some mAW towards the bottom. During the winter periods when the water column is more homogeneous, the water mass corresponds to mAW. It is interesting to note that NL2, which is situated north of P1 and south of the PF, looks like its an interface and often have wPW impacting the conditions.

Furthermore, we want to investigate how the different water masses found on the transect were formed, (and if the properties of the different water masses change seasonally). To get some insights, we look at the data points in CT-SA-space. In Figure 4.7 (left) we have plotted the data points from each cruise in CT-SA space, with boxes indicating the ranges for the eight water masses. Figure 4.7 (right) shows the same data points, but colored by the stations' respective latitudes, as a tool to pinpoint the data points in space. We ask the reader to be careful of doing a direct comparison between the TS plots, as the spatial coverage of the NL transect is fairly variable throughout the study period.

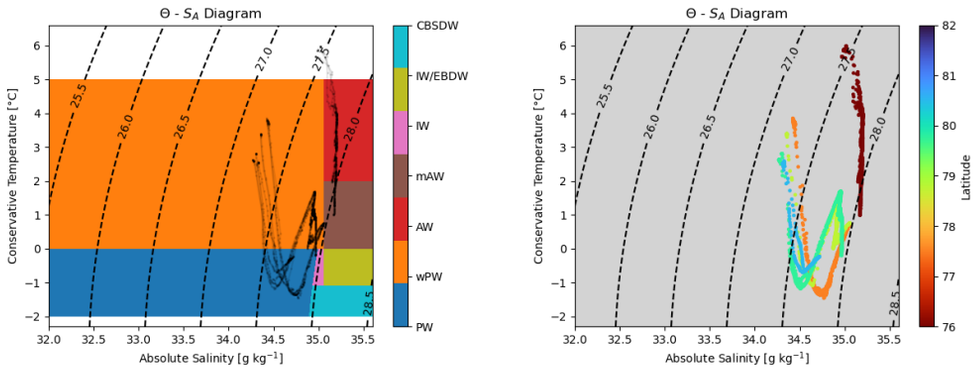

(a) JC1-2: August 2018

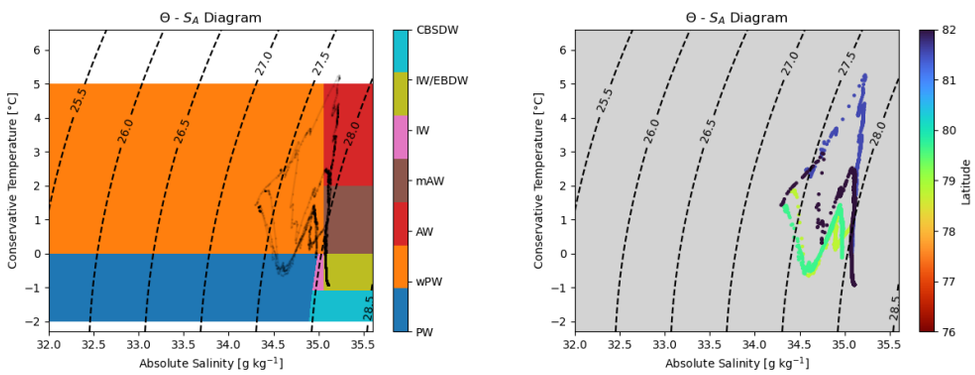

(b) Paleo: October 2018

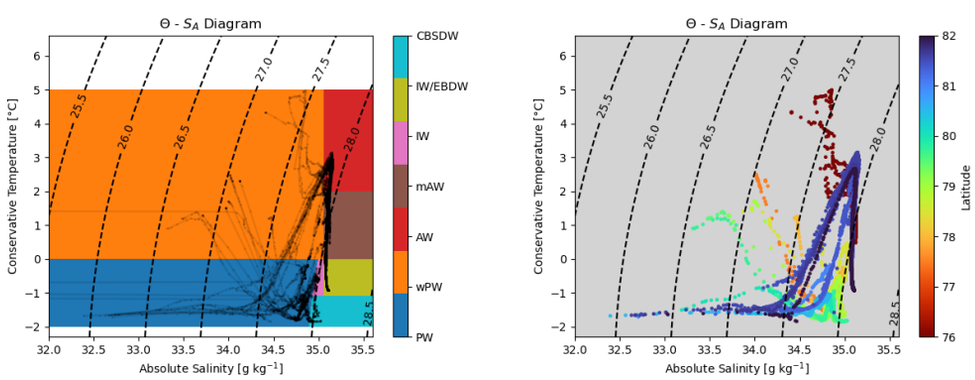

(c) SSQ3: August 2019

Figure 4.7: CT-SA plots displaying the NL data points from each cruise. The CT-SA plot to the left indicate the water mass classification of the single datapoints, while the plot to the right shows the latitude of the datapoits

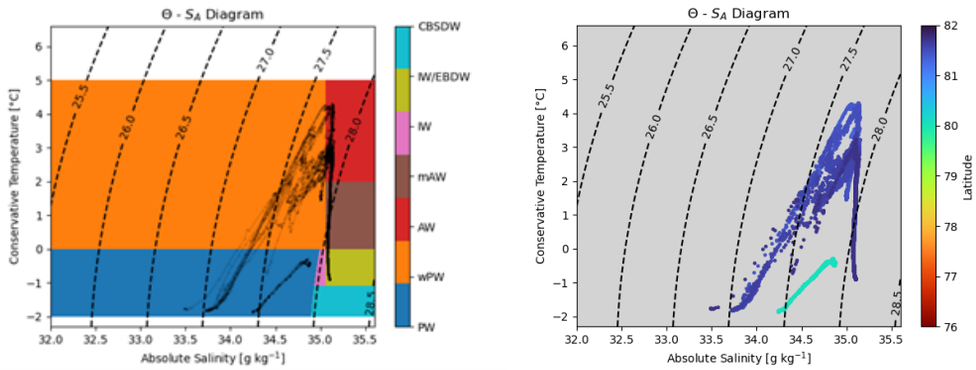

(d) MSC19: November 2019

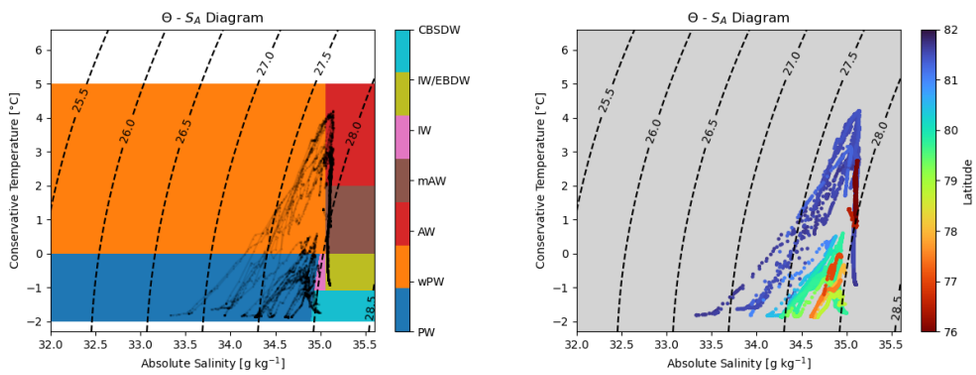

(e) SSQ4: November/December 2019

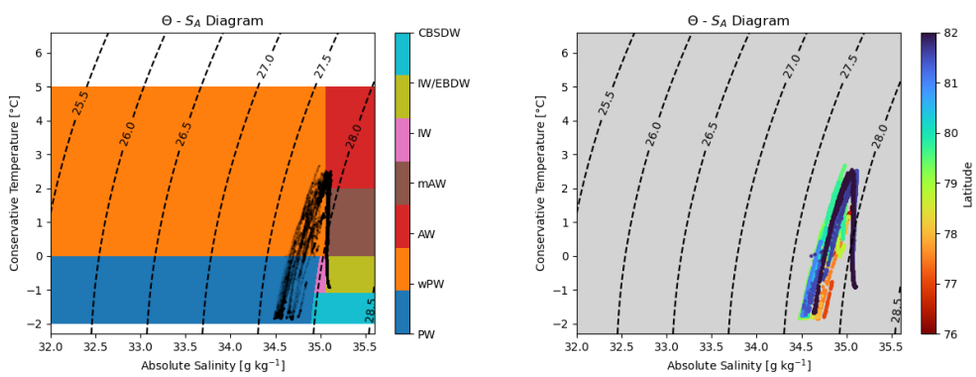

(f) SSQ1: March 2021

Figure 4.7: Continued.

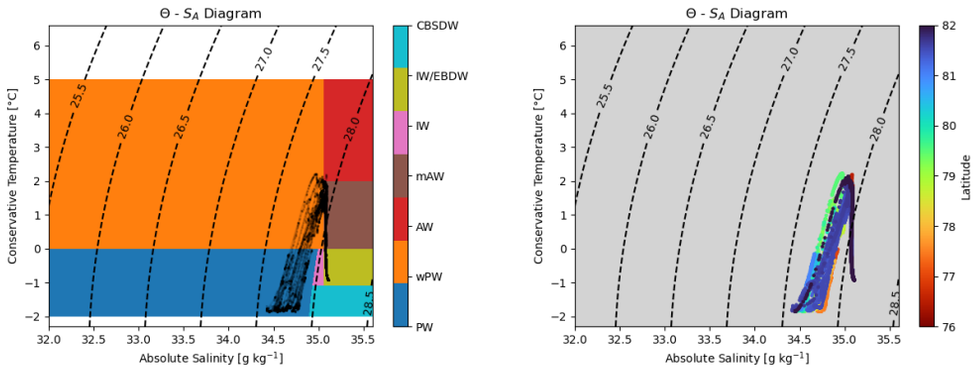

(g) SSQ2: May 2021

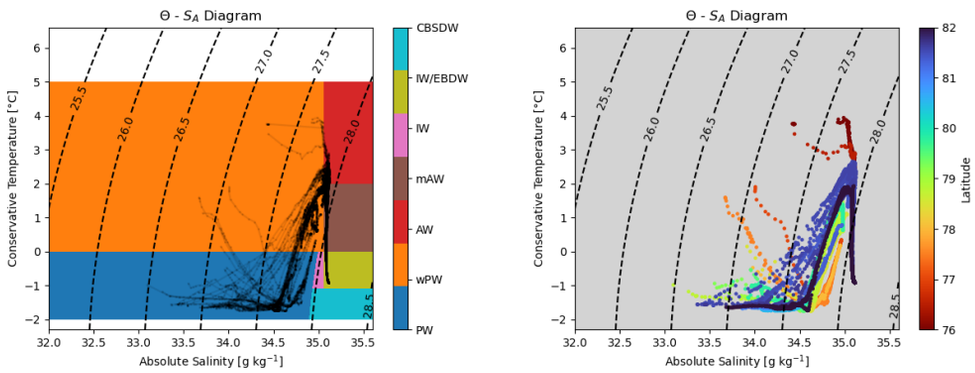

(h) JC2-1: July 2021

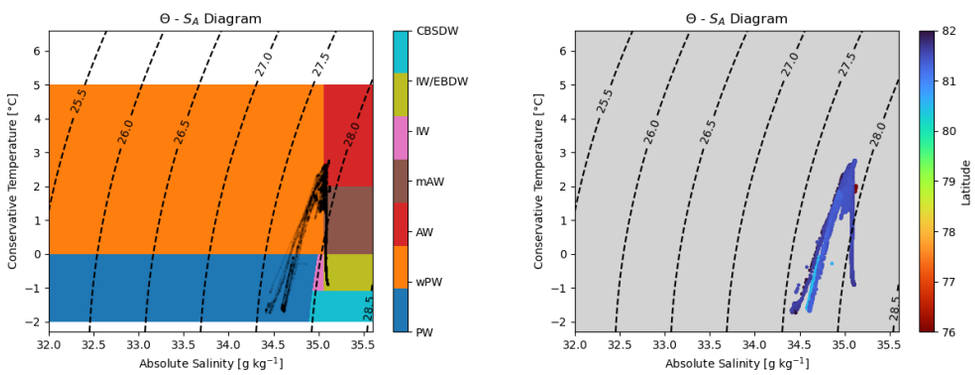

(i) JC3: February/March 2022

Figure 4.7: Continued.

From the CT-SA plots, we see the general picture of a lot more variability/higher spread in the water mass properties during summer (SSQ3, JC2-1, etc.) compared to measurements from winter and spring (SSQ1, SSQ2, JC3 etc.). This

regards the temperature parameter, but especially the ranges of salinity. The variability is reflected in the stratification of the water column, where the increased range in temperature and salinity during summer corresponds to increased stratification. This can be seen as the data points/lines during summer move across several the isopycnals. Oppositely, most of the datapoins on the NL transect align more parallel to the isopycnals during winter and spring (besides the datapoints the vertical line), and indicate overall weaker stratification.

All cruises that have CTD data in the shelf area and/or into the Nansen Basin (P7), show a typical feature that visually looks like an upward pointing arrow. On the right side of the "arrow", the line goes almost straight down vertically. Here we see that AW cools down to mAW, which cools down even further and becomes IW/EBDW. The coldest IW/EBDW (below approx. -1° C), which also is situated deepest in the water column (figure not shown) is additionally seen to have a slight increase in salinity (compared to the IW/EBDW, mAW, and AW higher up in the water column.).

On the left side of the "arrow" we have cold and fresh PW. This PW mixes with the AW and creates wPW. The mixing products is seen on the vertical line(s) between the PW and AW. The general increased water property variability during summer is also prominent for the data points in the north/arrow. We see that the ranges in salinity increase for the PW, which also is reflected in the mixing products of the PW and AW.

For stations in the Northern Barents Sea, we find wPW during summer that is not a mixing product, but rather a result of freshening and warming of the PW. This is the case for wPW found at the surface in August 2019 (JC1-2), in August 2019 (SSQ3) and in July 2021 (JC2-1). Visually inspecting the CT-SA plots for the CBSDW recorded for SSQ3 and SSQ4 between P4 and P3, we see that this WM has freezing point temperatures, and increased salinity compared to the PW. In tracking the profiles backward, it looks like the CBSDW comes from PW that has been cooled down (extensively), as well as receiving added salt. Tracking the profiles where pure IW, which was only recorded once for SSQ3 at the bottom of NL5, also seems to be coming from PW, but with added salinity. However, the source PW for IW is not as cold as the source PW for CBSDW.

4.3 Heat and Freshwater Content

In Figure 4.8 we show the heat and freshwater content for the upper 15 to 100 m of the water column for each conducted NL station during the study period.

The figure reveals an overarching picture of relatively high HC for the stations north of 81° N and south of the Polar front (approximately <77° N) , and low to moderate values for the area in between. Particularly high values are seen in the vicinity of P6 (approximately 81.5° N) on the shelf break during October 2018 and November 2019. However, the amount of heat varies considerably along the short stretch of the shelf within each cruise. In addition, we see a substantial temporal variation in HC in-between the cruises for this area.

While the figure reveals an overall trend of low heat content between 81 and 77° N, we still see some spatial, seasonal, and interannual fluctuations in this area. In particular, the two measurements from 2018 stands out with remarkably higher values compared to the other measurements. During the measurement of March (SSQ1) and May (SSQ2) of 2021 the HC is even close to 0 for large parts of this stretch. South of the Polar Front of 77° N the heat content generally increases towards the lower latitudes. The highest calculated values for the transect is found here at P1. Especially high values are captured for P1 in August (JC1-2) 2018, and again in October (MSC20) 2020.

The figure reveals that the fresh water content typically mirrors the trends in HC; where the heat content is high, the freshwater content tends to be low, - and vice versa. We see that the high variability in HC on the shelf, further corresponds to high variability in FWC. Interestingly, we find the highest calculated values for FWC (above 2m), and some of the lowest calculated values (~ 0) within a small stretch on the shelf during the same cruise surveys (as seen for MSC19, SSQ4 etc.).

Where the HC is low between 81 and 77° N the FWC is relatively high for the transect. For the measurements of March (SSQ1) and May (SSQ2) of 2021; the low values of heat do not respond to high values of FWC. Instead, we see some of the lowest values of FWC in this region for these two surveys. The lowest FWC is found south of the PF. Here, we even see negative values of FWC due to a higher amount of water being more saline than the set AW limit of 35.06 $g\,kg^{-1}$. The high content of heat captured for P1 in August (JC1-2) 2018 and October (MSC20) 2020, correspond to the lowest values of FWC calculated on the transect.

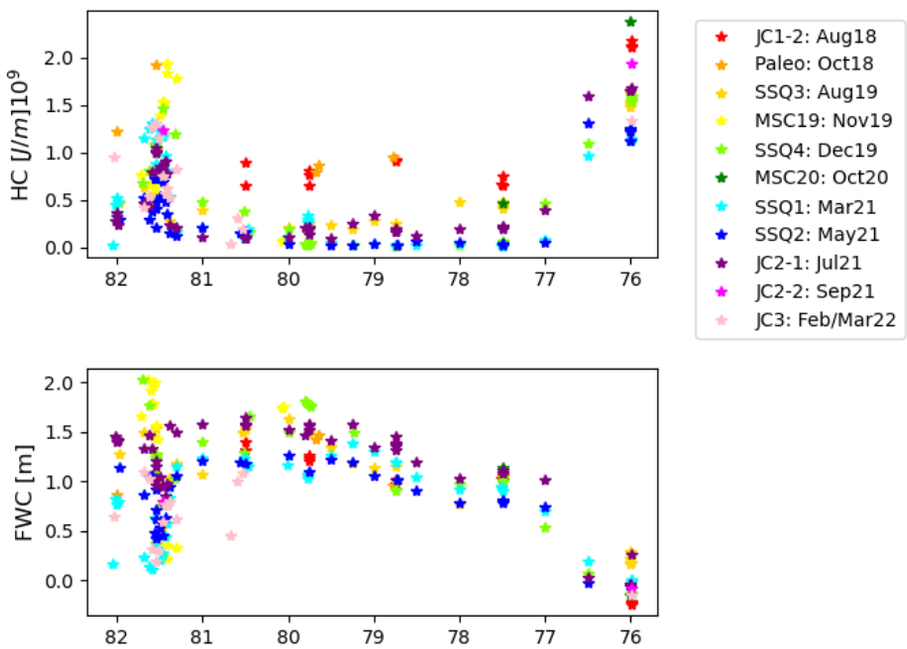

Figure 4.8: Calculated heat and freshwater content in the upper 15-100 m along the NL transect (by latitude (° N); x-axis) for all cruises.

4.4 Current Measurements

In this section we present the results from the current measurements, encompassing both types of ADCP data. The velocity profiles have been made into transect plots using the same Laplacian interpolation method as described for the temperature and salinity transects. The resulting plots show the u- and v-components of the currents. Here, positive u velocity values indicate eastward motion, whilst negative values indicate a westward flow. For the v velocities, positive values indicate flow towards the north, while negative values imply southward flow. As most of the NL transect is aligned in a north-to-south direction, the u velocities then show flow across the transect, while the v velocities indicate the flow direction along the transect. For easier comparison between the two ADCP types, the S-ADCP data are displayed in panels above the upper L-ADCP data.

The L-ADCP data in Figure 4.9 reveal relatively modest u- and v- velocities across the transects, while the S-ADCP data display some stronger velocity component values. The plots also reveal that there is quite some spatial variability in current directions along the transect, as well as temporal variations

from cruise to cruise. Nevertheless, some discernible trends or patterns can be detected. Notably, the u-component of velocity consistently exhibits positive values in the vicinity of P6. This is assumed to show the Atlantic Water boundary current (AWBC), which is known to flow along the shelf break in a predominantly eastward direction. The positive u-components in the vicinity of P6 are prevalent for all transects where there are measurements for the shelf (SSQ3, SSQ4, SSQ1, SSQ2, JC2-1, JC2-2, and JC3).

Although the eastward flow of the current is consistent in the data, the north-south component appears to fluctuate. According to the data, the flow direction of the AWBC is north-easterly in August 2019(SSQ3)(according to the L-ADCP data) and in February/March 2022 (JC3), while the flow is mainly in a south-easterly direction in November/December 2019 (SSQ4) and in July 2021 (JC2-1). At one particular instance in August/September 2021 (JC2-2), the S-ADCP and L-ADCP even showed a discrepancy in flow directions for the AWBC. Here, the S-ADCP data show a south-easterly direction of the AWBC, whereas the L-ADCP data suggests a north-easterly flow. For both March (SSQ1) and May (SSQ2) of 2021, station P6 was placed in the interface between a north-south flow division. The temperature minimum previously described for the AWBC at these two instances makes it hard to pinpoint the location of the current on the shelf. Thereby it is also hard to determine the flow direction (in terms of the north-south component).

Additionally, the AWBC seems to exhibit variability in both current speed and vertical extent of the flow. For instance, during the measurements from February/March 2022 (JC3) the current appears narrow and strong. At other times, the current extends over a larger vertical stretch with lower speed values, such as seen in March 2021 (SSQ1). Any seasonal patterns concerning speed values or extent have, however, not been detected.

As we have previously discussed based on temperature and salinity maxima values, the positioning of the AWBC seems to vary around P6 throughout the study period. Trying to locate the AWBC based on the eastward component velocities, it appears that the positioning varies both south and north of P6. Thus, it is worth noting that the positioning of the temperature and salinity maxima does not always correlate with the positioning of the eastward flow.

Another interesting feature to observe on the transects is that P5 seems to be placed in the interface between some stronger, deviating current systems. Two different flow regimes can usually be seen on each side of P5. This division is most visible for the north-south component (as seen for SSQ4), although in some instances the division is clearest for the west-east component (seen for SSQ3). Overall, we see that the resulting flow directions on each side of P5 vary considerably throughout, without any clear pattern. This diverting current flow

around P5 exhibits some of the highest velocity component values recorded on the transects.

For the Barents Sea, the data reveal a complex and intricate system of currents. The current direction fluctuates significantly as one traverses the area from north to south; a trend that regards both velocity components. It appears that the flow direction and speed generally vary less with depth, than horizontally.

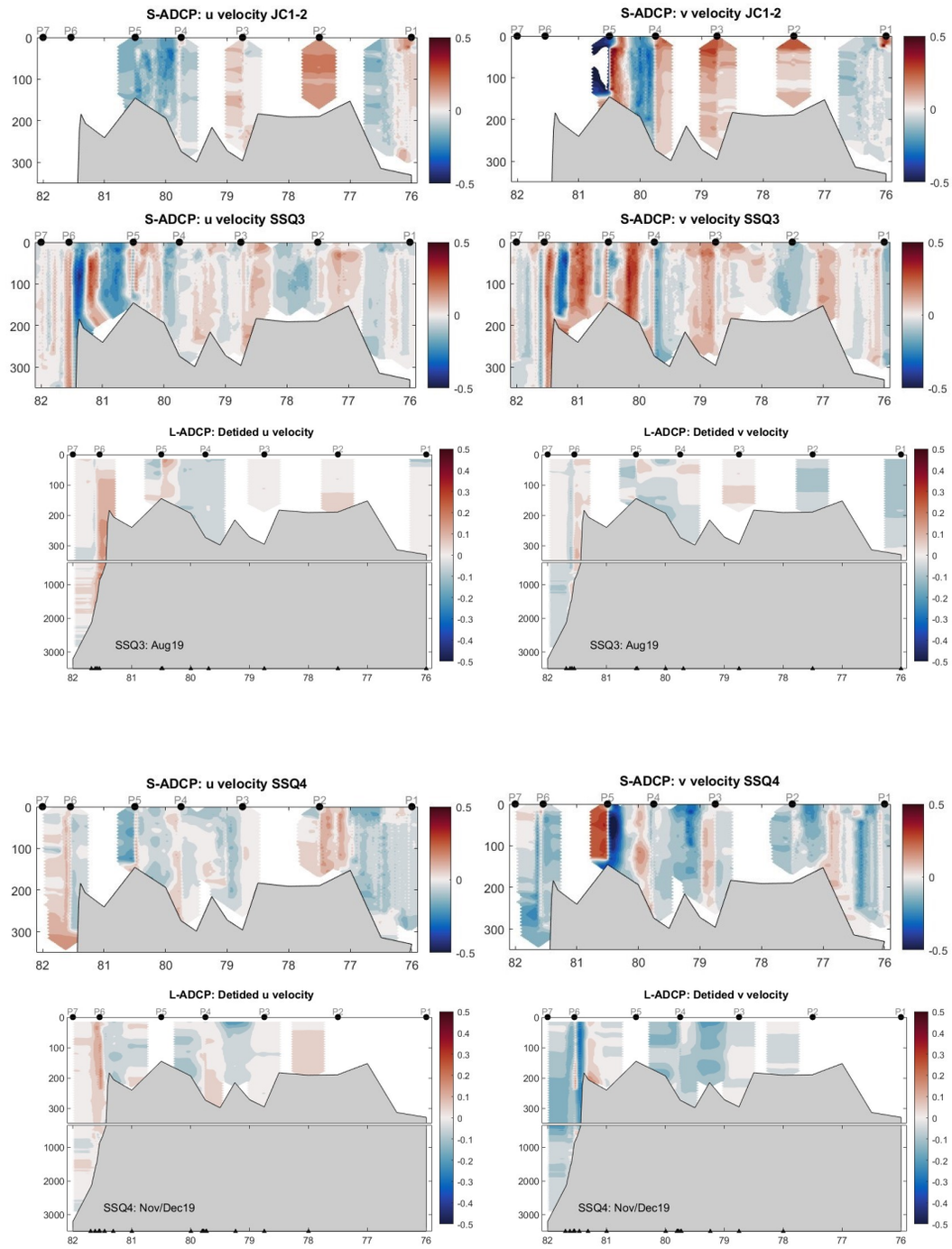

Figure 4.9: Transect plots of S-ADCP and L-ADCP current velocities against depth (in meters; y-axis) and latitude (° N; x-axis). The left panels display the u-component, while the right panels show the v-component of the current velocities. The positions of the seven process stations are indicated with black dots on top of the panel, while the black arrows at the bottom (for the L-ADCP transects) indicate where measurements are taken. Grey shading indicates the seafloor.

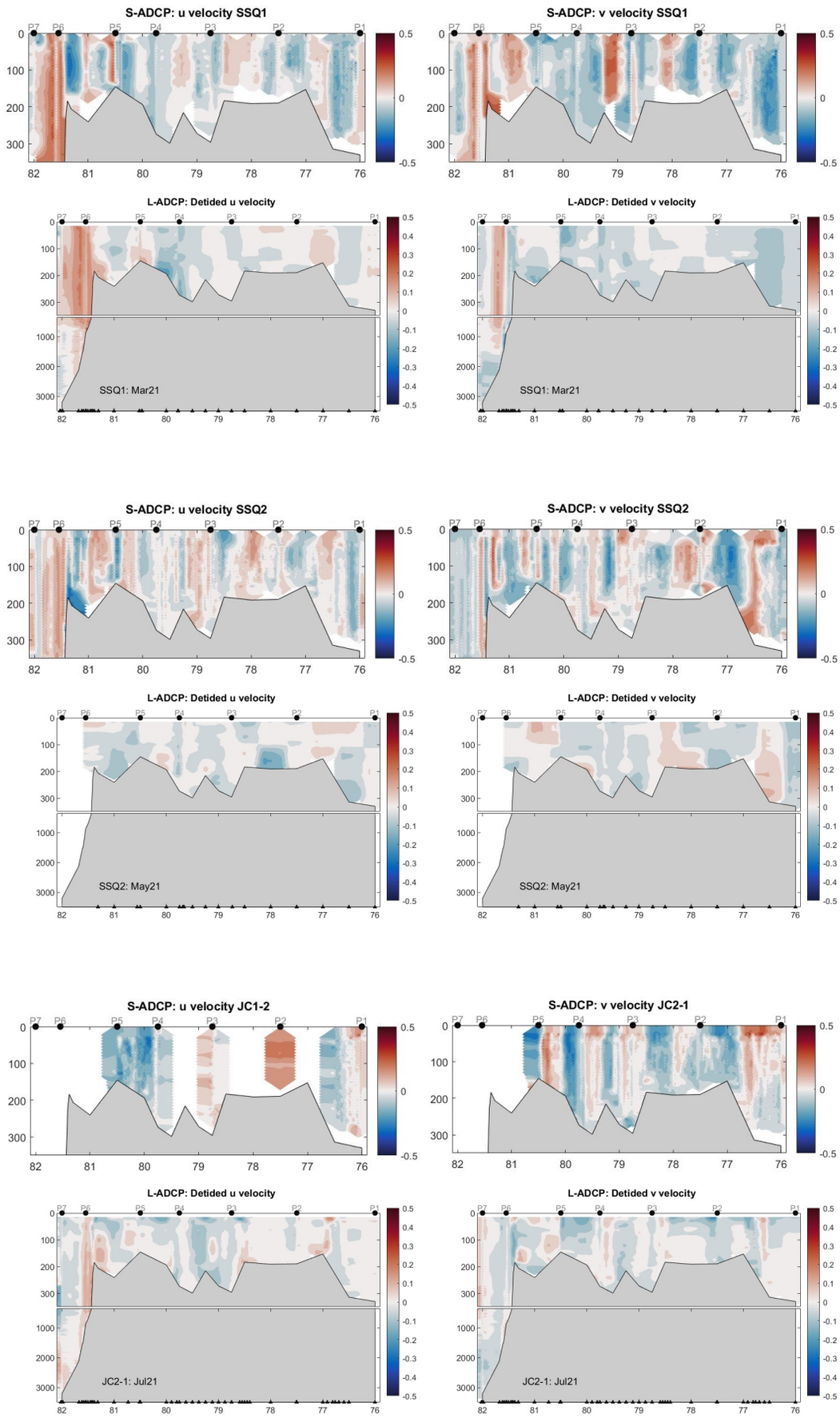

Figure 4.9: Continued.

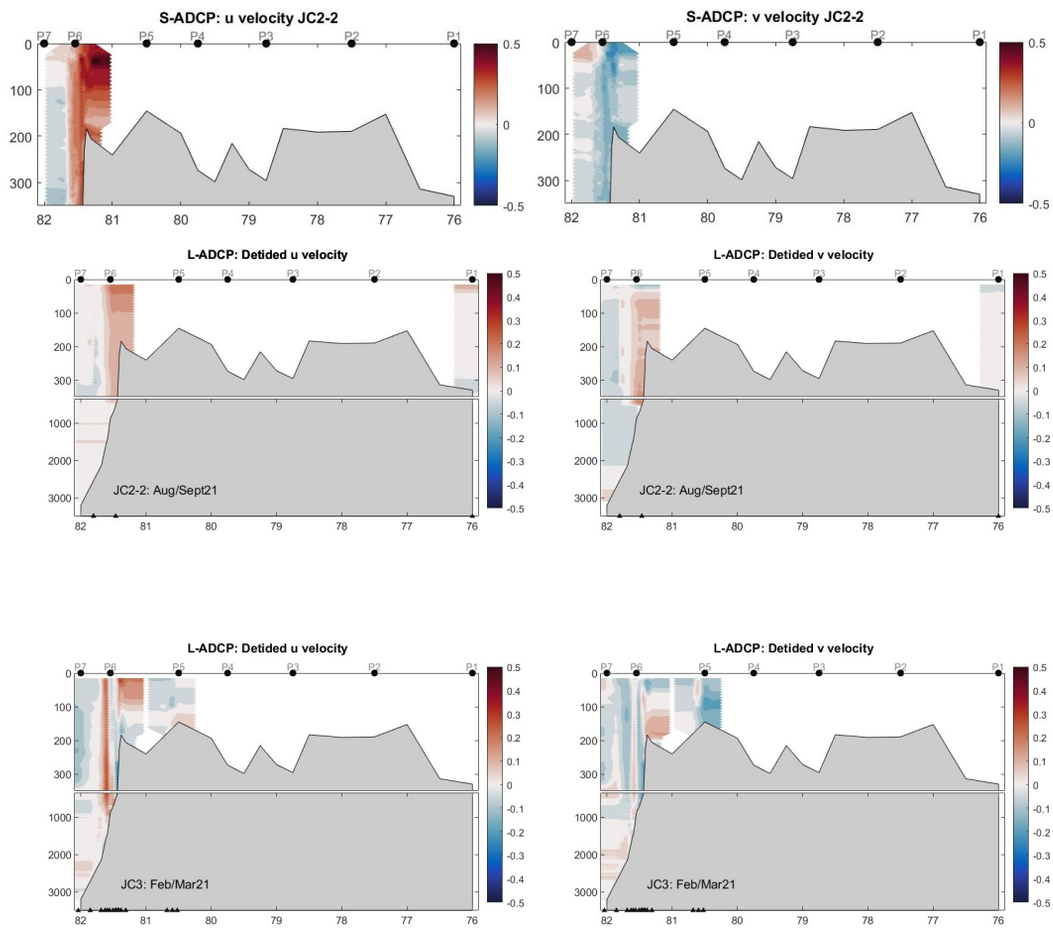

Figure 4.9: Continued.

5

Discussion

5.1 Atmospheric and sea ice forcing

We will start discussing our results by addressing the third research question first: How did sea ice and atmospheric forcing impact the water column properties?

In 2018, the first year of the Nansen Legacy study period, the transect was visited twice: one time during the summer (JC1-2; August) and again in the autumn (Paleo; October). However, only a few NL stations were conducted on each visit, and so the spatial resolution of the transect was rather limited that year. Based on the few hydrographic measurements, the data suggest an overall warm and salty water column across the transect, at least in relative terms. This aligns with the findings by Aaboe et al. (2021), which report that 2018 was a year with high anomalies in both oceanic temperature and salinity.

Particularly high were the recorded temperatures for the upper water column that year. For both (the summer and the autumn) measurements, we observe a layer of (solar-) heated wPW in the top of the water column for all conducted NL stations. These are the only two measurements where wPW characterizes the "surface" for stations across the whole transect, even for the stations in the north. Fig.4.1 reveals that the entire transect had been ice-free from May onward that year. In the northern part of the transect, there had even been periods of open water during the winter. This aligns with findings by Lundesgaard et al. (2021), who report anomalously low values of SIC for the shelf break area north of

Svalbard for the February-July period of 2018. This prolonged period of open water, exposing the whole transect to heat input from solar radiation, could be a contributing factor to the high surface temperatures recorded that summer and autumn. Fig. 4.2 also displays (somewhat) elevated air temperature during the summer season of 2018. This could be another warming driver, possibly contributing with sensible heat input into the surface layer.

The warmest wPW layer was found towards the south of the transect, measuring close to 6° C in the top water column for P1 that August (JC1-2). This happens to be the highest temperature recorded on the transect during the study period. The warm temperatures are reflected in the SST (Fig.4.2), revealing temperatures even above 6 degrees in the uppermost water column at P1. The layer of wPW was however relatively shallow, limited to the ~ 30 m (Fig.4.6(a),7.3). Beneath the wPW at P1, there was a deep layer of AW that summer, with some of the warmest temperatures recorded for this AW layer (CT above 5° C). Tracing the origin of the wPW on the CT-SA plot (Fig4.7(a)), it appears that the wPW stems from the warmest AW, albeit with some freshwater mixed in. The warming signal from this AW, combined with the solar and atmospheric heat input restricted to a shallow lower-density surface layer that the wPW represents, could possibly explain the elevated temperatures measured for P1 at this instance.

The warm oceanic temperatures, - including the elevated surface layer temperatures, are reflected in the calculated heat content throughout the transect for these two surveys. Most notable are the values for the stations in the Northern Barents Sea, which display the highest calculated heat content for that region (Fig.4.8). Fig. 4.1 reveals that the onset of sea ice for the transect later that year did not occur before late December/January 2018/2019. The high values of HC in the upper water column across the transect, especially in the northern Barents Sea region, could possibly be an explanation for the late onset of sea ice on the transect that winter season.

For the next hydrographic measurement of SSQ3 (Fig.4.4(c)), August 2019, the water column is relatively cold and fresh, especially in the Northern Barents Sea. Although it is late in the summer, sea ice is still present in the northern part of the transect. A substantial layer of PW is present in the upper and/or intermediate water column, - stretching from P7 down to P2. This belt of PW could indicate a water column that has been substantially impacted by present or previous sea ice coverage. Only where the sea ice has retreated (south of P4) do we see a shallow layer of (solar-heated, and freshened) wPW that has developed in the surface (Fig.4.6(c)).

A substantial transport of sea ice into the Barents Sea during the winter season of 2019 has been reported by Aaboe et al. (2021) and Lundesgaard et al. (2022).

The sea ice import resulted in an increased amount of added freshwater into the upper ocean of the Northern Barents Sea from the sea ice melting. This high input of meltwater is evident in our own data, where the upper water column for the transect of SSQ3, August 2019, experiences the freshest surface water recorded during the study period (see Figs. **??**(c), 4.7 (c), 4.8). The import of sea ice was also reported to contribute to a significant re-cooling of the surface water. This is evident in the SST graph (Fig. 4.2), which displays the coldest temperatures for all P-stations that summer season.

The CBSDW recorded towards the bottom of the water columns between P3 and P4 (Fig.4.6(c), 7.3, 7.3), indicates that there also has been local production of sea ice in the vicinity. The CT-SA plot reveals that the CBSDW has low temperatures, - close to freezing point, and increased salinity compared to the PW and wPW (Fig.4.4(c)). Based on its physical properties and lines on the CT-SA diagram, we can hypothesize that the CBSDW has been formed from PW that has been cooled down to the freezing point temperature. The added salt comes from brine released during sea ice formation. Fig.4.2 reveals a period of low air temperatures from January 2019 onwards, in combination with low SST, indicating favorable environmental conditions for sea ice formation in the Northern Barents Sea. The water column properties, in addition to the placement of the CBSDW at the water column base, suggest that there has been a (thermo-)haline circulation of the water sometime that winter or spring, which has sunk to the bottom of the water column.

The calculated heat content in the upper ocean is overall low for SSQ3. The cold, fresh surface layer together with the cooler overall air temperatures, could possibly allow for an early onset of sea ice freezing the subsequent autumn, when the sea ice in the north started forming in October 2019. By the next hydrographic measurements in November and December 2019, sea ice covers the transect down to NL4. The fresh summer surface layer has disappeared and the mixed layer deepened. Likely, this can attributed to mixing caused by the increased wind speeds and cooler air temp (causing thermal convection) progressing through the autumn season.

The winter season of 2019/2020 had an early and prolonged period of sea ice cover, including a rather substantial coverage down to the southern part of the transect. The high sea ice cover coincided with a prolonged period of low air temperatures across all P-stations and correspondingly low SST in the surface. Conversely, when the atmosphere and ocean begin to heat up during springtime, we see a steep increase for both parameters. By summer 2020, the air temperature and SST from the reanalysis show the highest temperatures occurring on the transect. With the high sea ice coverage during the winter and spring, followed by extensive heating and open water during summer, we expect that the surface would be highly stratified, with a warm, fresh surface

layer by the end of the summer. The only hydrographic measurements we have from 2020 are from October (autumn season) during the MSC20 cruise, and only for two NL stations (P1 and NL2) in the south. These measurements do reveal high temperatures throughout the water column, as well as the highest heat content calculated for P1. This supports the hypothesis that the water column during the summer of 2020 was indeed particularly warm.

The next hydrographic measurements we have are for March (SSQ1) and May (SSQ2) of 2021. The transect is then sea ice-covered from the very north of the transect down to the polar front. The freshwater content for the transect at these two measurments are some of the lowest calculated values. A possible explination is that there has been local sea ice production in the area, contributing with brine to the water column beneat. By the summer measurments in July (JC2-1) the heat content had increased, in line with the retreat of the sea ice up to around 80° N.

Recently, Koenig et al. (2023) investigated the seasonal evolution of the water column for the Northern Barents Sea (~ 77 to ~ 88° N) from late winter to late summer of 2021. The study involved, among other elements, the same hydrographic data from the SSQ1, SSQ2, and JC1-2 cruise. Their findings revealed that the sea ice meltwater and the timing of ice-free conditions controlled the stratification and heat content in the upper water column in the area. The influence of sea ice on the upper ocean environment is apparent in our findings. In particular, we see how the water mass classification in the upper water column is related to the sea ice cover and its retreat. During periods of sea ice cover, PW dominates the water column beneath. wPW develops at the surface once the ice has retreated and can receive input of heat, resulting in increased upper ocean stratification.

5.2 Currents

In the area north of 81° N, the circulation is dominated by the AWBC which predominately flows eastward along the Svalbard continental slope. Relative to the other current velocities measured on the transect, the AWBC appears to be a strong current. The consistency and strength of the AWBC, in combination with dominance of Atlantic water properties in the surrounding layers, indicates that the AWBC shapes the hydrographic environment in the intermediate water column.

It appears that station P5 often is situated within, or close to, a system where the currents flow in opposite directions. Typically, the discrepancy is strongest for the north-south component, although sometimes it is more pronounced for

the west-east component. Rather seldom is there a strong discrepancy for both components at the same time. The bifurcating currents appear to be mainly barotropic, as there is little change in current speed throughout the water column on each side of P5. The station is situated at the edge of a shallow plateau just northeast of Kvitøya, with depressions both to the north and south of the station. Thus, this flow system could be connected to of the presence of Kvitøya, or the complex bathymetry in the area. However, there is little consistency in either flow direction or the dominant velocity component, and we can not conclude that the flow is being topographically steered (in the depressions). There is also a possibility that this is a tidal current that the AOTIM tidal model does not properly filter out. How this current system impacts the water column properties in the area is not known. We would assume that the strong shear would have a substantial mixing effect throughout the whole water column. Although most profiles are dominated by one water mass, PW, the profiles at P5 are not particularly well mixed.

According to Lind and Ingvaldsen (2012), Lundesgaard et al. (2022), and The Nansen Legacy (2022), a smaller branch of Atlantic-origin water from the AWBC enters the Barents Sea in the north, subsequently reappearing as a deep southwestward flow in the close vicinity of P4. Our measurements do confirm a weak prevailing south-to-southwesterly flow in the lower water column at P4. Using the water mass classification according to Sundfjord et al. (2020), the water mass at the lower part of station P4 does not classify as any Atlantic-type of water for any of the measurements, nor does the area around it. Instead, the lower and intermediate water column were classified as wPW in 2018 and 2021, and as PW and CBSDW (with a few datapoints of wPW) in 2019 (see fig.7.3). The SA profiles at P4 do show high salinity values($>$34.8) for all profiles below $\sim$ 150 m depth. The profiles from 2018 even show salinity values up to 35 at this depth interval. However, only one profile had salinity above the Atlantic limit set to 35.06, and in this case, the water was so cold that it was classified as CBSDW. It appears that the recorded water, although it might have an Atlantic origin, was too fresh to classify as any Atlantic-type WM. From the CT-SA plot for this wPW it does look like it has Atlantic origin, but mixed with fresh PW.

According to The Nansen Legacy (2022) and Kolås et al. (2023), the lower part of P3 should have a deep northeasterly flow of Atlantic-signature water, - which in contrary to the flow at P4, comes from the Atlantic branch that enters the Barents sea (BSBW) in the south. In our current measurements we do find a north to slightly north-easterly flow in the lower water column for the measurments in August (SSQ3) and November/December (SSQ4) of 2019. From the current measurments in 2021, the flow in the deep parts at P3 seems to be mainly southerly, such as seen in March (SSQ1), May (SSQ2) and August (JC2-1). Looking at the water masses at P3, mAW do show up at the bottom 50m

for the profile conducted in September/October 2018 (Paleo). This is however the only instance where the water has both the temperature and salinity values high enough to classify as Atlantic-type. Predominantly, the intermediate to lower water column here classifies as wPW.

The overall picture of the currents in the Barents Sea is that they are weak and highly varying, such that no clear patterns are visible to us. The complex currents variation displays the complexity of the topography with deep trenches and shallow banks. More research is needed to uveil the characteristics of the flow patterns in this area.

5.3 Seasonality

The seasonal variations in the AWBC translate into seasonal differences in the hydrographic properties. The highest temperatures recorded for the AWBC during the study period occurred/was measured during the autumn and early winter, with core temperatures above 5° C in October 2018 and above 4° C in November and December 2019. We do not have measurements for P6, nor other parts of the shelf area, for other autumn periods to explore this aspect further. However, Renner et al. (2018) also found the warmest water for the AWBC during autumn, which might indicate a more systematic pattern.

The coldest temperatures for AWBC was recorded in May 2021 (SSQ2) at 1-2° C, and classifies as mAW. Due to lack of continuity in seasonal measurements/profiles, we do not have sufficient data to explore the seasonal evolution of the AWBC temperatures from winter, spring to summer in further detail. For the EBDW layer beneath, minimal seasonal variations is observed throughout the study period.

In general, we can see that the process stations P5, P4, P3, and P2 are in the Arctic domain of the Barents Sea, where PW and wPW are the most dominant water masses for the stations. For the Northern Barent Sea, the seasonality seems to be driven mainly by the sea ice cover and the retreat of it. It is interesting to note that none of the profiles recorded for the process stations in this region show any homogenious profiles to the bottom. This could imply that convection during autumn/winter/spring typically does not go down the whole water column in this area.

The hydrographic measurements at P1 indicate a water column that is highly Atlantic-dominated all year around. This aligns with our expectations of the water column characteristics at P1 considering the station's location within the Atlantic domain of the Barents Sea, and within the close proxy of one of

the current divisions transporting Atlantic-origin water northwards. All of the profiles conducted during the summer seasons reveal a three-layer structure of water masses, with a lower-density layer of wPW at the top, warm AW in the intermediate layer, and mAW towards the bottom. Although there is a marginal increase in stratification during summer, the stratification at P1 is overall considered weak. This corresponds well with the descriptions of the Atlantic domain in the Barents Sea by Lind et al. (2018) of a well-mixed water column with Atlantic properties.

By the profiles conducted in the autumn, we see that the surface layer of wPW has disappeared, and the mixed layer (ML) deepened. Instead, AW is characterizing the ML, but with colder properties than the AW in the intermediate layer. As the station is typically ice-free during the autumn season, the water column can be affected by thermal cooling and wind forcing at the ocean-air interface. With an atmosphere typically colder than the ocean surface at this time, both of these processes can lead to increased heat loss from the ocean to the atmosphere. The heat loss can further induce thermal convection, and in combination with physical mixing by the increased wind speeds at P1 during autumn, the depth of the mixed layer increases. As a result, warm AW from the intermediate layer can be mixed into the homogenious ML, supplying the surface with heat.

The hydrographic measurements from the winter season, although sparse, reveal a homogenious water column of mAW. By the vertical lines on the CT-SA plot, the mAW appears to be a cooled off verison of the AW, - a layer that by winter time has disappeared. This gives us an indication that there has been a further heat loss to the atmosphere duing the winter months, and thermal convection all the way to the bottom of the water column. This makes sense due to the low stratification. The profiles of current velocities at P1 and the surrounding area reveal low to moderate values. Based on this, and the progression of the water column properties throughout the seasons, we do believe that the local processes is more defining for the water column at P1 than the advective processes.

None of the profiles reveal freezing point temperatures at the upper 15m at their respective time of measurement. The SST for P1 also shows that the temperature in the surface rarely cools down to freezing point temperature during the study period, besides a few occasions during the cold winters of 2019 and 2020. The calculated heat content for the upper water column is the highest for P1 of all the NL stations, indicating that a lot of heat is stored in the water column throughout the year. This could explain why P1 is largely ice-free, even through most of the winter.

5.4 Limitations and Future work

Certain limitations and future areas of study have come to our attention while working on this dataset. Firstly, the resolution of the hydrographic (CTD) data is such that we do not have measurements for all four seasons within one yearly cycle at any instance during the study period. Thus, we are trying to create a picture of the seasonal evolution or seasonal patterns based on measurements from different seasons spread over several years. This is not ideal as we know there are significant interannual variations in the hydrography for the Barents Sea. Hence, distinguishing between water column properties that are caused by interannual variations and those that are more systematic seasonal traits, is challenging.

Whilst we had to remove the upper 15m of the CTD profiles due to possible disturbances and inaccuracy of the measured water column properties, the resulting gap of data between the very surface and the 15m level poses yet another challenge in our analysis. The stratification of the upper water column typically increases during summer, and the surface can compose high gradients (of water column properties) and shallow layers. Thus, we have no means to unveil the full characteristics of the summer surface layer, nor understand the full interactions at the air-ocean interface. It also poses a knowledge gap in regards to understanding the interactions between sea ice and the water layer beneath. Potentially, a shallow, cold, low-density layer, with suitable conditions for local sea ice production, could be present at the surface without being evident in the data. To pinpoint whether the sea ice cover is a product of local ice formation or ice advection, sea ice drift data would be required, which however are limited in the marginal ice zone. The lack of observations limits our investigations into sea ice influence on the water column properties of the under-ice water layer. A more complete study into the seasonal progression of the water column is therefore yet to be explored in future studies.

By removing the top 15 m, the calculated values for heat and freshwater content are also impacted. As the highest amount of heat and freshwater typically are situated in the uppermost surface in the more stratified water column during summer, we expect the calculated values in our study to be less than what they would be had the upper 15 m been included. In the autumn and winter, when the mixed layer deepens due to wind and convection, the properties tend to be spread more evenly in the upper 15-100 m stretch. In relative terms, the calculation for these seasons could be more representative if compared to other studies. However, as previously stated, the values should not be compared directly to studies where the upper 15 m has been included.

A certain mismatch between the S-ADCP and L-ADCP data is found in regard to current speed and/or direction. This signals that we should treat the accuracy

of these velocity measurements with some caution. A possible explanation for the mismatch could be related to the resolution of measurements. Whereas the L-ADCP data have measurements only where the CTD is cast, - and the transects are highly a result of interpolation, the S-ADCP data contain measurements on a 5-minute interval. For this reason, the S-ADCP data is thought to offer some finer details regarding flow direction and strength. Another plausible cause for the differences in the ADCP data could be related to the de-tiding of the data, which might not be sufficient for the Barents Sea area. The strong and deviating current system found close to station P5, hypothesized to be a tidal current close to Kvitøya, could support this theory. Lastly, we must mention the error codes that occurred during the processing of the raw L-ADCP data (see Section 3.2.2), which might have caused errors in the resulting current direction. This could also be a potential source for the discrepancy. For further studies, these error messages should be addressed.

The mismatch in the L-ADCP and S-ADCP data, in combination with the pronounced variability in the current characteristics, generally makes it difficult to interpret and determine the flow regimes on the transect. This holds especially true for the Barents Sea area, where little consistency is found. The sparse measurement coverage, both spatially and temporally, further complicates the analysis. We have therefore not been able to detect any discernible seasonal patterns in the flow across the transect. Further analysis, in addition to more observational data points, could be beneficial for future studies.

Lastly, it is worth to mention that the area we have investigated is rather vast and encompasses different flow regimes, origins of water masses, and water mass transformations. An in-depth analysis of these aspects is beyond the scope of this thesis. We have rather focused on giving an overview of hydrographic conditions along the transect during 2018-2022, using simple and fundamental oceanic parameters and tools of analysis. Thus, we recognize that there is a lot of potential to explore this dataset in further depth, especially concerning the driving mechanisms behind the flow dynamics and water mass interactions.

/6

Summary and conclusion

In this thesis, we have investigated the hydrographic conditions along the Nansen Legacy main transect across the Central Barents Sea and up into the Nansen Basin of the Arctic Ocean. The dataset encompasses observational CTD and ADCP data collected through the Nansen Legacy project between the years of 2018-2022, as well as atmospheric parameters from reanalysis product ERA-5 and remotely sensed satellite data of sea ice concentration (OSI-SAF) for the same period. The study has aimed to investigate the seasonal, interannual, and lateral variations in water masses, water mass transformations, and circulation across the transect.

Our analysis shows that the NL transects can be divided into three domains reflecting the lateral differences in water masses, seasonal evolution, heat- and freshwater content, and flow regimes. In the northern part of the transect (>81° N), the water column properties were controlled by the Atlantic Water Boundary Current (AWBC), transporting warm and salty AW along the continental slope north of Svalbard. The warmest AWBC temperatures were measured during autumn and early winter, supplying heat to the surrounding water. The coldest AWBC temperatures were recorded during the late winter of 2021, although we can not say whether this is an interannual variation or a more systematic seasonal pattern due to the sparse measurements during winter. Our results suggest that the water column is more controlled by advective processes, at least in the intermediate depths. The water column structure in the region follows the typical layering with Polar Water (PW) and/or warm Polar Water (wPW) on top followed by Atlantic Water (AW), modified Atlantic

Water (mAW), and Eurasian Basin Deep water(EBDW).

In the northern Barents Sea (81-77° N) the conditions were highly Arctic-dominated with PW and wPW as the most prevailing water masses. The upper to intermediate water column was typically dominated by cold and fresh PW, while the lower water column was occupied by wPW between P4 and P3. The seasonal evolution of the water column appears to be shaped by the sea ice cover at the surface, and to some extent also the advection of wPW with Atlantic-origin from both south and north of the Barents Sea.

The southernmost part of the transect was found to be highly Atlantic-dominated all year round. In general, the water mass of AW and mAW occupied large parts of the water column, with the latter water mass present for all conducted profiles (at station P1). For the summer measurements, a layer of fresher and warm wPW was detected in the upper water column, witnessing a seasonal evolution involving increased heat - and meltwater – input to the surface. This makes it a 3-layer structure of WM during summer, with wPW at the top, AW in the intermediate layer, and mAW towards the bottom. The autumn measurements witnessed a water column that was cooled off and where the MLD had increased. Likely, this is a seasonal effect mainly driven by thermal cooling and increased wind speeds in the area. The few winter measurements displayed a homogeneous water column with MLD to the down to the bottom. In such, the water column appears to follows a more typical seasonal evolution that mianly follows the trends of the atmospheric forcing. It also appears that local processes are more dominant on the water mass properties here than advective processes.

The environmental conditions were rather variating on the interannual scale throughout the study period, especially in regards to the sea ice cover and the air temperature. The winter seasons of 2018/2019 and 2019/2020 can be considered cold. At periods, sea ice covered the whole transect, even down to the southernmost station below the Polar Front. In relative terms, the winters of 2018, 2021, and 2022 were warm, and the sea ice edge was found north of 76. The variation in sea ice cover is thought to explain some of the interannual variations in heat and freshwater content, as well as the seasonal development of water masses for the upper water column.

Due to the low measurement resolution of each season, and the high interannual variation in water column properties, it has been proven hard to distinguish the seasonal patterns from the interannuability. The same is true for the current data, where the data coverage has been even more scarce. The currents in the Barents Sea appears to be highly variating in both time and across the transect. Thus, we have not been able to detect any seasonality in the current flow.

Bibliography

S. Aaboe, S. Lind, S. Hendricks, E. Down, T. Lavergne, and R. Ricker. Sea-ice and ocean conditions surprisingly normal in the Svalbard-Barents Sea region after large sea-ice inflows in 2019. *Copernicus Marine Service Ocean State Report*, 14(sup1):s140–s148, 2021. doi: 10.1080/1755876X.2021.1946240.

K. Aagaard and R. A. Woodgate. Some thoughts on the freezing and melting of sea ice and their effects on the ocean. *Ocean Modelling*, 3(1-2):127–135, 2001.

M. Årthun, I. H. Onarheim, J. Dörr, and T. Eldevik. The seasonal and regional transition to an ice-free Arctic. *Geophysical Research Letters*, 48: e2020GL090825, 2021. doi: 10.1029/2020GL090825.

A. Beszczynska-Möller, R. A. Woodgate, C. Lee, H. Melling, and M. Karcher. A synthesis of exchanges through the main oceanic gateways to the Arctic Ocean. *Oceanography*, 24(3):82–99, 2011.

A. Beszczynska-Möller, E. Fahrbach, U. Schauer, and E. Hansen. Variability in Atlantic water temperature and transport at the entrance to the Arctic Ocean, 1997–2010. *ICES Journal of Marine Science*, 69:852–863, 2012.

Environmental Working Group. Environmental Working Group Joint U.S.-Russian Atlas of the Arctic Ocean, Version 1. Online, 1997. URL `https://nsidc.org/data/G01961/versions/1`.

EUMETSAT Ocean and Sea Ice Satellite Application Facility. OSI SAF Global Sea Ice Concentration (SSMIS), OSI-401-d, 2023.

I. Fer, A. K. Peterson, and F. Nilsen. Atlantic water boundary current along the southern Yermak Plateau, Arctic Ocean. *Journal of Geophysical Research: Oceans*, 128:e2023JC019645, 2023. doi: 10.1029/2023JC019645.

T. Gammelsrød, Ø. Leikvin, V. Lien, W. P. Budgell, H. Loeng, and W. Maslowski. Mass and heat transports in the NE Barents Sea: Observations and models.

Journal of Marine Systems, 75(1-2):56–69, 2009. doi: 10.1016/j.jmarsys.2008.07.010.

S. Gerland, R. B. Ingvaldsen, M. Reigstad, A. Sundfjord, B. Bogstad, M. Chierici, H. Hop, P. E. Renaud, L. H. Smedsrud, L. C. Stige, M. Årthun, J. Berge, B. A. Bluhm, K. Borgå, G. Bratbak, D. V. Divine, T. Eldevik, E. Eriksen, I. Fer, and P. Wassmann. Still Arctic?—The changing Barents Sea. *Elementa: Science of the Anthropocene*, 11(1), 2023. doi: 10.1525/elementa.2022.00088.

H. Hersbach, B. Bell, P. Berrisford, G. Biavati, A. Horá nyi, J. Muñ oz Sabater, J. Nicolas, C. Peubey, R. Radu, I. Rozum, D. Schepers, A. Simmons, C. Soci, D. Dee, and J.-N. Thé paut. Era5 hourly data on single levels from 1940 to present, 2023.

N. P. Holliday, S. A. Cunningham, C. Johnson, S. F. Gary, C. Griffiths, J. F. Read, and T. Sherwin. Multidecadal variability of potential temperature, salinity, and transport in the eastern subpolar North Atlantic. *Journal of Geophysical Research: Oceans*, 120:5945–5967, 2015. doi: 10.1002/2015JC010762.

R. Ingvaldsen, H. Loeng, and L. Asplin. Variability in the Atlantic Inflow to the Barents Sea Based on a One-Year Time Series from Moored Current Meters. *Continental Shelf Research*, 22:505–519, 2002. doi: 10.1016/S0278-4343(01)00070-X.

IOC, SCOR, and IAPSO. The international thermodynamic equation of seawater – 2010: Calculation and use of thermodynamic properties. Manuals and Guides 56, Intergovernmental Oceanographic Commission, UNESCO, 2010.

K. Isaksen, Ø. Nordli, B. Ivanov, and et al. Exceptional warming over the Barents area. *Scientific Reports*, 12:9371, 2022. doi: 10.1038/s41598-022-13568-5.

V. V. Ivanov, V. A. Alexeev, I. Repina, N. V. Koldunov, and A. Smirnov. Tracing Atlantic Water Signature in the Arctic Sea Ice Cover East of Svalbard. *Advances in Meteorology*, 2012:201818, 2012. doi: 10.1155/2012/201818.

E. M. Jones, M. Chierici, A. Fransson, K. M. Assmann, A. H. H. Renner, and H. H. Lødemel. Inorganic carbon and nutrient dynamics in the marginal ice zone of the Barents Sea: Seasonality and implications for ocean acidification. *Progress in Oceanography*, 219:103131, 2023. doi: 10.1016/j.pocean.2023.103131.

Z. Koenig, C. Provost, N. Villacieros-Robineau, N. Sennéchael, A. Meyer, J.-M. Lellouche, and G. Garric. Atlantic waters inflow north of Svalbard: Insights from IAOOS observations and Mercator Ocean global operational system

during N-ICE2015. *Journal of Geophysical Research: Oceans*, 122:1254.1273. doi: 10.1002/2016JC012424.

Z. Koenig, M. Muilwijk, H. Sandven, O. Lundesgaard, P. Assmy, S. Lind, K. M. Assmann, M. Chierici, A. Fransson, S. Gerland, E. Jones, A. H. H. Renner, and M. A. Granskog. From Winter to Late Summer in the Northwestern Barents Sea Shelf: Impacts of Seasonal Progression of Sea Ice and Upper Ocean on Nutrient and Phytoplankton Dynamics. *Progress in Oceanography*, 220:103174, 2023. doi: 10.1016/j.pocean.2023.103174.

E. H. Kolås, T. M. Baumann, R. Skogseth, Z. Koenig, and I. Fer. Western Barents Sea Circulation and Hydrography, past and present. *ESS Open Archive*, August 2023. doi: 10.22541/essoar.169203078.81082540/v1.

V. S. Lien and A. G. Trofimov. Formation of Barents Sea Branch Water in the north-eastern Barents Sea. *Polar Research*, 32, 2013. doi: 10.3402/polar.v32i0.18905.

V. S. Lien (ed). The physical nature and biological implications of the polar front: A value and vulnerability assessment of the Polar Front in the Barents Sea (in Norwegian). Fisken og Havet 8-2018, Institute of Marine Research, Bergen, Norway, 2018.

S. Lind and R. Ingvaldsen. Variability and impacts of Atlantic Water entering the Barents Sea from the north. *Deep Sea Research*, 62:70–88, 2012. doi: 10.1016/j.dsr.2011.12.007.

S. Lind, R. Ingvaldsen, and T. Furevik. Arctic warming hotspot in the northern Barents Sea linked to declining sea-ice import. *Nature Climate Change*, 8: 634–639, 2018. doi: 10.1038/s41558-018-0205-y.

H. Loeng. Features of the Physical Oceanographic Conditions of the Barents Sea. *Polar Research*, 10, 1991. doi: 10.3402/polar.v10i1.6723.

Ø. Lundesgaard, A. Sundfjord, and A. H. H. Renner. Drivers of interannual sea ice concentration variability in the Atlantic Water inflow region north of Svalbard. *Journal of Geophysical Research: Oceans*, 126:e2020JC016522, 2021. doi: 10.1029/2020JC016522.

Ø. Lundesgaard, A. Sundfjord, S. Lind, F. Nilsen, and A. H. H. Renner. Import of Atlantic Water and Sea Ice Controls the Ocean Environment in the Northern Barents Sea. *Ocean Science*, 18:1389–1418, 2022.

T. Martin, M. Steele, and J. Zhang. Seasonality and long-term trend of Arctic

Ocean surface stress in a model. *Journal of Geophysical Research*, 119:1723–1738, 2014. doi: 10.1002/2013JC009425.

T. McDougall and P. Barker. *Getting started with TEOS-10 and the Gibbs Seawater (GSW) Oceanographic Toolbox*, 2011. ISBN 978-0-646-55621-5.

M. Meredith, M. Sommerkorn, S. Cassotta, C. Derksen, A. Ekaykin, A. Hollowed, G. Kofinas, A. Mackintosh, J. Melbourne-Thomas, M. Muelbert, G. Ottersen, H. Pritchard, and E. Schuur. Polar Regions. In H.-O. Portner, D. Roberts, V. MassonDelmotte, P. Zhai, M. Tignor, E. Poloczanska, K. Mintenbeck, A. Alegría, M. Nicolai, A. Okem, J. Petzold, B. Rama, and N. Weyer, editors, *IPCC Special Report on the Ocean and Cryosphere in a Changing Climate*, pages 203–320. Cambridge University Press, Cambridge, UK and New York, NY, USA, 2019. doi: 10.1017/9781009157964.005.

A. Meyer, I. Fer, A. Sundfjord, and A. K. Peterson. Mixing rates and vertical heat fluxes north of Svalbard from Arctic winter to spring. *Journal of Geophysical Research: Oceans*, 122, 2017. doi: 10.1002/2016JC012441.

E. Olsen and C. von Quillfeldt. Identifisering av særlig verdifulle områder i Barentshavet og Lofoten. Technical report, Norsk Polarinstitutt/Havforskningsinstituttet, Tromsø/Bergen, 2003.

I. H. Onarheim and M. Årthun. Toward an ice-free Barents Sea. *Geophysical Research Letters*, 44(16):8387–8395, 2017. doi: 10.1002/2017GL074304.

I. H. Onarheim, T. Eldevik, L. H. Smedsrud, and J. C. Stroeve. Seasonal and regional manifestation of Arctic sea ice loss. *Journal of Climate*, 31(12):4917–4932, 2018. doi: 10.1175/JCLI-D-17-0427.1.

K. A. Orvik and Ø. Skagseth. Heat flux variations in the eastern Norwegian Atlantic Current toward the Arctic from moored instruments, 1995–2005. *Geophysical Research Letters*, 32:L14610, 2005.

C. Peralta-Ferriz and R. A. Woodgate. Seasonal and interannual variability of pan-Arctic surface mixed layer properties from 1979 to 2012 from hydrographic data, and the dominance of stratification for multiyear mixed layer depth shoaling. *Progress in Oceanography*, 134:19–53, 2015.

R. S. Pickart and W. M. Smethie Jr. Temporal evolution of the deep western boundary current where it enters the sub-tropical domain. *Deep Sea Research Part I: Oceanographic Research Papers*, 45:1053–1083, 1998. doi: 10.1016/s0967-0637(97)00084-8.

A. V. Pnyushkov, I. V. Polyakov, V. V. Ivanov, Y. Aksenov, A. C. Coward, M. Janout, and B. Rabe. Structure and variability of the boundary current in the Eurasian Basin of the Arctic Ocean. *Deep Sea Research Part I: Oceanographic Research Papers*, 101:80–97, 2015.

I. V. Polyakov et al. Greater role for Atlantic inflows on sea-ice loss in the Eurasian Basin of the Arctic Ocean. *Science*, 356:285–291, 2017. doi: 10.1126/science.aai8204.

M. Previdi, K. L. Smith, and L. M. Polvani. Arctic amplification of climate change: a review of underlying mechanisms. *Environmental Research Letters*, 16(9):093003, 2021. doi: 10.1088/1748-9326/ac1c29.

M. Rantanen, A. Y. Karpechko, A. Lipponen, K. Nordling, O. Hyvärinen, K. Ruosteenoja, T. Vihma, and A. Laaksonen. The Arctic has warmed nearly four times faster than the globe since 1979. *Communications Earth & Environment*, 3:168, 2022. doi: 10.1038/s43247-022-00498-3.

A. H. H. Renner, A. Sundfjord, M. A. Janout, R. B. Ingvaldsen, A. Beszczynska-Möller, R. S. Pickart, and M. D. Pérez-Hernández. Variability and redistribution of heat in the Atlantic Water boundary current north of Svalbard. *Journal of Geophysical Research: Oceans*, 123(9):6373–6391, 2018.

U. Schauer, H. Loeng, B. Rudels, V. K. Ozhigin, and W. Dieck. Atlantic water flow through the Barents and Kara Seas. *Deep Sea Research Part I: Oceanographic Research Papers*, 49(12):2281–2298, 2002.

Q. Shu et al. Arctic Ocean Amplification in a Warming Climate in CMIP6 Models. *Science Advances*, 8:eabn9755, 2022. doi: 10.1126/sciadv.abn9755.

L. H. Smedsrud, I. Esau, R. B. Ingvaldsen, T. Eldevik, P. M. Haugan, C. Li, V. S. Lien, A. Olsen, A. M. Omar, O. H. Otterå, B. Risebrobakken, A. B. Sandø, V. A. Semenov, and S. A. Sorokina. The role of the Barents Sea in the Arctic climate system. *Reviews of Geophysics*, 51:415–449, 2013. doi: 10.1002/rog.20017.

A. Sundfjord, K. M. Assmann, Ø. Lundesgaard, A. H. Renner, S. Lind, and R. B. Ingvaldsen. Suggested water mass definitions for the central and northern Barents Sea, and the adjacent Nansen Basin: Workshop Report. *The Nansen Legacy Report Series*, (8), 2020. doi: 10.7557/nlrs.5707.

The Nansen Legacy. Sampling Protocols: Version 10. The Nansen Legacy Report Series 32/2022, 2022. doi:10.7557/nlrs.6684.

D. Thomas and G. Dieckmann. *Sea Ice*. Blackwell Publishing, Oxford, United

Kingdom, 2nd edition, 2010. ISBN ISBN 978-1-4051-8580-6.

M.-L. Timmermans and J. Marshall. Understanding Arctic Ocean circulation: A review of ocean dynamics in a changing climate. *Journal of Geophysical Research: Oceans*, 125:e2018JC014378, 2020. doi: 10.1029/2018JC014378.

M. Visbeck. Deep velocity profiling using lowered acoustic Doppler current profilers: Bottom track and inverse solutions. *Journal of Atmospheric and Oceanic Technology*, 19:794–807, 2002. doi: 10.1175/1520-0426(2002)019, 0794:DVPULA.2.0.CO;2.

A. Wold, H. Hop, C. Svensen, J. E. Sø reide, K. M. Assmann, M. Ormanczyk, and S. Kwasniewski. Atlantification influences zooplankton communities seasonally in the northern Barents Sea and Arctic Ocean. *Progress in Oceanography*, 219:103133, 2023. doi: 10.1016/j.pocean.2023.103133.

R. A. Woodgate, K. Aagaard, R. D. Muench, J. Gunn, G. Björk, B. Rudels, and U. Schauer. The Arctic Ocean boundary current along the Eurasian slope and the adjacent Lomonosov Ridge: Water mass properties, transports and transformations from moored instruments. *Deep Sea Research Part I: Oceanographic Research Papers*, 48(8):1757–1792, 2001.

/7
Appendix

7.1 Appendix A – Station table

Nansen LEGACY transect - stations							
Station name	Longitude (decimal)	Latitude (decimal)	Longitude (degrees)	Latitude (degrees)	Depth (m)	Type of station	Comment
NLEG25	**30,0000**	**82,0000**	**030 00.00 E**	**82 00.00 N**	**3000**	**Process study station P7**	
NLEG24	30,5258	81,6828	030 31.55 E	81 40.97 N	2807		*A-TWAIN*
NLEG23	30,6647	81,6165	030 39.88 E	81 36.99 N	1913		*A-TWAIN*
NLEG22	30,7667	81,5895	030 46.00 E	81 35.37 N	1551		*A-TWAIN*
NLEG21	**30,8548**	**81,5463**	**030 51.29 E**	**81 32.78 N**	**865**	**Process study station P6**	***A-TWAIN, shelf-break***
NLEG20	30,9618	81,5025	030 57.71 E	81 30.15 N	698		*A-TWAIN, shelf-break*
NLEG19	31,0775	81,4580	031 04.65 E	81 27.48 N	486		*A-TWAIN, shelf-break*
NLEG18	31,1448	81,4318	031 08.69 E	81 25.91 N	264		*A-TWAIN, shelf-break*
NLEG17	31,2468	81,4107	031 14.81 E	81 24.64 N	204		*A-TWAIN, shelf-break*
NLEG16	31,2933	81,3822	031 17.60 E	81 22.93 N	189		*A-TWAIN, shelf-break*
NLEG15	31,3487	81,3098	031 20.92 E	81 18.59 N	195		*Arctic Price near-shelf-station*
NLEG14	34,0000	81,0000	034 00.00 E	81 00.00 N	216		*Vardø-N, Kvitøybanken*
NLEG13	**34,0000**	**80,5000**	**034 00.00 E**	**80 30.00 N**	**167**	**Process study station P5**	***Vardø-N, Kvitøybanken***
NLEG12	34,0000	80,0000	034 00.00 E	80 00.00 N	209		*Vardø-N, Kvitøybanken*
NLEG11	**34,0000**	**79,7500**	**034 00.00 E**	**79 45.00 N**	**332**	**Process study station P4**	***Vardø-N, trench east of Kong Karl***
NLEG10	34,0000	79,5000	034 00.00 E	79 30.00 N	293		*Vardø-N, trench east of Kong Karl*
NLEG09	34,0000	79,2500	034 00.00 E	79 15.00 N	215		*Vardø-N, trench east of Kong Karl*
NLEG08	34,0000	79,0000	034 00.00 E	79 00.00 N	266		*Vardø-N, trench east of Kong Karl*
NLEG07	**34,0000**	**78,7500**	**034 00.00 E**	**78 45.00 N**	**301**	**Process study station P3**	***Vardø-N, trench east of Kong Karl***
NLEG06	34,0000	78,5000	034 00.00 E	78 30.00 N	180		*Vardø-N, Storbanken*
NLEG05	34,0000	78,0000	034 00.00 E	78 00.00 N	193		*Vardø-N, Storbanken*
NLEG04	**34,0000**	**77,5000**	**034 00.00 E**	**77 30.00 N**	**190**	**Process study station P2**	***Vardø-N, Storbanken***
NLEG03	34,0000	77,0000	034 00.00 E	77 00.00 N	154		*Vardø-N, Storbanken*
NLEG02	31,2200	76,5000	031 13.20 E	76 30.00 N	308		*Vardø-N, Storbanken*
NLEG01	**31,2200**	**76,0000**	**031 13.20 E**	**76 00.00 N**	**322**	**Process study station P1**	***Vardø-N, Hopendjupet***

Figure 7.1: Name, position, depth, etc. for each defined NL station in the Nansen Legacy main transect. The comment section refers to an associated project and/or the geographical location of the station. Source of table: The Nansen Legacy (2022) Sampling Protocols: Version 10. The Nansen Legacy Report Series 32/2022. DOI: `https://doi.org/10.7557/nlrs.6684`

7.2 Appendix B – Pcolour plots of CT and SA

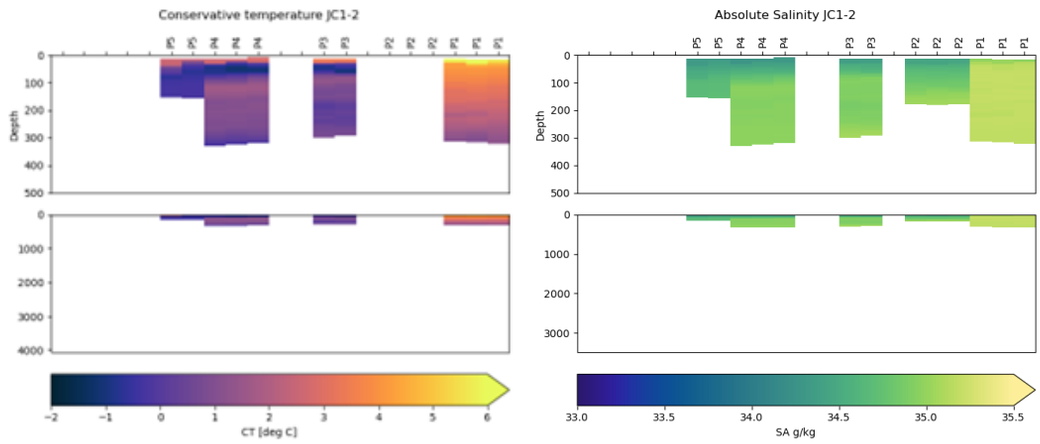

(a) JC1-2: August 2018

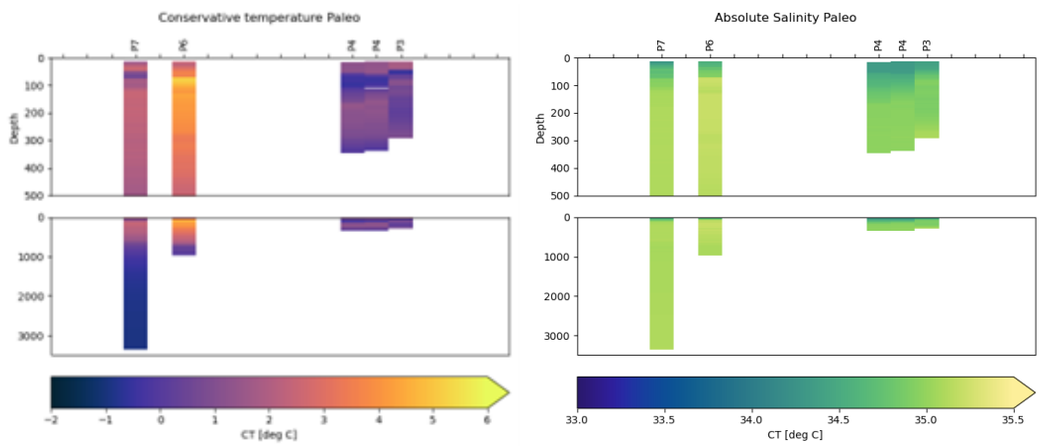

(b) Paleo: October 2018

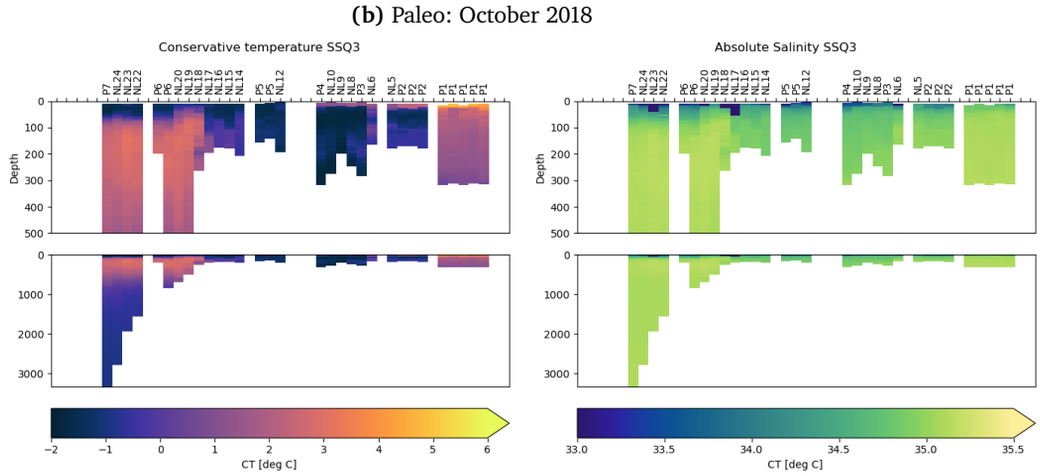

(c) SSQ3: August 2019

Figure 7.2: Pcolour plots of Conservative Temperature and Absolute Salinity for each of the cruises. Each column refers to a conducted profile. Thus, for some NL stations where several profiles were conducted, several columns are displayed for that same station.

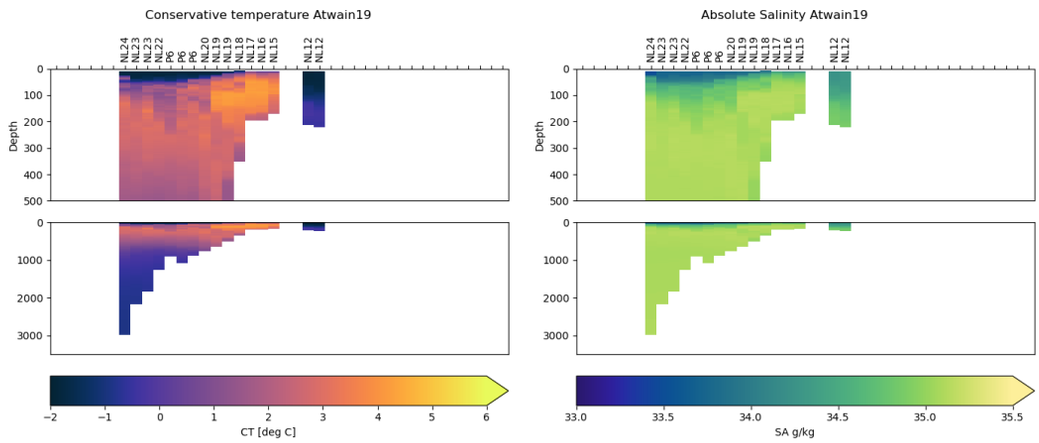

(d) MSC19: November 2019

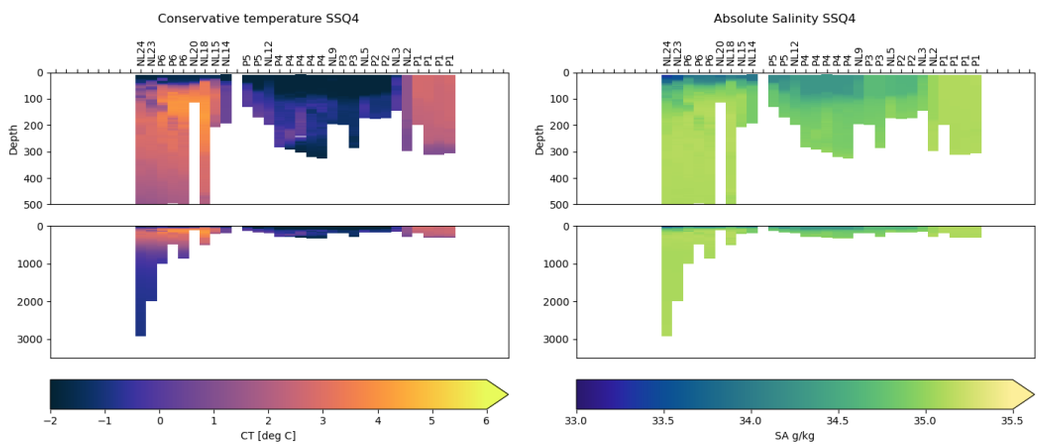

(e) SSQ4: November/December 2019

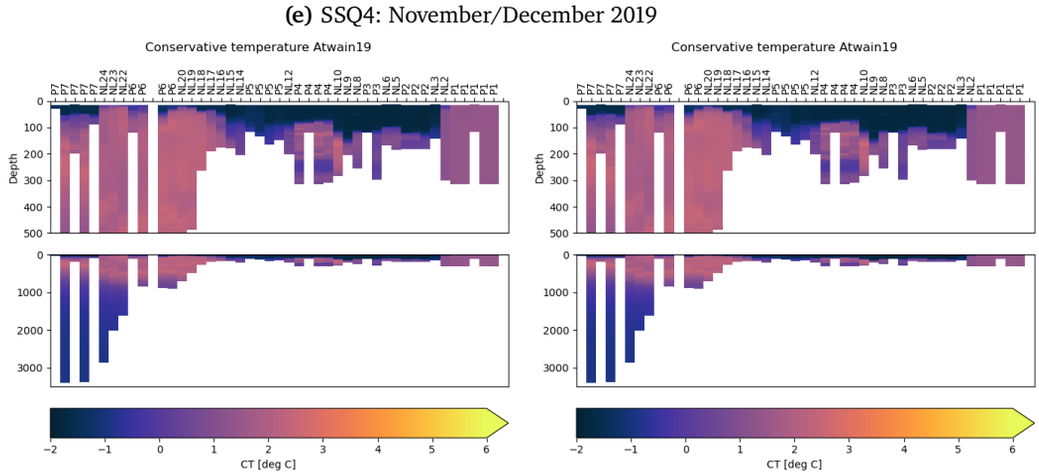

(f) SSQ1: March 2021

Figure 7.2: Continued.

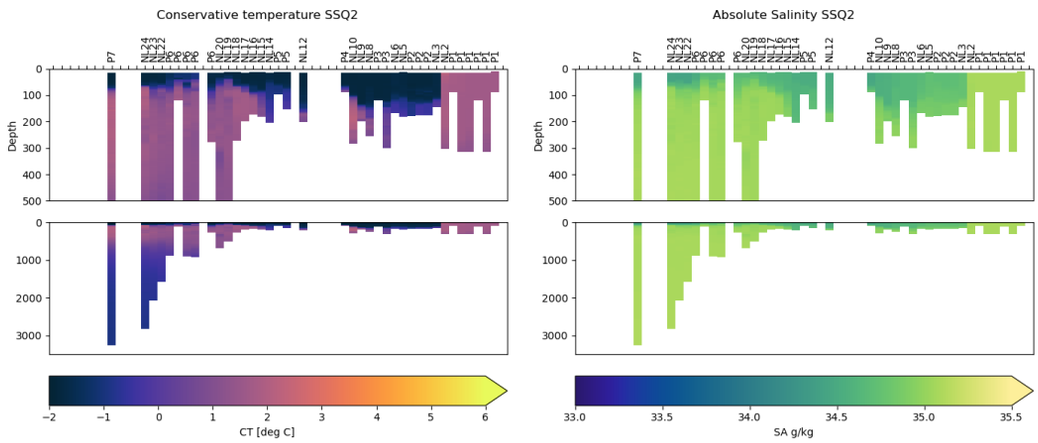

(g) SSQ2: May 2021

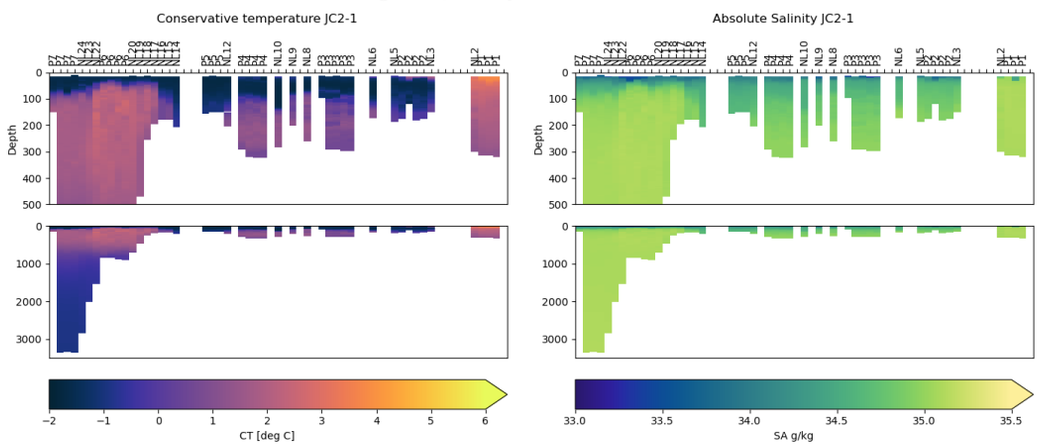

(h) JC2-1: August 2021

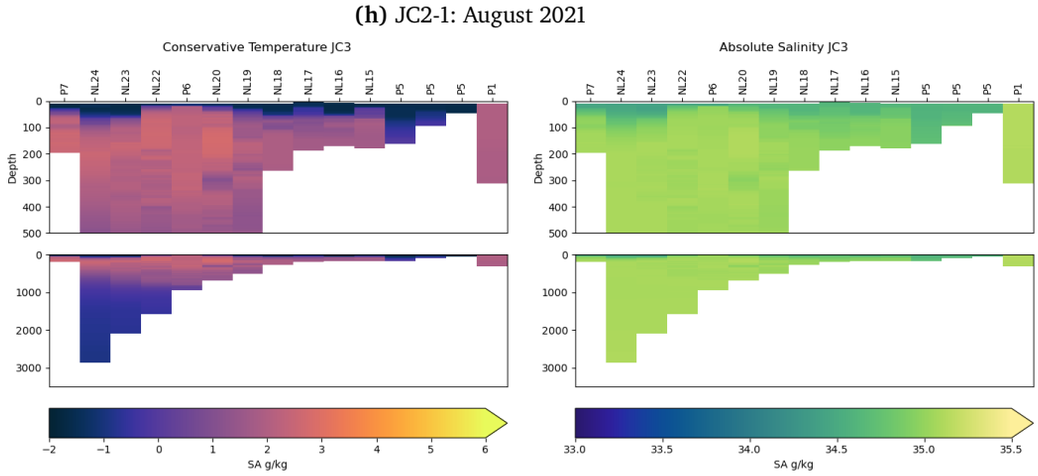

(i) JC3: February/March 2022

Figure 7.2: Continued.

7.3 Appendix C – P-station profiles including water masses

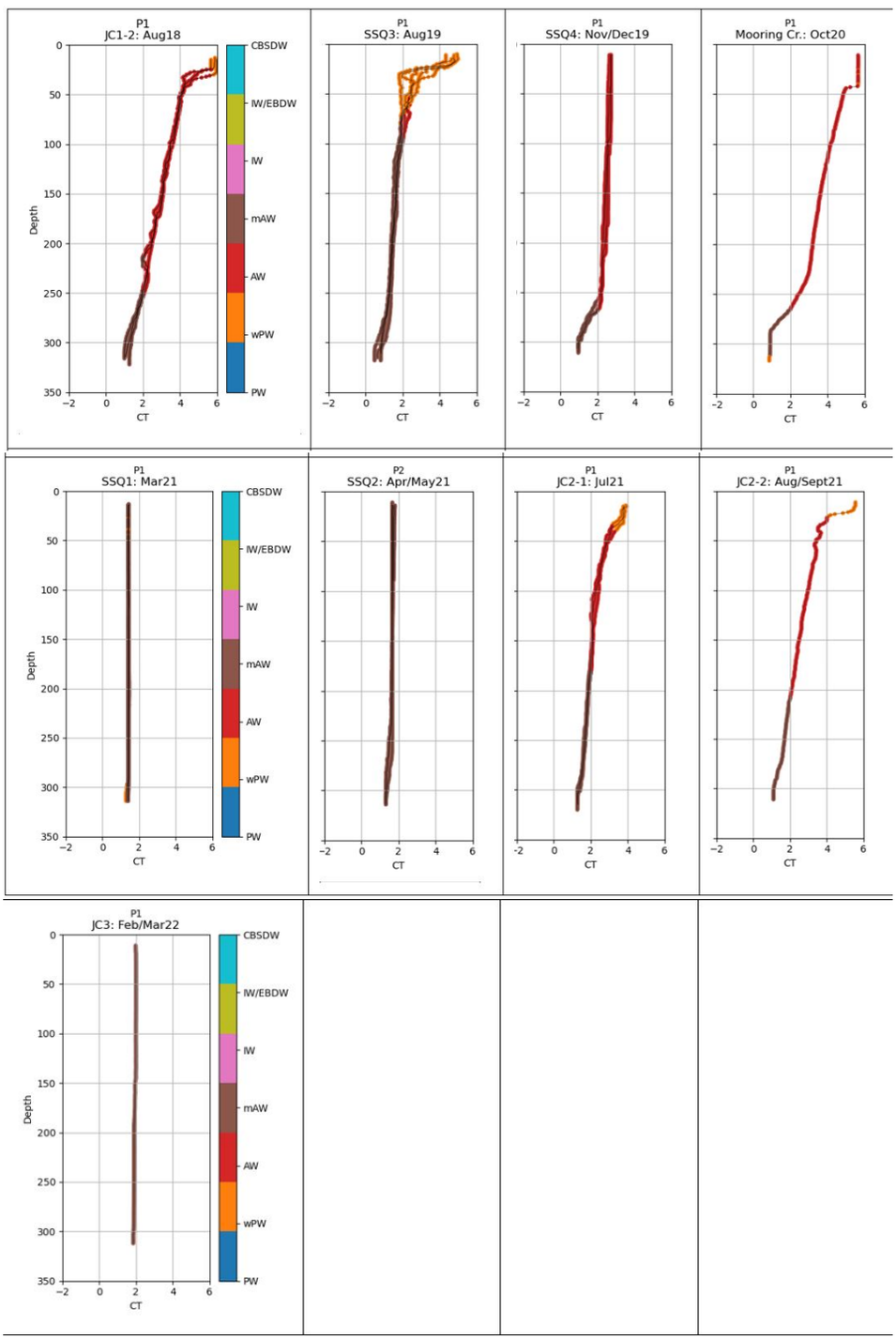

(a) Vertical profiles at P1

Figure 7.3: Profiles of Conservative Temperature for the 7 P-stations, with the corresponding water masses plotted on top. The profiles are shown in chronological order, displaying the evolution throughout the study period. Regarding P7, the displayed profile depth is limited to 15-1000m

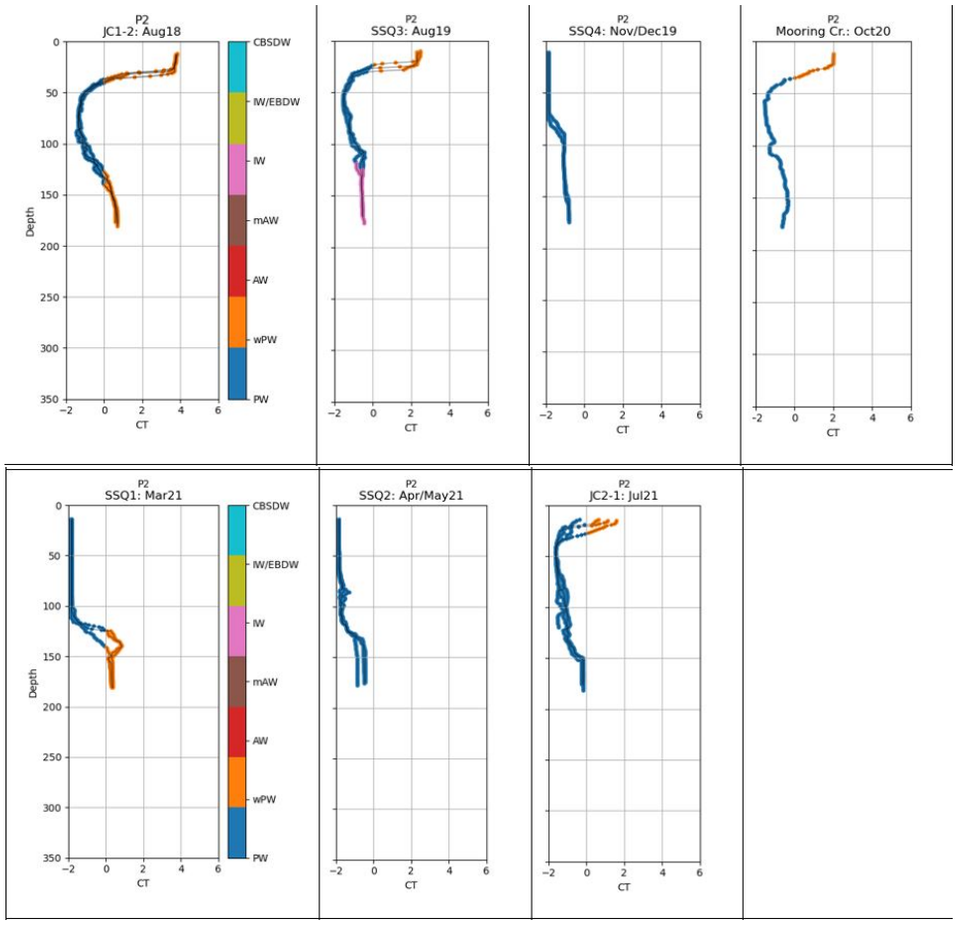

(b) Vertical profiles at P2

Figure 7.3: Continued.

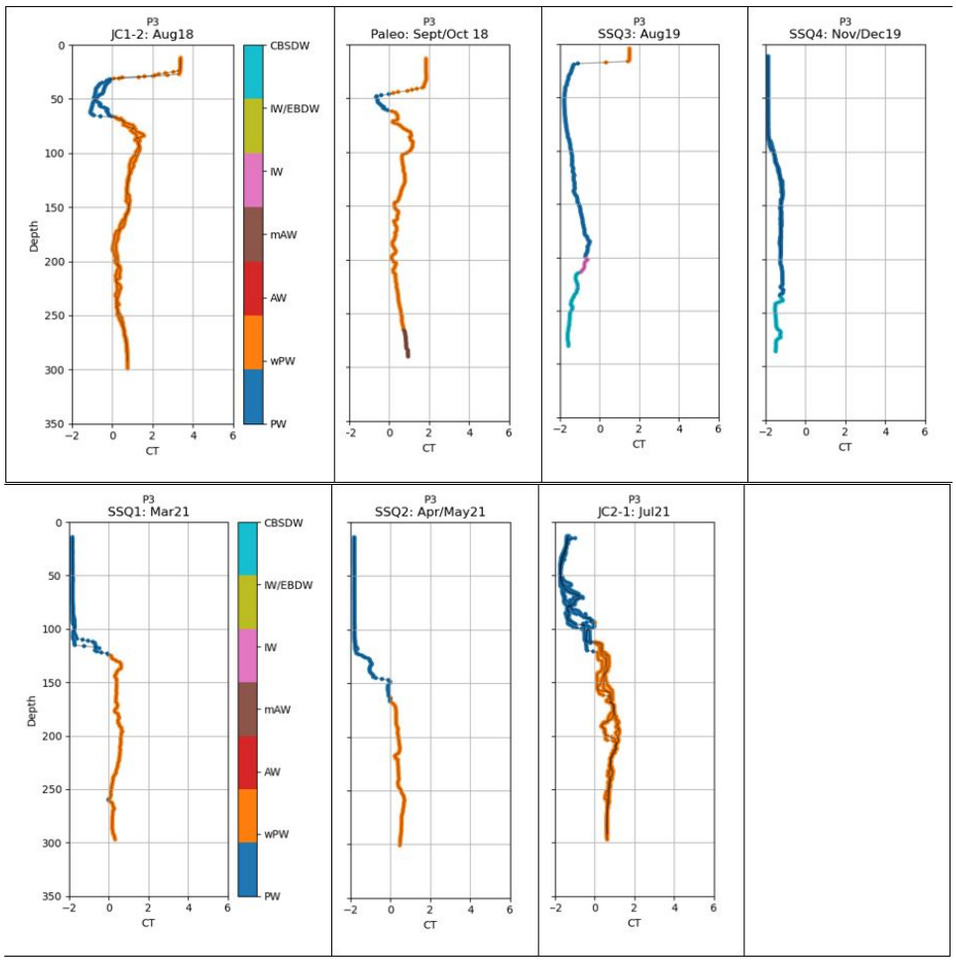

(c) Vertical profiles at P3

Figure 7.3: Continued.

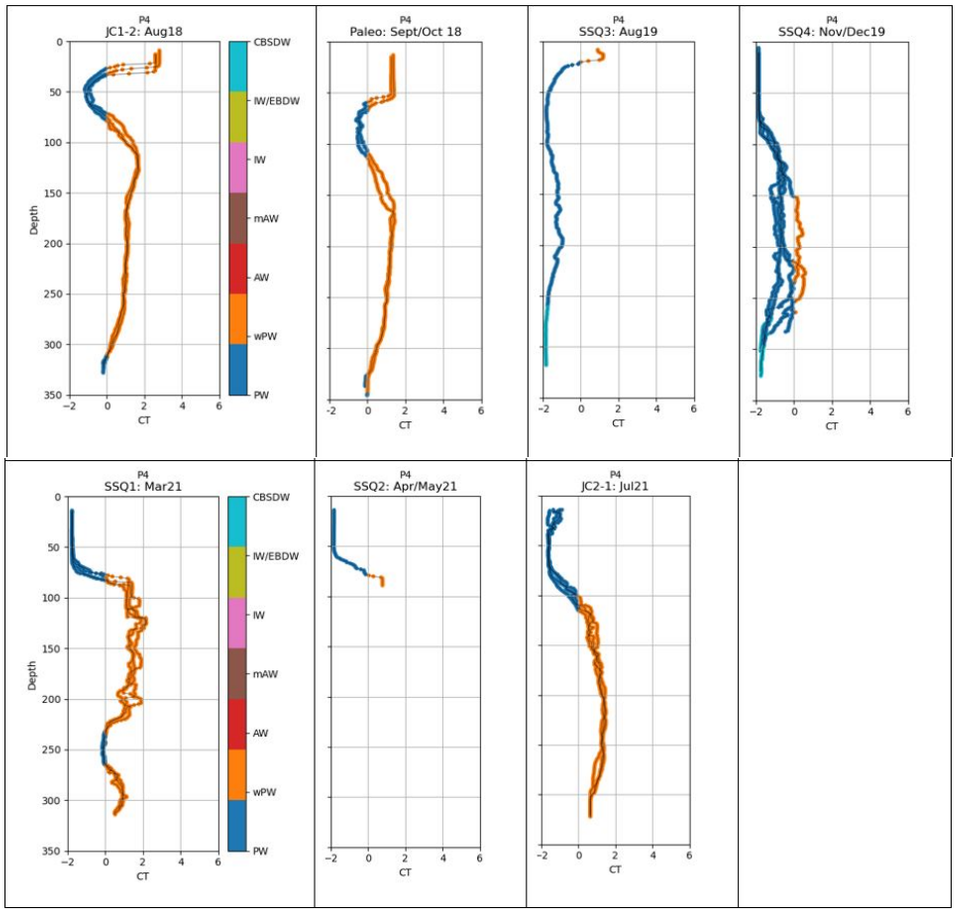

(d) Vertical profiles at P4

Figure 7.3: Continued.

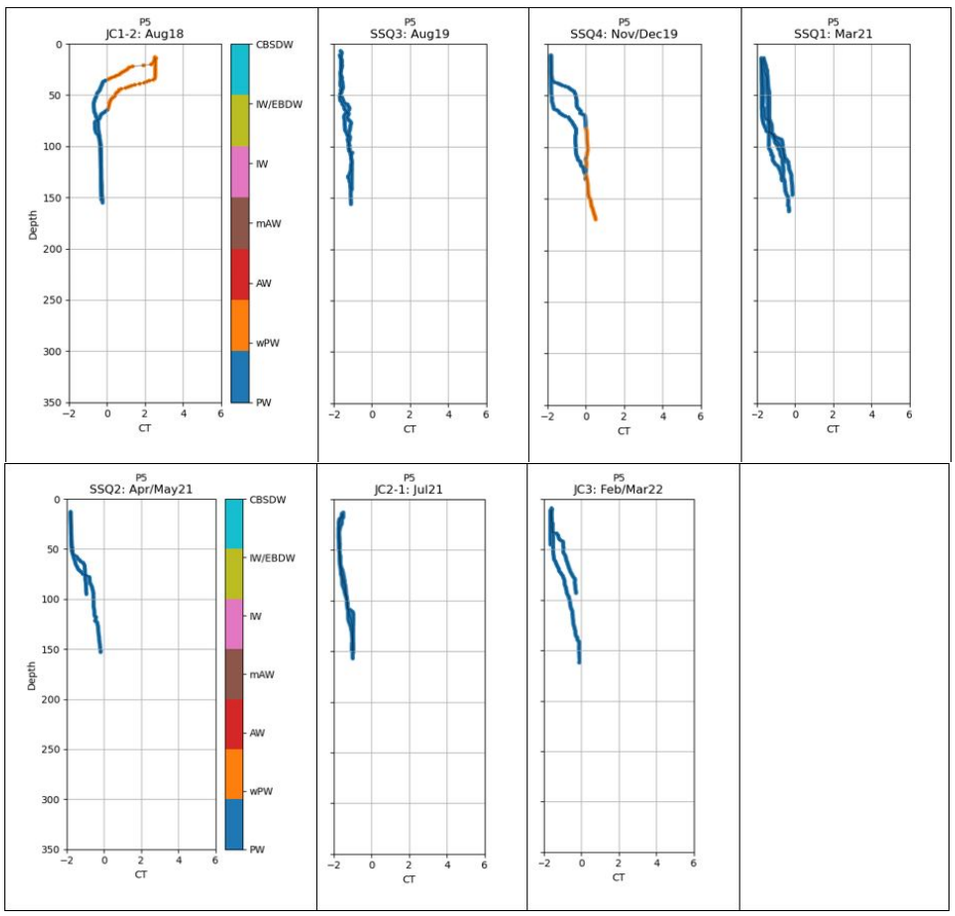

(e) Vertical profiles at P5

Figure 7.3: Continued.

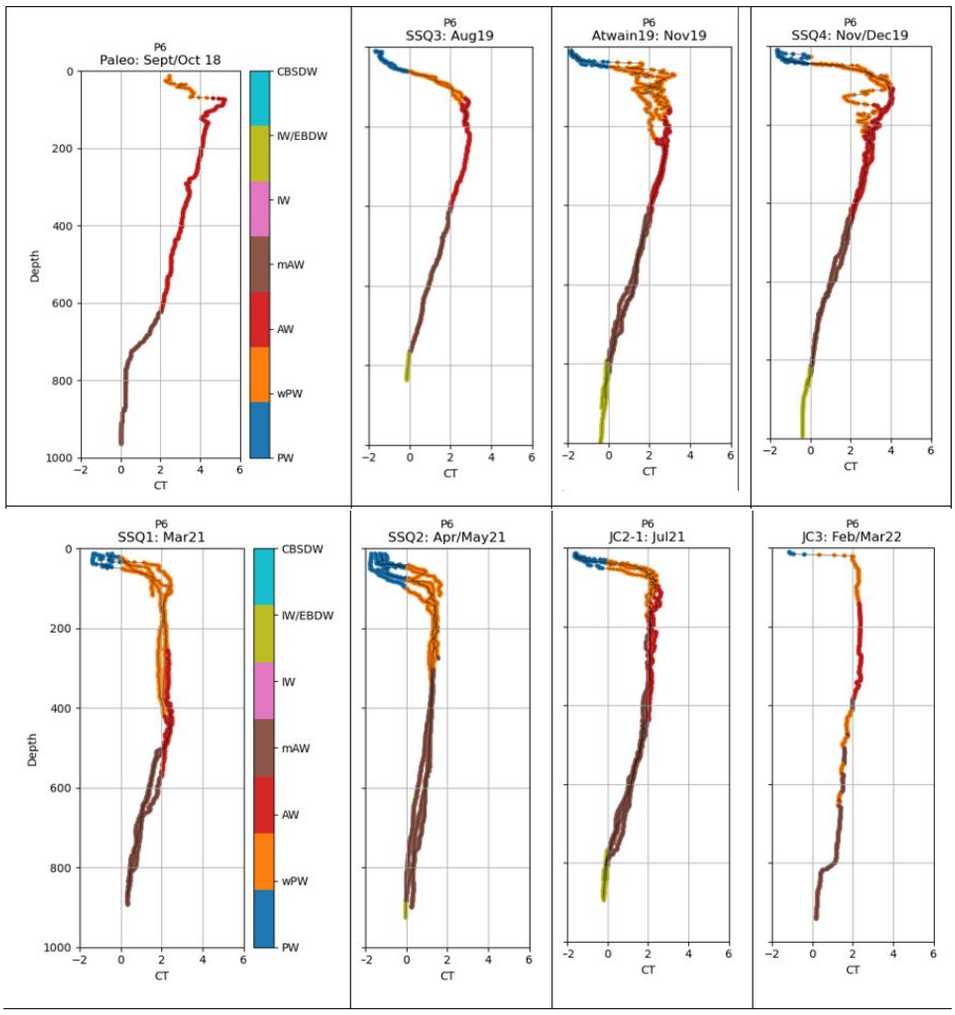

(f) Vertical profiles at P6

Figure 7.3: Continued.

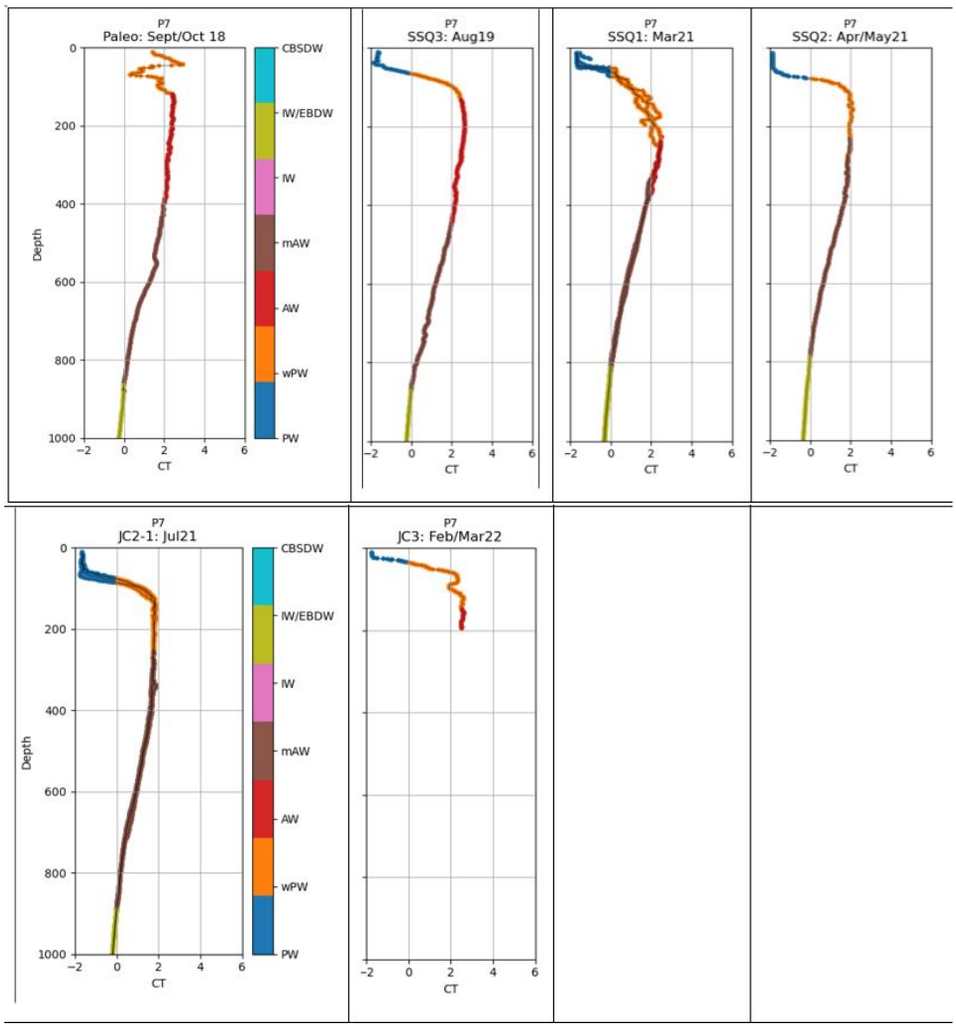

(g) Vertical profiles at P7

Figure 7.3: Continued.